Significant reduction of unequal population exposure to climate extremes by achieving the carbon neutrality

Seok-Geun Oh[1], Jung Choi[1], Min-Jee Kang[1], Sujong Jeong[2,3], Seung-Ki Min[4,5], Sang-Wook Yeh[6], Yeon-Hee Kim[4], and Seok-Woo Son[1,3*]

[1]School of Earth and Environmental Sciences, Seoul National University, Seoul, South Korea

[2]Department of Environmental Planning, Seoul National University, Seoul, South Korea

[3]Climate Technology Center, Seoul National University, Seoul, South Korea

[4]Division of Environmental Science and Engineering, Pohang University of Science and Technology, Pohang, Gyeongbuk, South Korea

[5]Institute for Convergence Research and Education in Advanced Technology, Yonsei University, Incheon, Republic of Korea

[6]Department of Marine Science and Convergence Engineering, Hanyang University, ERICA, Ansan, South Korea

December 2023

***Corresponding author:** Seok-Woo Son (seokwooson@snu.ac.kr)

Key points (Limit 140 character including spaces):

- By the 2050s, carbon neutrality reduces population exposure to climate extremes by 87–98% compared to current global warming rates.
- Africa and Asia are projected to experience the most dramatic reductions in population exposure to climate extremes by achieving the carbon neutrality.
- In North America, Europe, and Oceania, climate extreme change plays a more important role in population exposure to climate extremes.

Abstract

Climate extremes, such as hot temperature and heavy precipitation events, have devastating effects on human societies. As the planet gets warmer, they have become more intense and more frequent. To avoid irreversible damages from climate extremes, many countries have committed to achieving net-zero anthropogenic carbon emissions, or carbon neutrality, by the 2050s. Here, we quantify the impact of carbon neutrality on population exposure to climate extremes using multi-model projections from the Coupled Model Intercomparison Project Phase 6 (CMIP6) Shared Socioeconomic Pathway (SSP)1-1.9 and SSP3-7.0 scenarios. It is found that the increasing population exposure to hot-temperature and heavy-precipitation extremes under SSP3-7.0 scenario can be substantially reduced by 87–98% in the late 21st century by achieving the carbon neutrality based on SSP1-1.9 scenario. The benefits of carbon neutrality are particularly pronounced in Africa and Asia. The potential benefits of carbon neutrality are also significant in North America, Europe, and Oceania, where a reduction in climate extremes is more than twice as important as population decline in reducing population exposure to climate extremes. These results provide important scientific support for ongoing efforts to achieve net-zero carbon emissions by the 2050s to reduce potential climate risk and its inequity across continents.

Plain Language Summary

To avoid irreversible damages from climate extremes in a warming climate, net-zero anthropogenic carbon emissions, or carbon neutrality, has been proposed. However, how much damages from climate extremes can be mitigated by achieving the carbon neutrality has not been quantitatively assessed. Here, we show that achieving carbon neutrality could lead to a significant and widespread reduction in population exposure to hot-temperature and heavy-precipitation extremes by 87–98% in the late 21st century. The benefits of carbon neutrality are particularly large in Africa and Asia. Even in North America, Europe, and Oceania, where the developed countries are concentrated, population exposure to climate extremes is projected to decrease significantly, primarily due to reduced climate extremes with a minor contribution of population decline. This finding underscores the critical importance of ongoing efforts to achieve net-zero carbon emissions by the 2050s to reduce potential climate risk and its inequity across continents.

1. Introduction

As the threat of global warming became a reality, the Paris Agreement was proposed in 2015 to "hold the increase in the global average temperature to well below 2°C against preindustrial levels and pursue efforts to limit the temperature increase to 1.5°C" (UNFCCC, 2015). Its potential benefits have often been highlighted through the analyses of climate model simulations (e.g., Park et al., 2018; King et al., 2021; Nashwan & Shahid, 2022). Such studies have reported that 0.5°C less warming compared to 2°C warming can lead to a significant reduction in the areas damaged by climate change. However, these studies are mainly based on relatively low-emission scenarios compared to high-emission scenarios (e.g., O'Neill et al., 2016; Oin et al., 2021) rather than carbon-neutrality scenarios which take into account socioeconomic and environmental changes, technological development and innovation, and policy coordination to achieve net-zero emissions by the 2050s (Gidden et al., 2018).

While the Paris Agreement focuses on mean surface air temperature (UNFCCC, 2015), more attention should be paid to climate extremes. Climate extremes, such as hot-temperature and heavy-precipitation events, are rapidly increasing with global warming, exerting destructive impacts on human societies (e.g., Kharin et al., 2013; Li et al., 2021; Xie et al., 2022). By reducing CO_2 emissions, the frequency and intensity of climate extremes are projected to decrease significantly (e.g., Jo et al., 2022; Kim et al., 2022; Nashwan & Shahid, 2022). However, it has not yet been quantified how much the population exposure to climate extremes can be reduced by achieving carbon neutrality, although it can provide critical context for establishing effective climate mitigation policies.

Here, we investigate the impact of carbon neutrality on population exposure to hot-temperature and heavy-precipitation events by examining multi-model projections from the Coupled Model Intercomparison Project Phase 6 (CMIP6, Eyring et al., 2016). In particular, we compare the Shared Socioeconomic Pathway (SSP)1-1.9 scenario, which describes a transition to a carbon-neutral society around the 2050s and net carbon absorption thereafter, with the SSP3-7.0 scenario, which is based on regional rivalry over carbon emissions policy (Fig. 1; O'Neill et al., 2016; Oin et al., 2021), and quantitatively assess the projected reduction in global and regional population exposure to hot-temperature and heavy-precipitation extremes. The relative importance of changes in population and extreme events in reducing population exposure to climate extremes is also examined.

2. Data and Methods

2.1. Datasets

To calculate climate extremes, daily maximum temperature and precipitation for historical simulations (1985–2014) and future projections (2015–2100) under two different SSP scenarios from eight CMIP6 models (Eyring et al., 2016) are used (Table 1). Specifically, the SSP3-7.0 and SSP1-1.9 scenarios, which are the high and very low greenhouse gas emission scenarios, respectively (O'Neill et al., 2016; Oin et al. 2021), are compared. The former assumes the current rate of global warming to be maintained until 2100 (i.e., regional rivalry scenario), while the latter assumes net-zero carbon emissions by the 2050s (i.e., carbon neutrality scenario) (Figure 1). All variables of interest are computed at each land grid point

and then intercompared across six continents, i.e., North America, South America, Europe, Africa, Asia, and Oceania (Figure S1; Iturbide et al., 2020).

2.2. Climate extremes based on GEV analysis

This study uses the annual maximum of daily maximum temperature (TXx) and annual maximum daily precipitation (RX1day) as indices of hot temperature and heavy precipitation extremes, respectively, following the Expert Team on Climate Change Detection and Indices (ETCCDI; Zhang et al. 2011). To estimate the rare events occurring once in 10, 30, or 50 years, we first fit TXx and RX1day at every grid point of each model's native resolution to the generalized extreme value (GEV, Kharin et al., 2013) distribution during the historical (1985–2014) and future (2071–2100) periods. The GEV estimation for 30-year time window is based on the assumption that temperature or precipitation extremes remain approximately stationary within 30-year period (Kim et al., 2020; Li et al., 2021).

The cumulative density function (CDF) of the GEV distribution for variable x is defined as follows:

$$F(x;\mu,\sigma,\xi) = \begin{cases} exp\left[-exp\left\{-\frac{x-\mu}{\sigma}\right\}\right] & \text{for } \xi = 0 \\ exp\left[-\left\{1+\xi\frac{x-\mu}{\sigma}\right\}^{-\xi^{-1}}\right] & \text{for } \xi \neq 0 \text{ and } \xi\frac{x-\mu}{\sigma} > -1 \end{cases} \quad (1)$$

where μ, σ, and ξ represent the location, scale, and shape parameters, respectively. The GEV parameters are estimated using the L-moments method (Hosking, 1990), which has been used for the small sample size (Hosking, 1990; Kim et al., 2020). The quantile function of GEV (X)

is derived by inverting a CDF for a given probability p as below.

$$X_p = \begin{cases} \mu - \sigma \ \ln[-\ln(p)] \ \text{ for } \ \ \xi = 0 \\ \mu - \frac{\sigma}{\xi}\ln\left[1 - (-\ln(p))^{-\xi}\right] \ \text{ for } \ \xi \neq 0. \end{cases} \quad (2)$$

The 10-, 30-, and 50-year return values for the historical and future periods are calculated when p=0.90, 0.967, and 0.98 (as the exceedance of the annual extreme with probability = 10%, 3.3%, and 2%), respectively. In this study, we mainly focus on the return values of 30-year, which is the most realistic but large enough period that can be obtained from the current reanalysis dataset (see supporting information). After the GEV estimation, climate extreme indices are interpolated to a common 1°×1° grid using a bilinear remapping, and then multi-model ensemble statistics are computed. This procedure allows to minimize the discrepancy arising from different data resolutions (Kim et al., 2020; Li et al., 2021). Further details on the model evaluation and projection for the historical and future climate extremes can be found in the supporting information.

2.3. Population exposure

Population exposure is one of the key indicators of the impact of climate extremes on human societies (e.g., Jones et al., 2018; Chen & Sun, 2021). It is closely intertwined with climate risk, as the impacts of climate change are felt most acutely by vulnerable populations (e.g., Jones et al., 2018; Chen & Sun, 2021). Population exposure represents the accumulative number of people exposed to climate extremes (unit: person-days), and is computed by multiplying the population count of an area by the number of climate extremes that occur there.

In this study, the 10-, 30-, and 50-year return values of TXx and RX1day, estimated from the historical period of 1985–2014 (Figures S2b and 2e), are used as the threshold values to identify the hot-temperature and heavy-precipitation extremes. The number of climate extreme events at each native model grid is counted as the number of extreme days exceeding the threshold values in each year for the period of 1985–2100. After interpolating the result into a common 1°×1° grid, the historical population exposure is defined as the integrated product of the number of climate extremes from 1985 to 2014 and the historical population count in 2010 (Figure S3a; Jones & O'Neill, 2016). For the future population exposure, the future population counts in 2020, 2030, …, 2090, and 2100 under SSP1 and SSP3 scenarios (Figures S3b–3h; Jones & O'Neill, 2016) are used to match the SSP1-1.9 and SSP3-7.0 scenarios. For example, the population counts in 2020 and 2030 are used to calculate the population exposure for the period of 2020–2029 and 2030–2039, respectively.

2.4. Reduction rate of population exposure and its contributing factor

To quantify the benefit of carbon neutrality, the reduction rate (%, Jones et al., 2018; Zhang et al., 2018; Lei et al., 2022) of population exposure to climate extremes by achieving the carbon neutrality is calculated as follows:

$$\text{Reduction rate (\%)} = \frac{\Delta SSP_{370} - \Delta SSP_{119}}{\Delta SSP_{370}} \times 100 \quad (3)$$

where △ stands for the difference of the aggregated population exposure between the future (2071–2100) and historical (1985–2014) periods. Here, the changes in population exposure can

be attributed to the three factors, i.e., climate extreme, population, and climate extreme-population interaction factors (e.g., Jones et al., 2018; Lei et al., 2022; Zhang et al., 2022) as below:

$$\Delta SSP_{370} = P_{hist} \times \Delta C_{370} + C_{hist} \times \Delta P_{370} + \Delta C_{370} \times \Delta P_{370}$$

$$\Delta SSP_{119} = P_{hist} \times \Delta C_{119} + C_{hist} \times \Delta P_{119} + \Delta C_{119} \times \Delta P_{119} \quad (4)$$

where P and C are the population and the number of extreme days, respectively. The terms ΔP and ΔC are the changes in the population and number of extreme days in the future period with respect to the historical period, respectively. Subscripts of C and P denote the historical climate or SSP scenario. Therefore, the three terms on the right side of Eqn. (4) represent the roles of climate extreme (CLM), population (POP), and their interaction (INT) changes, respectively. By combining Eqns. (3–4), the reduction rate can be decomposed as follows:

$$\text{Reduction rate (\%)} = \frac{CLM_{370} - CLM_{119}}{\Delta SSP_{370}} \times 100 + \frac{POP_{370} - POP_{119}}{\Delta SSP_{370}} \times 100 + \frac{INT_{370} - INT_{119}}{\Delta SSP_{370}} \times 100 \quad (5)$$

The first term represents the contribution of climate extreme changes to the total reduction rate (%) of population exposure to climate extremes. Similarly, the second and third terms represent the contribution of population and climate extreme-population interaction changes, respectively, to the total reduction rate (%).

3. Results

3.1. Global population exposure to climate extremes

Figure 2 presents the time series of global population exposure to hot-temperature and

heavy-precipitation extremes for the period of 2015–2100 under the SSP1-1.9 and SSP3-7.0 scenarios compared to the historical period of 1985–2014. If global warming keeps continuing without a transition to the carbon-neutral society in the 2050s, the population exposures to hot-temperature and heavy-precipitation extremes that exceed the historical 30-year return values (Figures S2b and S2e) are anticipated to increase up to 192 billion and 1.87 billion person-days, respectively, at the end of the century (red lines in Figures 2a and 2b). Given the fact that population exposures in the historical period are 0.21 billion and 0.17 billion person-days, respectively, they are approximately 914 and 11 times larger than the historical values. The increasing trends are particularly noticeable after the 2050s. The inter-model spread does not cross the zero line after the year 2043 for hot-temperature extremes and the year 2067 for heavy-precipitation extremes. This indicates that increasing population exposures to climate extremes under the high-emission scenario are distinct in the late 21st century compared to the historical period. The same trends are also found when population is fixed to the historical level (orange lines in Figures 2a and 2b). However, they are only half of that with time-varying population (compare red and orange lines). This suggests that population changes and climate-population interaction changes are also important in determining population exposure to climate extremes in the high-emission scenario.

The transition to the carbon-neutral society in the 2050s results in a minimal shift in population exposure to climate extremes, accompanied by reduced model spread which indicates the robust multi-model projections (blue lines and shading in Figures 2c and 2d). The population exposure in the carbon neutrality scenario is less than one-tenth of that in the high-

emission scenario (compare Figures 2a,b and 2c,d; note the different scale of the *y*-axis between the two scenarios). The population exposures to hot-temperature and heavy-precipitation extremes slightly increase by approximately 4.65 billion and 0.19 billion person-days (approximately 22 and 1.12 times larger than the historical values), respectively, until the middle of the 21st century, then decrease afterward. However, these changes have a large uncertainty, with a model spread often crossing the zero line, revealing that future population exposures to climate extremes are indistinguishable from historical ones if the carbon neutrality is successfully achieved.

The reduced population exposures to hot-temperature and heavy-precipitation extremes by achieving the carbon neutrality are 187 billion and 1.68 billion person-days in the year 2100, respectively (Figures 2e and 2f). These correspond 90 and 98% reductions for heavy-precipitation and hot-temperature extremes, respectively, from the high-emission scenario (purple lines in Figures 2e and 2f). Inter-model spread does not cross the zero line in the late 21st century for both climate extremes. This result highlights the importance of carbon neutrality in mitigating climate change risks.

3.2. Regional population exposure to climate extremes

The increasing population exposure to climate extremes under the high-emission scenario is more pronounced in densely populated areas. Some land regions, where population is dense (Figure S3a), are expected to have an increasing population exposure to hot-temperature extremes by ten million person-days or more in 2071–2100 (Figure 3a). The people

238 in those regions are anticipated to experience more intense hot-temperature events, over 4 °C
239 hotter than the historical events (upper panel of Figure S4a). In particular, people living in
240 South America, Africa, Arabian Peninsula, and South Asia would be more frequently exposed
241 to heat-related extremes, more than 20 days per year, compared to those living in other regions
242 (bottom row of Figure S4a). For heavy-precipitation extremes, a large population exposure,
243 greater than one million person-days, is projected to occur only in African and Asia monsoon
244 regions (Figure 3b). It is expected that African and Asian people would experience more intense
245 (over 40 mm/day) and frequent (over 0.5–1.0 days per year) heavy-precipitation extremes
246 under the high-emission scenario (Figure S5a).

247 While the global population exposure to climate extremes may increase only
248 marginally under the carbon-neutral scenario, the regional changes remain noteworthy. The
249 large population exposure to hot-temperature extremes, greater than one million person-days,
250 is still found in the late 21st century in African and Asian monsoon regions as well as
251 Mediterranean and western Europe (Figure 3c). It contrasts to the population exposure to
252 heavy-precipitation extremes which is less than one-tenth million person-days in most regions
253 (Figure 3d). This result suggests that even if carbon neutrality is achieved, some regions could
254 be exposed to higher heat-related climate risks than the historical level. However, carbon
255 neutrality can still significantly reduce the number of people, exceeding ten million in each
256 region, who may potentially be exposed to climate extremes under the high-emission scenario
257 (Figures 3e and 3f).

258 To quantify the regional changes in the late 21st century, the area-aggregated total

population exposures to hot-temperature and heavy-precipitation extremes are calculated in Figures 4a and 4b. Globally, an increasing population exposure to hot-temperature extremes is projected to continue under the high-emission scenario, by approximately 106 billion person-days (the first bar in Figure 4a). This value is approximately 461 times higher than the historical value of 0.23 billion person-days. If carbon neutrality is achieved, only 2.50 billion person-days are expected to increase, with the population exposure to hot-temperature extremes being substantially reduced. Although much smaller than hot-temperature extremes, the globally-aggregated population exposure to heavy-precipitation extremes is also expected to increase up to 1.43 billion person-days in the high-emission scenario (approximately 7 times higher than 0.20 billion person-days in the historical period; see the leftmost bar in Figure 4b). If carbon neutrality is achieved, only 0.17 billion person-days are expected to increase, with the population exposure to heavy-precipitation extremes again being substantially reduced.

Such reductions are largest in African and Asian continents (AF and AS in Figures 4a and 4b). If the current "regional rivalry" for the carbon emissions policy is maintained, African and Asian continents would have the highest or second-highest population exposures to both hot-temperature and heavy-precipitation extremes in the late 21st century (Figures 4a and 4b). Their sum accounts for 79% of global population exposure to hot-temperature extremes and 88% of global population exposure to heavy-precipitation extremes. Here, it is important to note that African continent would become the region most suffering from increasing climate extremes despite its relatively low carbon emissions (Mann, 2023). It exemplifies an inequality of climate risk.

3.3. Benefits of carbon neutrality and its contributing factors

The impact of carbon neutrality is further examined by calculating the reduction rate of population exposure to climate extremes (Eq. 3; Figures 4c and 4d). The global reduction rates for hot-temperature and heavy-precipitation extremes in the late 21st century reach up to 98% and 87%, respectively (first gray bars in Figures 4c and 4d). The reduction rate for hot-temperature extremes is similar across all continents, ranging from 93 to 99% (Figure 4c). However, the reduction rate for heavy-precipitation extremes varies considerably from one continent to another, ranging from 20 to 91%, with the largest reduction in Africa, Asia, and South America (Figure 4d; see also Figure S7). This result suggests that the carbon neutrality can reduce the inequality of climate risk across continents.

The relative contributions of climate extreme, population, and their interaction changes on the reduction rate (Eq. 5) are further evaluated in Figures 4c and 4d. The climate extreme change itself explains about half of the global reduction rate (first red bars in Figures 4c and 4d). The contribution of population change is negligible (first yellow bars), while that of interaction change is comparable to climate extreme change (first blue bars). The latter is due to the enormous changes in Africa which is associated with significant future increases in both population and the number of extreme days across all regions of Africa (Figures S3f and S12; see also bottom panel of Figures S4 and S5). It suggests a synergistic effect between climate extreme and population changes in the African continent. Asia is also expected to experience significant increase in population and the number of extreme days (Figure S3g; see also bottom

301 panel of Figures S4 and S5). However, unlike Africa, interaction change contributes less than
302 climate extreme change (AS blue bars in Figures 4c and 4d). Given that climate extreme change
303 is positive across all regions of Asia (bottom panels of Figures S4 and S5), it results from the
304 opposing population trends from one country to another, i.e., an increasing trend in India but a
305 decreasing trend in China (Figure S12). Although South America also shows comparable
306 contributions of climate extreme and interaction changes (SA in Figures 4c and 4d), their
307 absolute values are much smaller than those in Africa and Asia (SA in Figures 4a and 4b).

308 In North America, Europe, and Oceania, the contribution of climate extreme change
309 surpasses that of the interaction change by more than twofold (compare red and blue color bars
310 of NA, EU, and OC in Figures 4c and 4d), because of rather slow and small population growth
311 under the high-emission scenario (Figures S3c, S3e, and S3h; see also Figure S13). In particular,
312 for heavy precipitation extremes, the climate extreme changes dominate the reduction rates in
313 these continents with even negative contributions of the population and interaction changes
314 (Figure 4d). It indicates that climate extreme change plays a predominant role in reducing the
315 population exposure to climate extremes in these continents. This result also suggests that the
316 potential benefits of carbon neutrality can be significant even in developed countries by
317 reducing the occurrence of climate extremes.

318

319 **3.4. Sensitivity to return intervals of climate extremes**

320 More intense climate extremes, that substantially deviate from their climatologies, can
321 result in more significant social damages, particularly when they are beyond the tolerable

ranges of ecological systems and human infrastructures. In this regard, the sensitivity of the reduction rate shown in Figures 4c and 4d to the return intervals of climate extremes is tested. The 10-, 30-, and 50-year return events are particularly considered (Figure 5). Note that all analyses in previous sections are conducted with 30-year return events and repeated here as references. The reduction rate increases for longer return events for hot-temperature extremes (Figure 5a), indicating an increasing benefit of carbon neutrality for more intense hot-temperature extremes. A small inter-model spread for longer return events further indicates that this benefit is robust across all continents (Figure 5a).

In contrast, the reduction rate for heavy-precipitation extremes does not systematically increase for longer return events (black lines in Figure 5b). The inter-model spread is also large, indicating that the risk of heavy-precipitation extremes has a relatively high uncertainty compared to hot-temperature extremes, presumably due to their localized and complex nature. In particular, North America, Europe, and Oceania show a relatively larger inter-model spread because of different climate sensitivity of individual models to the forcing. In these continents, climate extreme change is much more important than the other two factors, with increasing return intervals (Figure S8). Other continents, such as South America, Africa, and Asia, where the population exposure to heavy-precipitation extremes is high, show a relatively small inter-model spread, suggesting a relatively higher model consistency.

4. Discussion and conclusions

The present study evaluates the impact of carbon neutrality on population exposure to

343 climate extremes in the late 21st century. If the current “regional rivalry” over the carbon
344 emissions policy is maintained in this century, population exposures to hot-temperature and
345 heavy-precipitation extremes, exceeding their historical 30-year return values, are projected to
346 increase by 461 and 7 times, respectively, over the historical values. Such drastic increases can
347 be significantly reduced by 87–98% by achieving the carbon neutrality. This result supports
348 the critical importance of ongoing efforts to achieve net-zero carbon emissions by the 2050s to
349 reduce potential climate risks and their inequity across continents.

350 The reduction in population exposure to climate extremes through carbon neutrality is
351 greatest in Africa and Asia. However, as most countries in these continents are currently
352 developing (Figure S6), conflicts between carbon neutrality and economic development may
353 arise. Such conflicts may increase the uncertainty in future projection of population exposure
354 to climate extremes (e.g., Liu et al., 2017; Chen & Suh, 2021; Lei et al., 2022). Another point
355 of note is the contrasting population trends projected for Asian countries, i.e., an increasing
356 trend in India but a decreasing trend in China (Figure S12). This calls for further investigation
357 into the potential benefits of carbon neutrality for individual countries (e.g., Das et al., 2022;
358 Xie et al., 2022). In North America, Europe, and Oceania, reducing climate extremes by
359 achieving carbon neutrality plays a more important role than population decline in reducing
360 population exposure to climate extremes. This indicates that the potential benefits of carbon
361 neutrality can be substantial even in developed countries. It becomes more apparent when
362 considering more intense hot-temperature extremes, for which the reduction rates are much
363 larger with a better agreement between the models (i.e., smaller inter-model spread).

The findings of the present study do not hold only for extremely rare events. Other extreme indices of temperature and precipitation (Zhang et al. 2011) consistently show the net benefits of carbon neutrality (Figures S9–S11). Among others, the number of consecutive dry days, representing drought, in South America and Africa is projected to decrease considerably from the high-emission to carbon-neutrality scenarios (Figures S10o and S10p). This result is consistent with Park et al. (2018), who reported that limiting global warming to 1.5°C constrains the emergence of aridification.

The year of net-zero carbon emissions in the SSP1-1.9 scenario is decades earlier than in other mitigation scenarios (e.g., SSP1-2.6), resulting in weaker warming in the late 21st century (Meinshausen et al., 2020). By conducting the sensitivity experiments for a net-zero carbon emission year by 2050 and 2060, Lei et al. (2022) reported that more active carbon neutrality policy could further reduce the population exposure to heat extremes. The present study supports the need for more active net-zero carbon emissions policy by the 2050s.

It should be recalled that this study is based on concentration-driven simulations from the CMIP6 project (Quilcaille et al., 2023). The concentration-driven simulations often exaggerate future climate changes compared to the emission-driven simulations (Nicholls et al., 2021; Quilcaille et al., 2023). In this regard, the emissions-driven simulations may be more useful for investigating the merits of the Paris Agreement's goals (Terhaar et al., 2022).

While this study has addressed the impact of carbon neutrality on climate extremes and population exposure, it is still important to explore the importance of vulnerability which serves as a critical determinant in assessing the extent to which communities and ecosystems

fare in a warming climate (Cardona et al., 2012; Jones et al., 2018). Because vulnerability depends on regional location, social and economic development, and the nature of climate extremes (e.g., Cardona et al., 2012; Jones et al., 2018), assessing the impact of carbon neutrality on vulnerability may be useful in developing and implementing equitable and sustainable climate risk mitigation strategies.

Acknowledgements

This research was supported by Basic Science Research Program through the National Research Foundation of Korea (NRF) funded by the Ministry of Education (RS-2023-00238065). This research was also supported by the Research Program for the carbon cycle between oceans, land, and atmosphere of the NRF funded by the Ministry of Science and ICT (2021M3I6A1086807), and Korea Environment Industry & Technology Institute (KEITI) through Project for developing an observation-based GHG emissions geospatial information map, funded by Korea Ministry of Environment (MOE) (RS-2023-00232066). All authors thank every group involved in Coupled Model Intercomparison Project Phase 6 (CMIP6) model output data provided by World Climate Research Programme (WCRP) CMIP6 Community. We also thank Jones & O'Neill and Iturbide & co-authors for sharing their dataset and providing guidance. Special thanks for two anonymous reviewers for their relevant contribution in the different processes of the revisions of this work.

Conflict of Interest

The authors declare no conflicts of interest relevant to this study.

Open Research

The data of eight global climate models from the Coupled Model Intercomparison Project Phase 6 (CMIP6) can be accessed at https://esgf-node.llnl.gov/search/cmip6/, and can also be accessed in Eyring et al. (2016). The projected gridded population dataset under Shared Socioeconomic Pathway 1 (SSP1) and SSP3 scenarios can be obtained in Jones and O'Neill (2016) or via http://sedac.ciesin.columbia.edu/data/set/popdynamics-1-8th-pop-base-year-projection-ssp-2000-2100-rev01/data-download. The mask dataset for the six continents in this study is available in Iturbide et al. (2020). The above raw data were post-processed using Fortran90 (https://www.intel.com/content/www/us/en/developer/articles/tool/oneapi-standalone-components.html#fortran), R version 4.0.3 (https://cran.r-project.org/bin/windows/base/old/4.0.3/), Grads version 2.2.1 (http://cola.gmu.edu/grads/downloads.php). The relevant post-processed dataset and analysis codes for Figures 1 to 5 in the main text are available at https://zenodo.org/records/10408749

Author contributions

All authors contributed to the study conception and design. Material preparation, data collection and analysis were performed by S.-G. Oh under supervision of S.-W. Son. The first draft of the manuscript was written by S.-G. Oh, J. Choi, M.-J. Kang, S. Jeong, S.-K. Min, S.-W. Yeh, Y.-H. Kim, and S.-W. Son and all authors commented on previous versions of the

manuscript. All authors read and approved the final manuscript.

Additional information

The methods and results of the model evaluation for the historical period of 1985–2014 are presented in the Supporting Information. The future changes in intensity and frequency of climate extremes under the SSP1-1.9 and SSP3-7.0 scenarios are also discussed in the Supporting Information.

References

Cardona, O. D., van Aalst, M. K., Birkmann, J., Fordham, M., McGregor, G., & Perez, R., et al. (2012). in Determinants of risk: exposure and vulnerability (eds Field, C. B. et al.) *Managing the Risks of Extreme Events and Disasters to Advance Climate Change Adaptation*. pp. 65–108 (Cambridge University Press, Cambridge, UK, and New York, NY, USA, 2012). A Special Report of Working Groups I and II of the Intergovernmental Panel on Climate Change (IPCC).

Chen, H., & Sun, J. (2021). Significant increase of the global population exposure to increased precipitation extremes in the future. *Earth's Future*, *9(9)*, e2020EF001941.

Das, J., Manikanta, V., & Umamahesh, N. V. (2022). Population exposure to compound extreme events in India under different emission and population scenarios. *Science of The Total Environment*, *806*, 150424.

Eyring, V., Bony, S., Meehl, G. A., Senior C. A., Stevens, B., Stouffer, R. J., & Taylor K. E.

448 (2016). Overview of the coupled model intercomparison project phase 6 (CMIP6)
449 experimental design and organization [Dataset]. *Geoscientific Model Development*, *9*,
450 1937–1958.

451 Gidden, M. J., Riahi, K., Smith, S. J., Fujimori, S., Luderer, G., & Kriegler, E. et al. (2018).
452 Global emissions pathways under different socioeconomic scenarios for use in CMIP6:
453 a dataset of harmonized emissions trajectories through the end of the century. *Geosci.*
454 *Model Dev. Discuss.*, https://doi.org/10.5194/gmd-2018-266

455 Hosking, J. R. M. (1990). L-moments: analysis and estimation of distributions using linear
456 combinations of order statistics. *Journal of the Royal Statistical Society*, *522*, 105–124.

457 Iturbide, M., Gutierrez, J. M., Alves, L. M., Bedia, J., Cerezo-Mota, R., & Cimadevilla E., et
458 al. (2020). An update of IPCC climate reference regions for subcontinental analysis of
459 climate model data: definition and aggregated datasets [Dataset]. *Earth System Science*
460 *Data*, *12*, 2959–2970.

461 Jo, S. Y., Seong, M. G., Min, S. K., Kug, J. S., Yeh, S. W., & An, S. I., et al. (2022). Hysteresis
462 behaviors in East Asian extreme precipitation frequency to CO2 pathway. *Geophysical*
463 *Research Letters*, *49*, e2022GL099814.

464 Jones, B., & O'Neill B. C. (2016). Spatially explicit global population scenarios consistent with
465 the shared socioeconomic pathways [Dataset]. *Environmental Research Letters*, *11*,
466 084003.

467 Jones, B., Tebaldi, C., O'Neill B. C., Oleson, K., & Gao J. (2018). Avoiding population

468 exposure to heat-related extremes: demographic change vs climate change. *Climatic*
469 *Change*, *146*, 423–472.

470 Kharin, V. V., Zwiers, F. W., Zhang, X., & Wehner, M. (2013). Changes in temperature and
471 precipitation extremes in the CMIP5 ensemble. *Climatic Change*, *119*, 345–357.

472 Kim, S. K., Shin, J., An, S. I., Kim, H. J., Im, N., & Xie, S. P., et al. (2022). Widespread
473 irreversible changes in surface temperature and precipitation in response to CO2 forcing.
474 *Nature Climate Change*, *12*, 834–840.

475 Kim, Y. H., Min, S. K., Zhang, X., Sillmann, J., & Sandstad, M. (2020). Evaluation of the
476 CMIP6 multi-model ensemble for climate extreme indices. *Weather and Climate*
477 *Extremes*, *29*, 100269.

478 King, A. D., Borowiak, A., Brown, J. R., Frame, D. J., Harrington, L. J., & Min, S. K., et al.
479 (2021). Transient and quasi-equilibrium climate states at 1.5°C and 2°C global warming.
480 *Earth's Future*, *9*, https://doi.org/10.1029/2021EF002274

481 Lei, Y., Wang, Z., Zhang, X., Che, H., Yue, X., & Tian, C., et al. (2022). Avoided population
482 exposure to extreme heat under two scenarios of global carbon neutrality by 2050 and
483 2060. *Environmental Research Letters*, *17*, 094041.

484 Li, C., Zwiers, F., Zhang, X., Li, G., Sun, Y., & Wehner, M. (2021). Changes in annual extremes
485 of daily temperature and precipitation in CMIP6 model. *Journal of Climate*, *34*, 3441–
486 3460.

487 Liu, Z., Anderson, B., Yan, K., Dong, W., Liao, H., & Shi, P. (2017). Global and regional

changes in exposure to extreme heat and the relative contributions of climate and population change. *Scientific Reports*, *7*(1), 43909.

Mann, M. E. (2023, October 24). G*reenhouse gas*. *Encyclopedia Britannica*. https://www.britannica.com/science/greenhouse-gas

Meinshausen, M., Nicholls, Z. R., Lewis, J., Gidden, M. J., Vogel, E., Freund, M., ... & Wang, R. H. (2020). The shared socio-economic pathway (SSP) greenhouse gas concentrations and their extensions to 2500. *Geoscientific Model Development*, *13*(8), 3571-3605.

Nashwan, M. S., & Shahid, S. (2022). Future precipitation changes in Egypt under the 1.5 and 2.0°C global warming goals using CMIP6 multimodel ensemble. *Atmospheric Research*, *265*, 105908.

Nicholls, Z., Meinshausen, M., Lewis, J., Corradi, M. R., Dorheim, K., Gasser, T., ... & Woodard, D. L. (2021). Reduced complexity Model Intercomparison Project Phase 2: Synthesizing Earth system knowledge for probabilistic climate projections. *Earth's Future*, *9*(6), e2020EF001900.

Oin, J., Su, B., Tao, H., Wang, Y., Huang, J., & Jiang T. (2021). Projection of temperature and precipitation under SSPs-RCPs scenarios over northwest China. *Frontiers of Earth Science*, *15(1)*, 23–37.

O'Neill, B. C., Tebaldi, C., van Vuuren, D. P., Eyring, V., Friedlingstein, P., & Hurtt, G., et al. (2016). The scenario model intercomparison project (ScenarioMIP) for CMIP6. *Geoscientific Model Development*, *9*, 3461–3482.

508 Park, C. E., Jeong, S. J., Joshi, M., Osborn, T. J., Ho, C. H., & Piao, S., et al. (2018). Keeping
509 global warming within 1.5°C constrains emergence of aridification. *Nature Climate*
510 *Change*, *8*, 70–74.

511 Quilcaille, Y., Gasser, T., Ciais, P., & Boucher, O. (2023). CMIP6 simulations with the compact
512 Earth system model OSCAR v3. 1. *Geoscientific Model Development*, *16*(3), 1129–
513 1161.

514 Terhaar, J., Frölicher, T. L., Aschwanden, M. T., Friedlingstein, P., & Joos, F. (2022). Adaptive
515 emission reduction approach to reach any global warming target. *Nature climate*
516 *change*, *12*(12), 1136–1142.

517 UNFCCC (2015). Conference of the Parties. Adoption of the Paris Agreement.
518 FCCC/CP/2015/10/Add.1, pp. 1–32, Paris.

519 Xie, W., Zhou, B., Han, Z., & Xu Y. (2022). Substantial increase in daytime-nighttime
520 compound heat waves and associated population exposure in China projected by the
521 CMIP6 multimodel ensemble. *Environmental Research Letters*, *17*, 045007.

522 Zhang, G., Wang, H., Gan, Y. Y., Zhang, S., Shi, L., & Zhao, J., et al. (2022). Climate change
523 determines future population exposure to summertime compound dry and hot events.
524 *Earth's Future*, *10(11)*, e2022EF003015.

525 Zhang, W., Zhou, T., Zou, L., Zhang, L., & Chen, X. (2018). Reduced exposure to extreme
526 precipitation from 0.5°C less warming in global land monsoon regions. *Nature*
527 *Communications*, *9*, 3153.

528 Zhang, X., Alexander, L., Hegerl, G. C., Jones, P., Tank, A. K., & Peterson, T. C. (2011) Indices
529 for monitoring changes in extremes based on daily temperature and precipitation data.
530 *WIREs Climate Chang*, *2*, 851–870.

531

532

533

534

535

536

537

538

539

540

541

542

543

544

545

546

547

548

549 **Table 1.** CMIP6 models used in this study.

No.	Model	Ensemble information	Institution	Horizontal Resolution (Lon x Lat)
1	CanESM5	r1i1p1f1	Canadian Earth System Model version 5, Canadian Centre for Climate Modelling and Analysis (Canada)	128 x 64
2	CNRM-ESM2-1	r1i1p1f2	National Center for Meteorological Research (France)	256 x 128
3	EC-Earth3	r4i1p1f1	ICHEC, The Irish Centre for High-End Computing, National University of Ireland (Ireland)	512 x 256
4	GFDL-ESM4	r1i1p1f1	NOAA/Geophysical Fluid Dynamics Laboratory, Earth System Model version 4 (USA)	288 x 180
5	MIROC-ES2L	r1i1p1f2	Atmosphere and Ocean Research Institute (The University of Tokyo), National Institute for Environmental Studies, and Japan Agency for Marine-Earth Science and Technology (Japan)	128 x 64
6	MPI-ESM-LR	r1i1p1f1	Max Planck Institute for Meteorology (Germany)	192 x 96
7	MRI-ESM2-0	r1i1p1f1	Meteorological Research Institute (Japan)	320 x 160
8	UKESM1-0-LL	r1i1p1f2	Met Office Hadley Centre (UK)	192 x 144

550

551

552

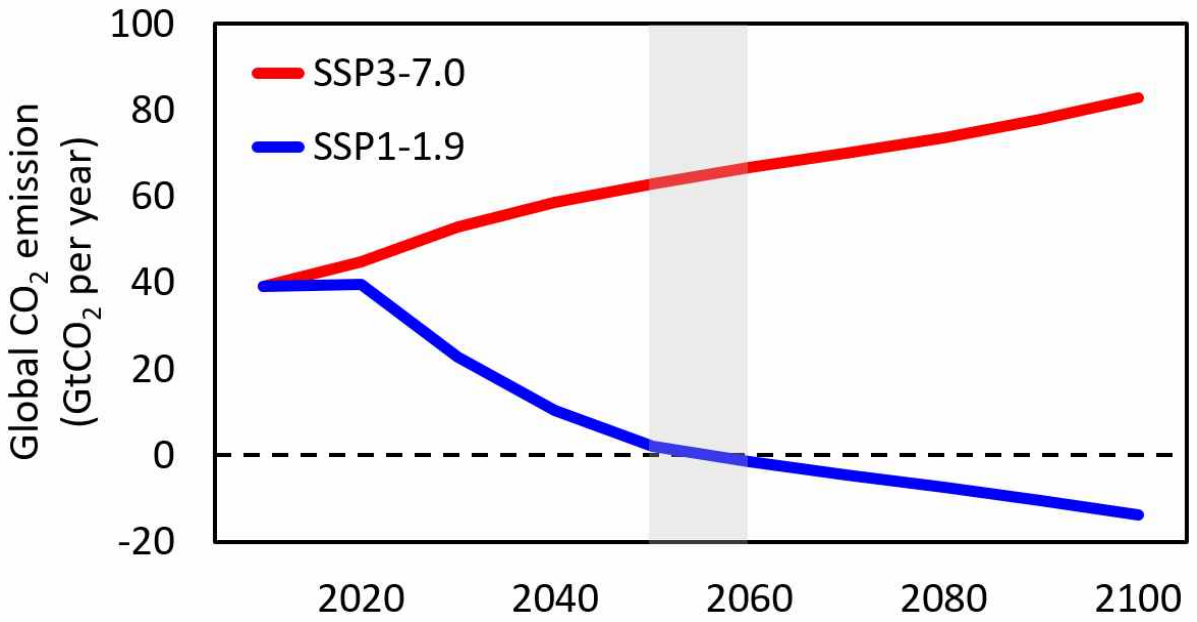

Figure 1. Time series of global CO_2 emissions in SSP1-1.9 and SSP3-7.0 scenarios. The vertical gray shading indicates the 2050s when net-zero emissions are achieved in the SSP1-1.9 scenario.

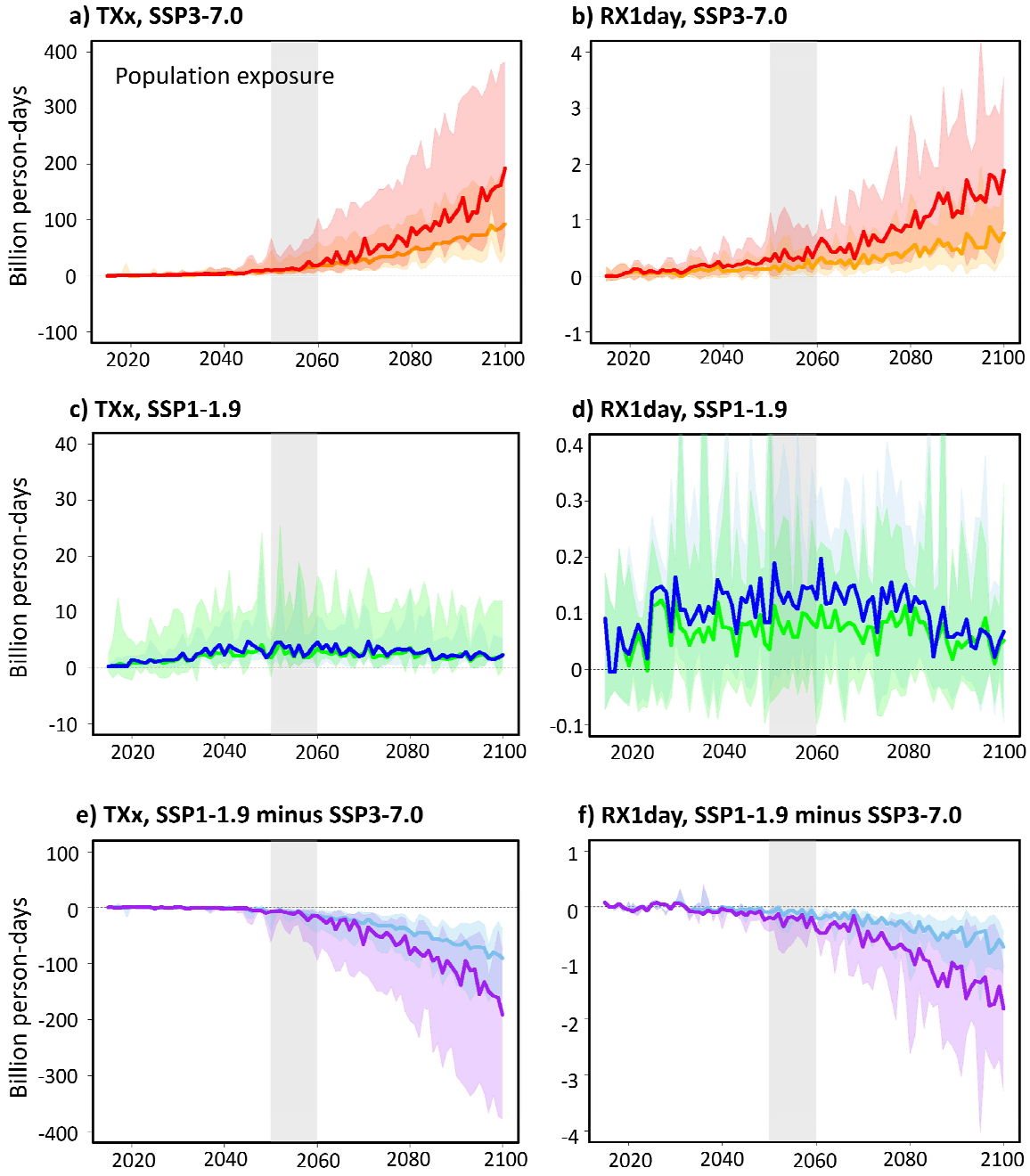

Figure 2. Temporal evolution of global population exposure to climate extremes. Time series of global population exposure (unit: person-days) to 30-year return events of (a) hot-temperature (TXx) and (b) heavy-precipitation (RX1day) for the period of 2015–2100. Blue

and red lines indicate the CMIP6 multi-model ensemble median with population change under SSP1-1.9 and SSP3-7.0 scenarios against the historical period of 1985–2014. Green and orange lines are the same as blue and red ones but with a fixed population to the historical period. Purple and sky-blue lines in the bottom row are the differences between SSP1-1.9 and SSP3-7.0 scenarios with time-varying and time-fixed populations, respectively. Shadings indicates the inter-model spread defined by the full range (min-max) for each scenario. The vertical gray shading denotes the 2050s when net-zero CO2 emissions occur in Fig. 1. Note that the range of the y-axis in SSP1-1.9 scenario is only one-tenth of that in SSP3-7.0 scenario.

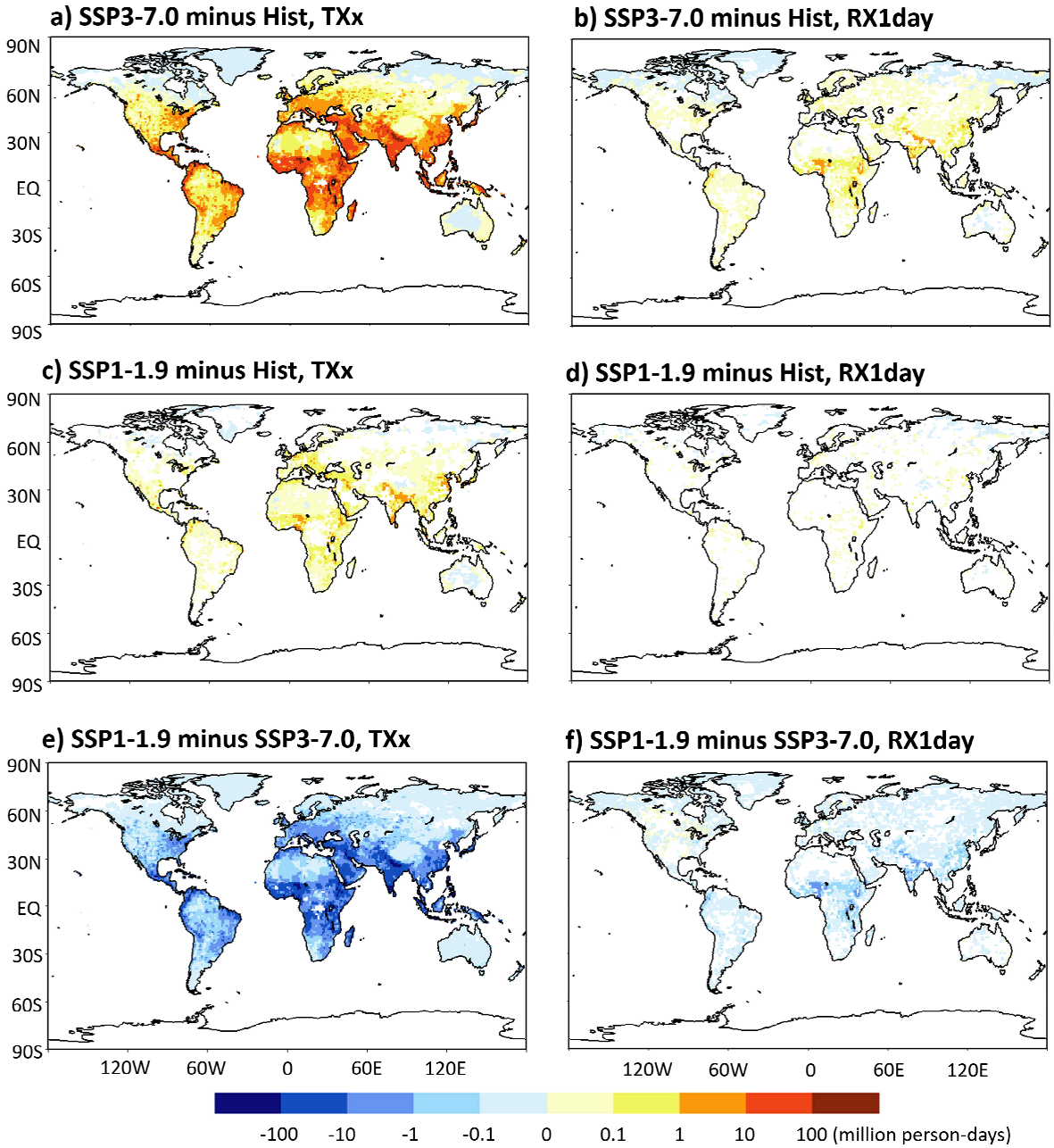

573

574 **Figure 3.** Projected changes of 30-year mean population exposure to climate extremes in the
575 late 21st century (2071–2100) compared to the historical period of 1985–2014. Changes of the
576 population exposure (unit: person-days) to 30-year return events of hot-temperature extreme

(TXx) under (a) SSP3-7.0 and (c) SSP1-1.9 scenarios and (e) their differences. Only grids where more than three-quarters of the models show the same sign to the multi-model ensemble median are presented. (b, d, f) Same as (a, c, e), but for heavy-precipitation extreme (RX1day).

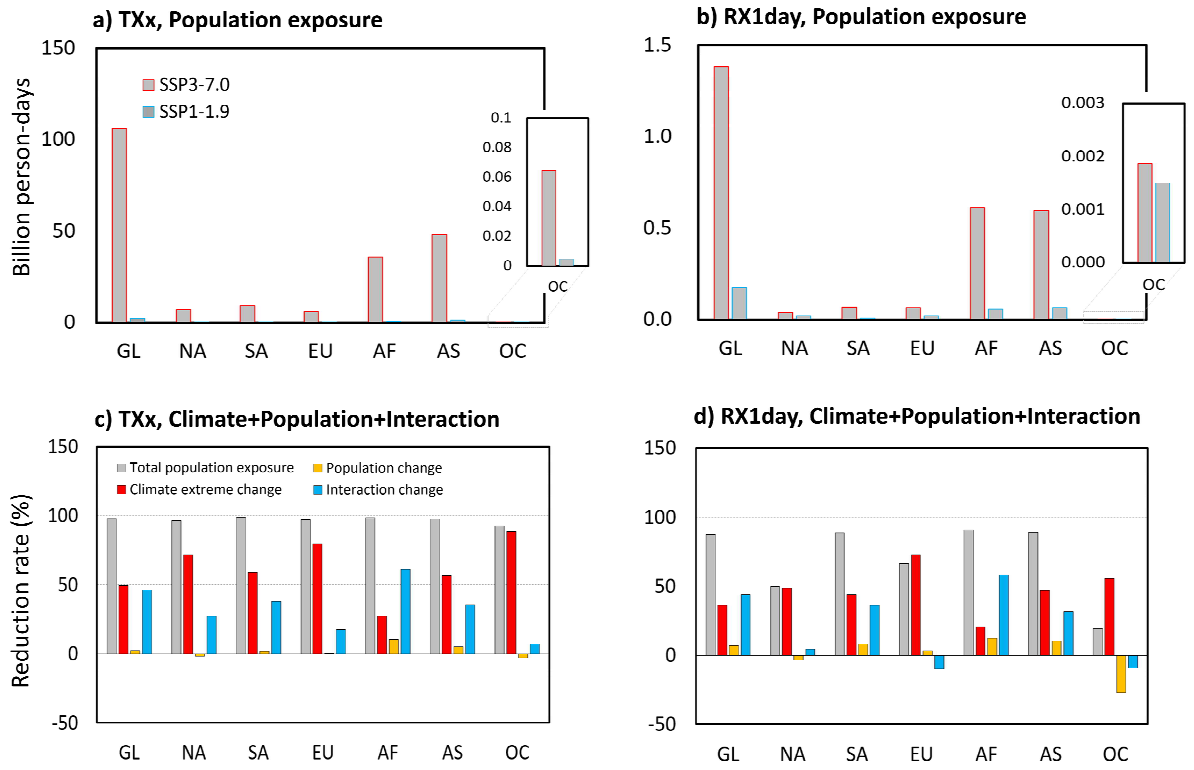

594

595 **Figure 4.** Changes of 30-year mean regionally-aggregated population exposures to climate
596 extremes in the late 21st century (2071–2100) compared to the historical (1985–2014) values,
597 and their reduction rate from SSP3-7.0 to SSP1-1.9 scenarios. (a) Area-aggregated population
598 exposure to 30-year return events of TXx over the globe (GL), North America (NA), South
599 America (SA), Europe (EU), Africa (AF), Asia (AS), and Oceania (OC). Red and blue outlined
600 bars indicate the SSP3-7.0 and SSP1-1.9 scenarios, respectively. (c) The reduction rate (%) of
601 population exposure to TXx from SSP3-7.0 scenario to SSP1-1.9 scenarios (gray), and the
602 relative contributions of climate (red), population (yellow), and climate-population interaction
603 (blue) changes. (b, d) Same as (a, c) but for RX1day. Note that the range of the y-axis is
604 different in (a) and (b).

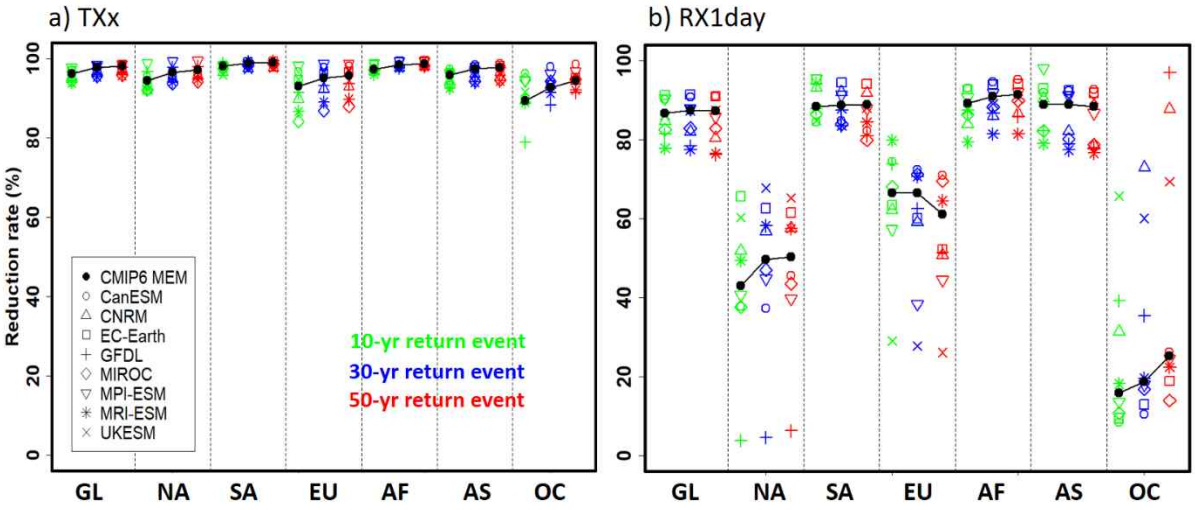

Figure 5. Regionally-aggregated reduction rate of population exposures to climate extremes for varying return periods. Area-averaged reduction rate (%) of population exposure to (a) TXx and (b) RX1day is shown for 10-year (green), 30-year (blue), and 50-year (red) return events. The periods of 1985–2014 and 2071–2100 are used as in Figs. 3c and d. Closed circles denote the CMIP6 multi-model ensemble median results, whereas other marks indicate individual models.

[Earth's Future]

Supporting Information for

Significant reduction of unequal population exposure to climate extremes by achieving the carbon neutrality

Seok-Geun Oh[1], Jung Choi[1], Min-Jee Kang[1], Sujong Jeong[2,3], Seung-Ki Min[4,5], Sang-Wook Yeh[6], Yeon-Hee Kim[4], and Seok-Woo Son[1,3*]

[1]School of Earth and Environmental Sciences, Seoul National University, Seoul, South Korea

[2]Department of Environmental Planning, Seoul National University, Seoul, South Korea

[3]Climate Technology Center, Seoul National University, Seoul, South Korea

[4]Division of Environmental Science and Engineering, Pohang University of Science and Technology, Pohang, Gyeongbuk, South Korea

[5]Institute for Convergence Research and Education in Advanced Technology, Yonsei University, Incheon, Republic of Korea

[6]Department of Marine Science and Convergence Engineering, Hanyang University, ERICA, Ansan, South Korea

December 2023

***Corresponding author:** Seok-Woo Son (seokwooson@snu.ac.kr)

Contents of this file

- **Text S1 to S3**
- **Figures S1 to S13**

Text S1. Model evaluation.

The fifth generation of the European Centre for Medium-Range Weather Forecast global reanalysis (ERA5, Hersbach et al. 2020) for the historical period of 1985–2014 is used as reference to evaluate the Coupled Model Intercomparison Phase 6 (CMIP6) models. The ERA5 data has higher spatial (30 km) and time resolution (hourly) than the other reanalysis data (i.e., ERA40, Uppala et al. 2005; ERA-Interim, Dee et al., 2011; NCEP/NCAR Reanalysis 1, Kalnay et al., 1996; NCEP-DOE Reanalysis 2, Kanamitsu et al., 2002), potentially making it more suitable to estimate and evaluate the climate extremes. Therefore, this dataset has been widely utilized as a reference data for temperature and precipitation extremes (e.g., Kim et al., 2020; Li et al., 2021; Oh & Sushama, 2021). The daily temperature and precipitation data at approximately 30 km resolution into common into 1°×1° grid and then calculated climate extreme indices, TXx and RX1day (Zhang et al. 2011), and Generalized Extreme Value (GEV) estimation to reduce the difference in spatial scales from CMIP6 models (1–2°).

This study uses the multi-model ensemble median (MEM), which is a more valid representative measure than the multi-model mean, because extremely large or small values can distort the mean. The model performance is basically evaluated based on the bias, root-mean-square error (RMSE), and correlation for spatial patterns of the estimated extreme values for the historical period of 1985–2014. The equations of the bias, RMSE and correlation are as

follow:

$$bias = \frac{1}{n}\sum_{i=1}^{n}(M_i - R_i)$$

$$RMSE = \sqrt{\frac{1}{n}\sum_{i=1}^{n}(M_i - R_i)^2}$$

$$correlation = \frac{\sum_{i=1}^{n}(M_i - \bar{M})(R_i - \bar{R})}{\sqrt{\sum_{i=1}^{n}(M_i - \bar{M})}\sqrt{\sum_{i=1}^{n}(R_i - \bar{R})}}$$

where n is the number of the total grids at land areas. The M_i and R_i denote the model and reanalysis at i th grid, respectively. The $\bar{M}$ nd $\bar{R}$ present the mean values over the land areas in the model and reanalysis, respectively. To compare the performance of MEM with that of each model, the combined metric of the RMSE and Taylor skill score (TSS, Taylor, 2001) is also used. The equation of TSS is like below:

$$TSS = \frac{(1 + correlation)^4}{4(SDR + \frac{1}{SDR})^2}$$

where SDR is the ratio of the spatial standard deviations of the model against to that of the reanalysis data. This score quantifies the similarity in the distribution and amplitude of the spatial pattern between the model and the reanalysis. The relative RMSE and TSS for each model and MEM are calculated by using their median values.

Text S2. Performance of CMIP6 MEM for historical period.

Compared with the ERA5 data, the CMIP6 MEM reproduces the spatial distribution

of the 30-year return value of TXx and RX1day reasonably well for the historical period of 1985–2014, with the spatial correlations of 0.95 and 0.84, respectively (Figures S2a–S2f). The 30-year return value of TXx is slightly overestimated by 0.1 to 3.0 °C in most land areas except for the high-latitude regions of the Northern Hemisphere, resulting in the global land average bias of 0.28 °C (Figure S2c). For the 30-year return value of RX1day, the CMIP6 MEM well captures typical large-scale features such as the intense precipitation extreme in the intertropical convergence zone (ITCZ) and African and Asian monsoon regions. However, the models underestimate the extreme precipitation by 20 to 100 mm/day depending precipitation zone, resulting in a global land average bias of -11.41 mm/day (Figure S2f).

Compared to a single model, the MEM shows a better performance in both the 30-year return values of TXx and RX1day (Figure S2g and S2h). This result is consistent with previous studies showing that the multi-model ensemble shows superior performance in reproducing mean and extreme climates than a single model (e.g., Oh & Suh, 2017; Kim et al., 2020; Li et al., 2021). Similar results are found for other return events, i.e., 10- and 50-year return value (not shown). It provides justification for the use of the CMIP6 MEM for future projection of the rare extreme events with varying return years.

Text S3. Response of climate extremes in the late 21st century to carbon neutrality.

If the current global warming is continued (i.e., SSP3-7.0 scenario), hot-temperature and heavy-precipitation extremes are expected to be strengthened in the late 21st century. The hot-temperature extreme is projected to experience a more intense warming event of above

4 °C over all land regions except Greenland (the first row of Figure S4a). Such extreme is expected to occur more than total 1000 days in South America, Africa, Arabia peninsula, and South Asia regions during the future period of 2071–2100 (the second row of Figure S4a). The heavy-precipitation extreme also reveals more intense and frequent events (Figure S5a) particularly in the African and Asian monsoon region where a dense population exists (Figure S3a).

Even if the transition to a carbon-neutral society is successful (i.e., SSP1-1.9 scenario), the intensity in both hot-temperature and heavy-precipitation extremes are still expected to increase with a range of 0.5–2°C and 0–20 mm/day, respectively. On a global average, the number of days in hot-temperature (heavy-precipitation) extreme increases up to total 100 days (5 days) compared to the historical period (Figures S4b and S5b). Although more intense and frequent climate extremes are also evident in the carbon neutrality scenario, the reduction rates, which estimate the benefit of carbon neutrality compared to the high emission scenario, are substantially large (Figures S4c and S5c; see Methods in main paper). Globally, a 71% decrease is found in the intensity of hot-temperature extreme (the first row of Figure S4c), while a more significant decrease (97%) is found in its frequency (the second row of Figure S4c). Similar reduction rates are revealed in the heavy-precipitation extreme, i.e., 75 and 76% decreases in its intensity and frequency, respectively (Figure S5c).

The difference between the scenarios with and without the net-zero carbon emission shows a large regional dependency, especially for the frequency (Figures S4c and S5c). For example, the frequency of the hot-temperature extreme exhibits large differences in the South

America, African, and Asian continents, while that of heavy-precipitation extreme shows a large difference in the African, North America, and Asian continents. Interestingly, the reduction rates of the intensity and frequency of the hot-temperature extremes are 68–81% and 94–98%, respectively, which implies a higher benefit of carbon neutrality in the frequency than in the intensity for all the continents (Figures S4c). On the other hand, the intensity and frequency of the heavy-precipitation extremes are reduced by 66–85% and 69–87% in net-zero carbon emission scenario, respectively. This result suggests that there are larger differences in reduction rate across continents, but smaller differences between frequency and intensity compared to hot-temperature extreme (Figure S5c). In summary, a transition to a carbon-neutral society around 2050 can lead to a more than twofold of reduction in both the intensity and frequency of hot-temperature and heavy-precipitation extremes for all the continents.

Acknowledgements

This research was supported by Basic Science Research Program through the National Research Foundation of Korea (NRF) funded by the Ministry of Education (RS-2023-00238065). This research was also supported by the Research Program for the carbon cycle between oceans, land, and atmosphere of the NRF funded by the Ministry of Science and ICT (2021M3I6A1086807), and Korea Environment Industry & Technology Institute (KEITI) through Project for developing an observation-based GHG emissions geospatial information map, funded by Korea Ministry of Environment (MOE) (RS-2023-00232066).

Reference

Dee, D. P., Uppala, S. M., Simmons, A. J., Berrisford, P., Poli, P., & Kobayashi, S., et al. (2011). The ERA-Interim reanalysis: configuration and performance of the data assimilation system. *Quarterly Journal of the Royal Meteorological Society*, *137*, 553–597.

Hersbach, H., Bell, B., Berrisford, P., Hirahara, S., Horanyi, A., & Munoz-Sabater, J., et al. (2020). The ERA5 global reanalysis. *Quarterly Journal of the Royal Meteorological Society*, *146*, https://doi.org/10.1002/qj.3803.

Kalnay, E., Kanamitsu, M., Kistler, R., Collins, W., Deaven, D., & Gandin, L., et al. (1996). The NCEP/NCAR 40-year reanalysis project. *Bulletin of the American Meteorological Society*, *77*, 437–472.

Kanamitsu, M., Ebisuzaki, W., Woollen, J., Yang, S.-K., Hnilo, J. J., & Fiorino, M., et al. (2002). NCEP-DOE AMIP-II reanalysis (R-2). *Bulletin of the American Meteorological Society*, *83*, 1631–1643.

Kim, Y. H., Min, S. K., Zhang, X., Sillmann, J., & Sandstad, M. (2020). Evaluation of the CMIP6 multi-model ensemble for climate extreme indices. *Weather and Climate Extremes*, *29*, 100269.

Kummu, M., Taka, M., & Guillaume, J. H. A. (2018). Gridded global datasets for gross domestic product and human development index over 1990 2015. *Scientific data*, *5*, 180004.

Li, C., Zwiers, F., Zhang, X., Li, G., Sun, Y., & Wehner, M. (2021). Changes in annual extremes of daily temperature and precipitation in CMIP6 model. *Journal of Climate*, *34*, 3441–3460.

761 Oh, S. G. & Sushama, L. (2021). Urban-climate interactions during summer over eastern North
762 America. *Climate Dynamics*, *57*, 3015–3028.

763 Oh, S. G., & Suh, M. S. (2017). Comparison of projection skills of deterministic ensemble
764 methods using pseudo-simulation data generated from multivariate Gaussian
765 distribution. *Theoretical and Applied Climatology*, 129, 243–262 .

766 Taylor K. E. (2001) Summarizing multiple aspects of model performance in a single diagram.
767 *Journal of Geophysical Research*, *106*, 7183–7192.

768 Uppala, S. M., KÅllberg, P. W., Simmons, A. J., Andrae, U., Bechtold, V. D. C., & Fiorino, M.,
769 et al. (2005). The ERA-40 Reanalysis. *Quarterly Journal of the Royal*
770 *Meteorological Society*, *131*, 2961–3012.

771 Zhang, W., Zhou, T., Zou, L., Zhang, L., & Chen, X. (2018). Reduced exposure to extreme
772 precipitation from 0.5°C less warming in global land monsoon regions. *Nature*
773 *Communications*, *9*, 3153.

774

775

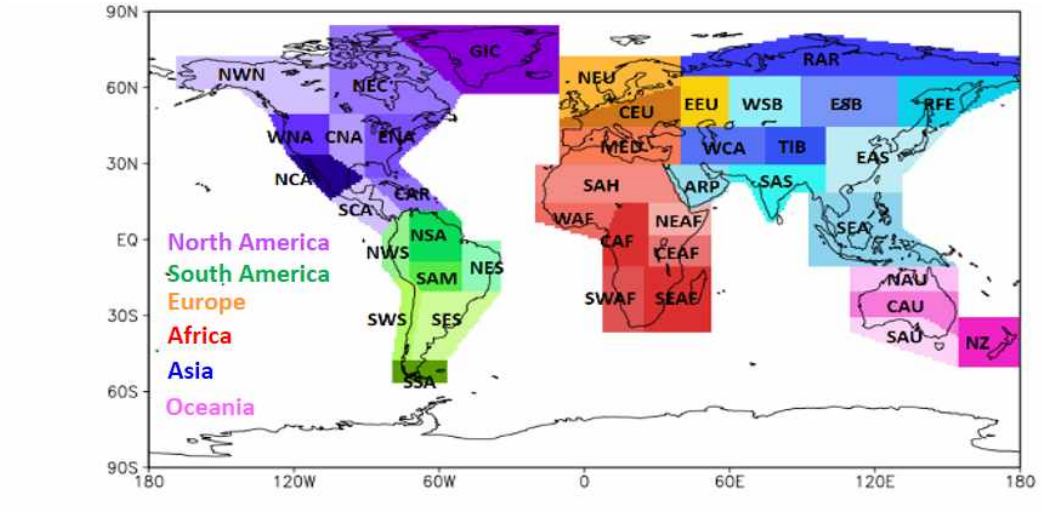

776

777 **Figure S1.** Sub-regional domain in the global land adopted from Iturbide et al. (2020). The
778 shaded colors indicate different continents: North America (purple series), South America
779 (green), Europe (orange), Africa (red), Asia (blue), and Oceania (pink).

780

781

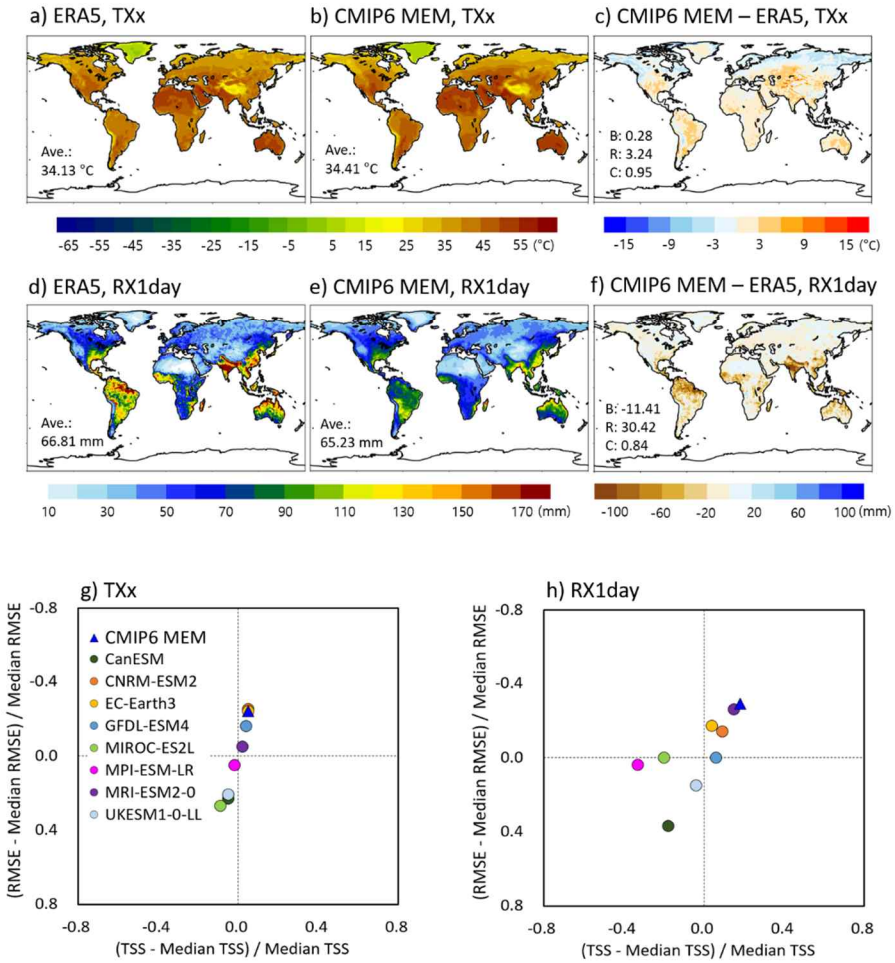

782

783 **Figure S2.** Estimates of 30-year return values of hot-temperature (TXx) and heavy-
784 precipitation (RX1day) extremes of (a, d) ERA5 reference data and (b, e) CMIP6 multi-model
785 ensemble median for the present period of 1985–2014, and (c, f) their differences. The area-
786 averaged value (Ave.), bias (B), root-mean-square error (R), and correlation (C) between the
787 CMIP6 multi-model ensemble median and ERA5 are indicated in sub-plot. Only land areas are
788 considered. (g, h) The relative performance of the CMIP6 models for 30-year return values of
789 TXx and RX1day, based on the root-mean-square error (RMSE) and Taylor skill score (TSS).
790 The symbol closer to the upper right corner indicates better performance.

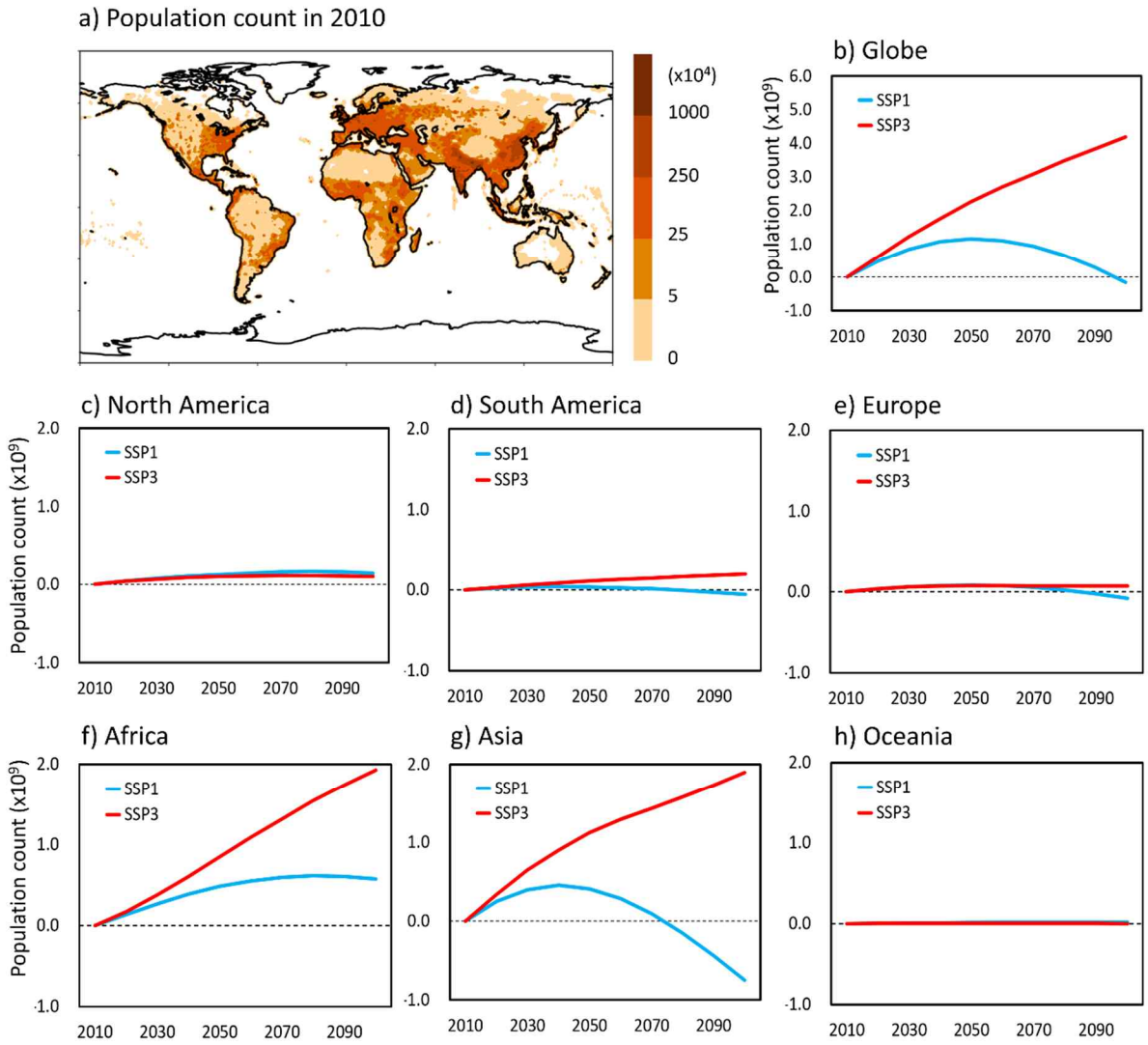

791

792 **Figure S3.** Spatial distribution of (a) population count (unit: number of persons) in 2010
793 estimated by NASA Socioeconomic Data and Application Center, and (b–h) time series of the
794 population change in the globe (GL), North America (NA), South America (SA), Europe (EU),
795 Africa (AF), Asia (AS), and Oceania (OC) under SSP1 and SSP3 scenarios at ten-year intervals
796 for the period of 2010–2100. Note that the y-axis range for GL is different from that of each
797 continent.

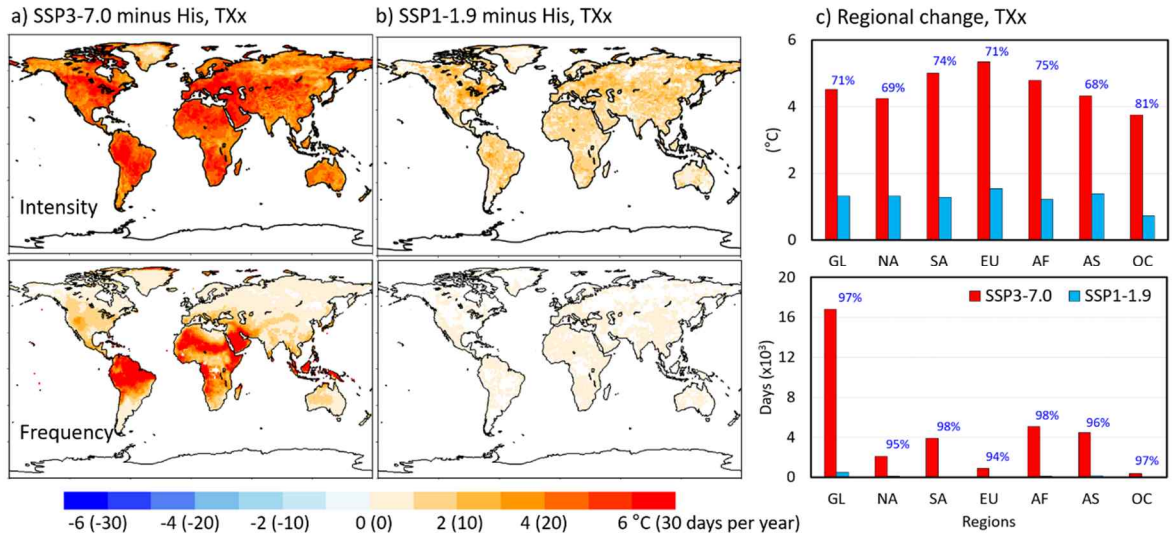

Figure S4. Projected changes of (a, b) spatial distribution in 30-year return value of TXx in the late 21st century (2071–2100) compared to the historical period of 1985–2014. (c) Changes in regionally-averaged or aggregated 30-year return value and its exceeding occurrence days for the North America (NA), South America (SA), Europe (EU), Africa (AF), Asia (AS), and Oceania (OC) are also presented. The CMIP6 multi-model ensemble median under the SSP1-1.9 and SSP3-7.0 scenarios are used. Only grids where more than three-quarters of the models used show the same sign are presented. Note that the relative reduction rate (%) in the SSP1-1.9 scenario compared to the SSP3-7.0 scenario is shown in blue above each bar.

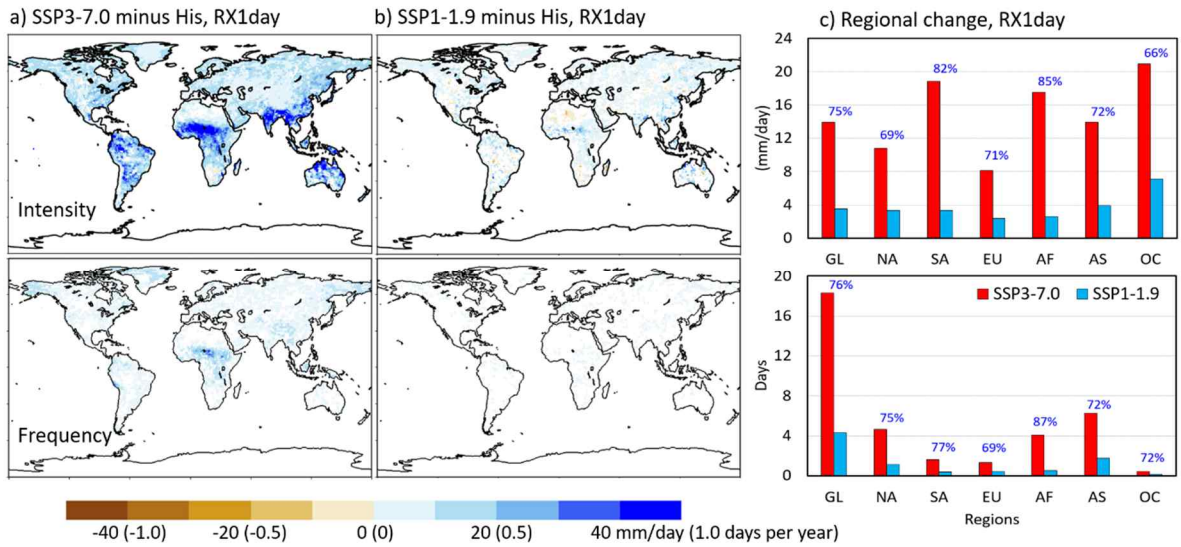

Figure S5. Same as Figure S4 but for 30-year return value of RX1day.

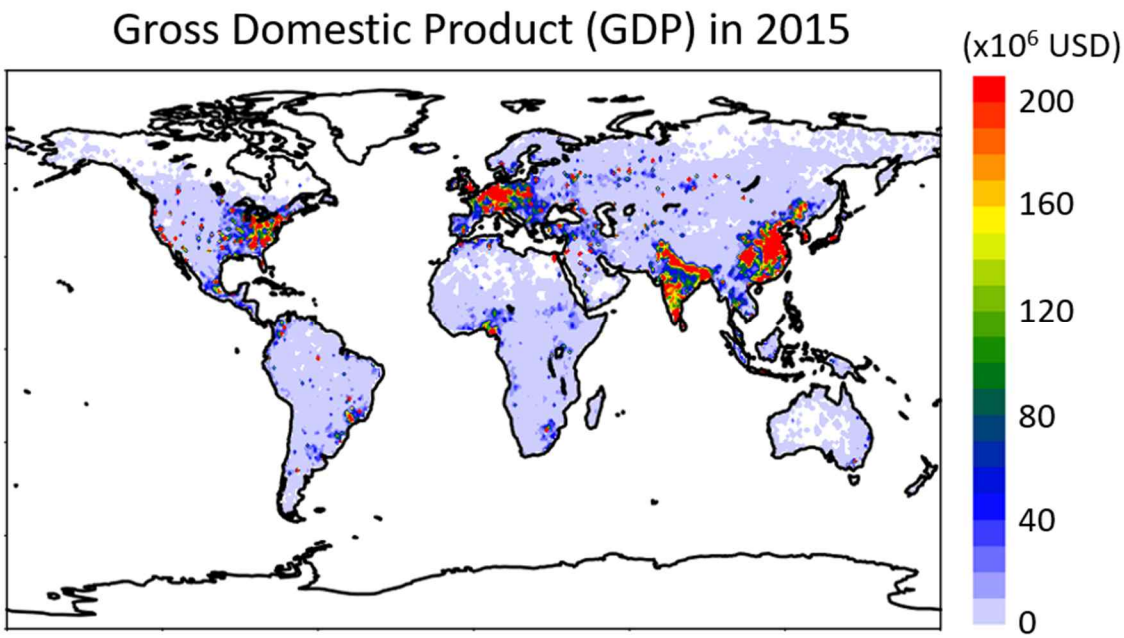

822

823 **Figure S6.** Gross Domestic Product (GDP, unit: US dollar) in 2015 estimated by Kummu et al.

824 (2020).

825

826

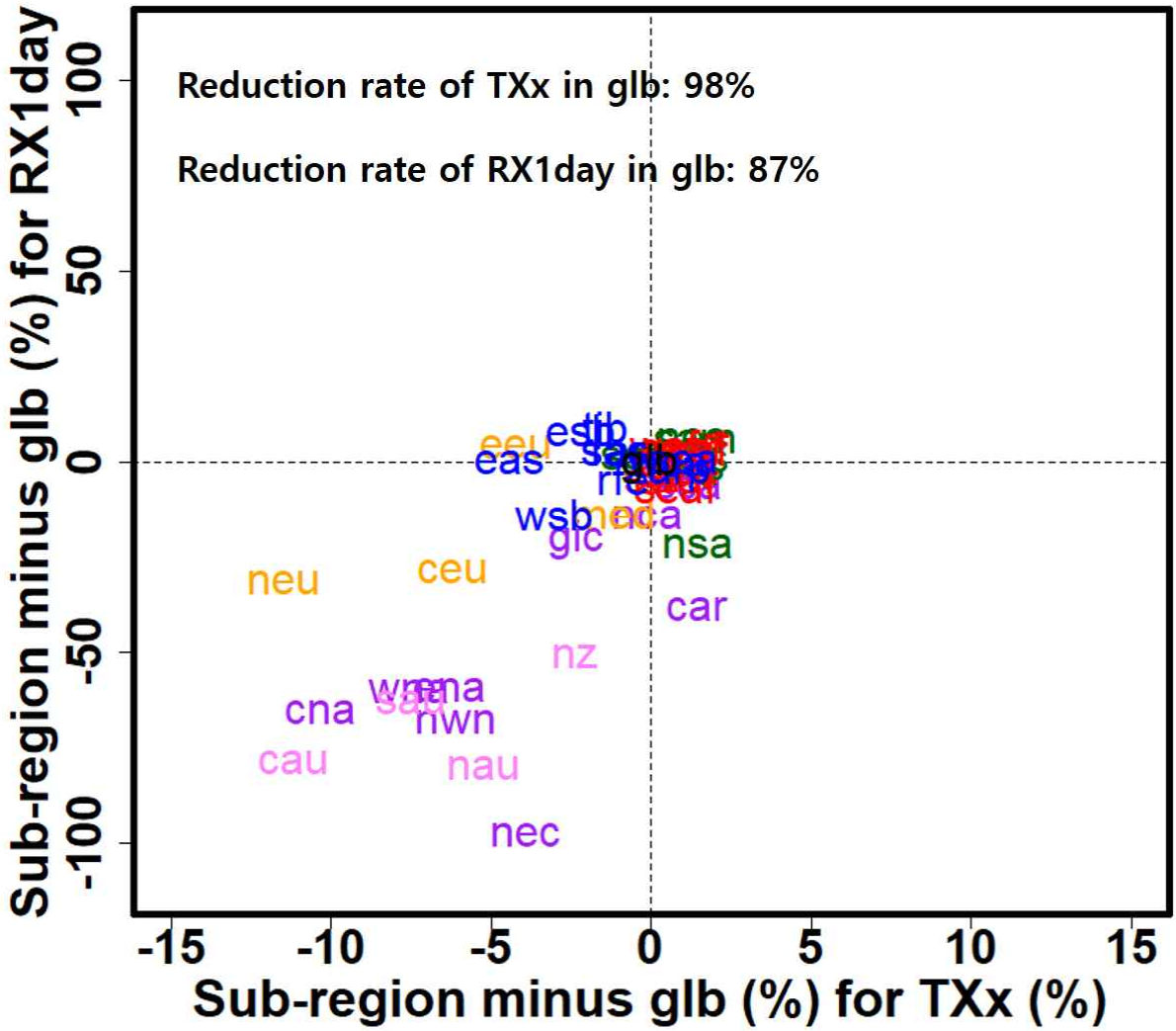

827

828 **Figure S7.** Comparison of relative reduction rate (%) of population exposure to extremely
829 high-temperature and heavy-precipitation events, that exceed the historical 30-year return
830 value of TXx and RX1day, in 41 sub-regions against that of the global region (glb). The
831 reduction rate (%) is calculated by comparing the population exposure changes under the SSP1-
832 1.9 scenario against the SSP3-7.0 scenario. Shaded colors indicate different continents: North
833 America (purple series), South America (green), Europe (orange), Africa (red), Asia (blue), and
834 Oceania (pink).

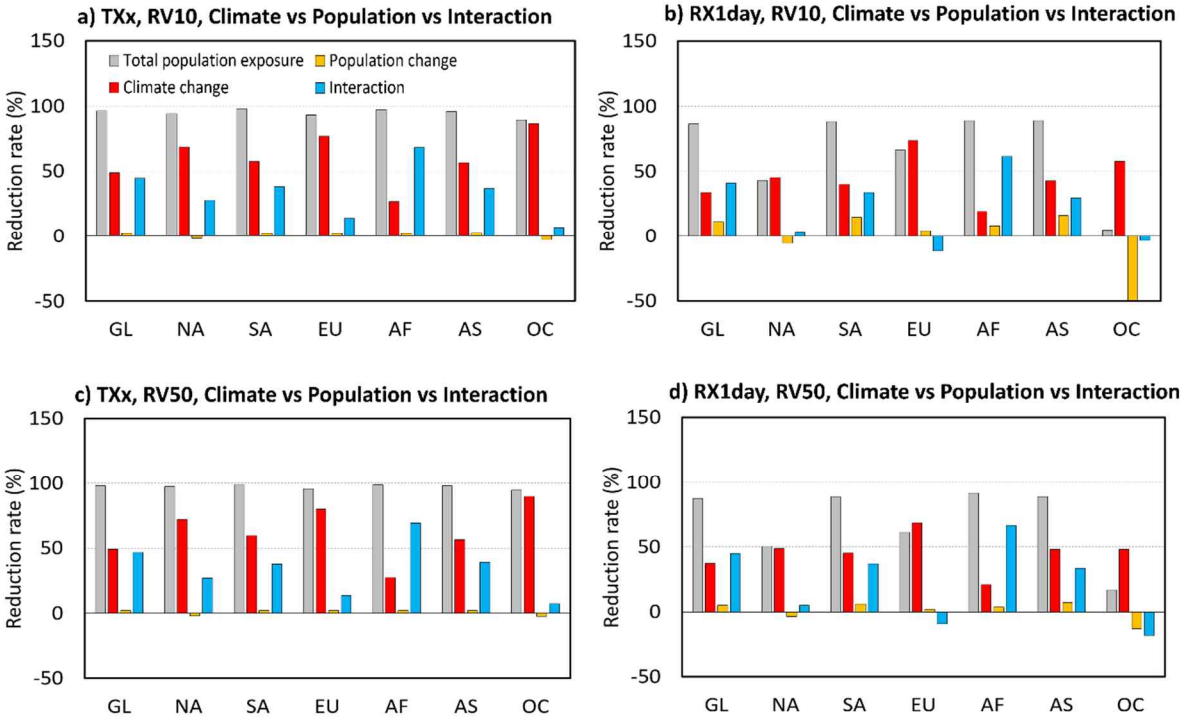

Figure S8. Reduction rate (%) of regionally aggregated population exposure for the 10- and 50-year return events (RV10 and RV50) of hot-temperature and heavy-precipitation in SSP1-1.9 relative to SSP3-7.0 scenarios and the relative contribution of climate, population, and climate-population interaction in the reduction rate.

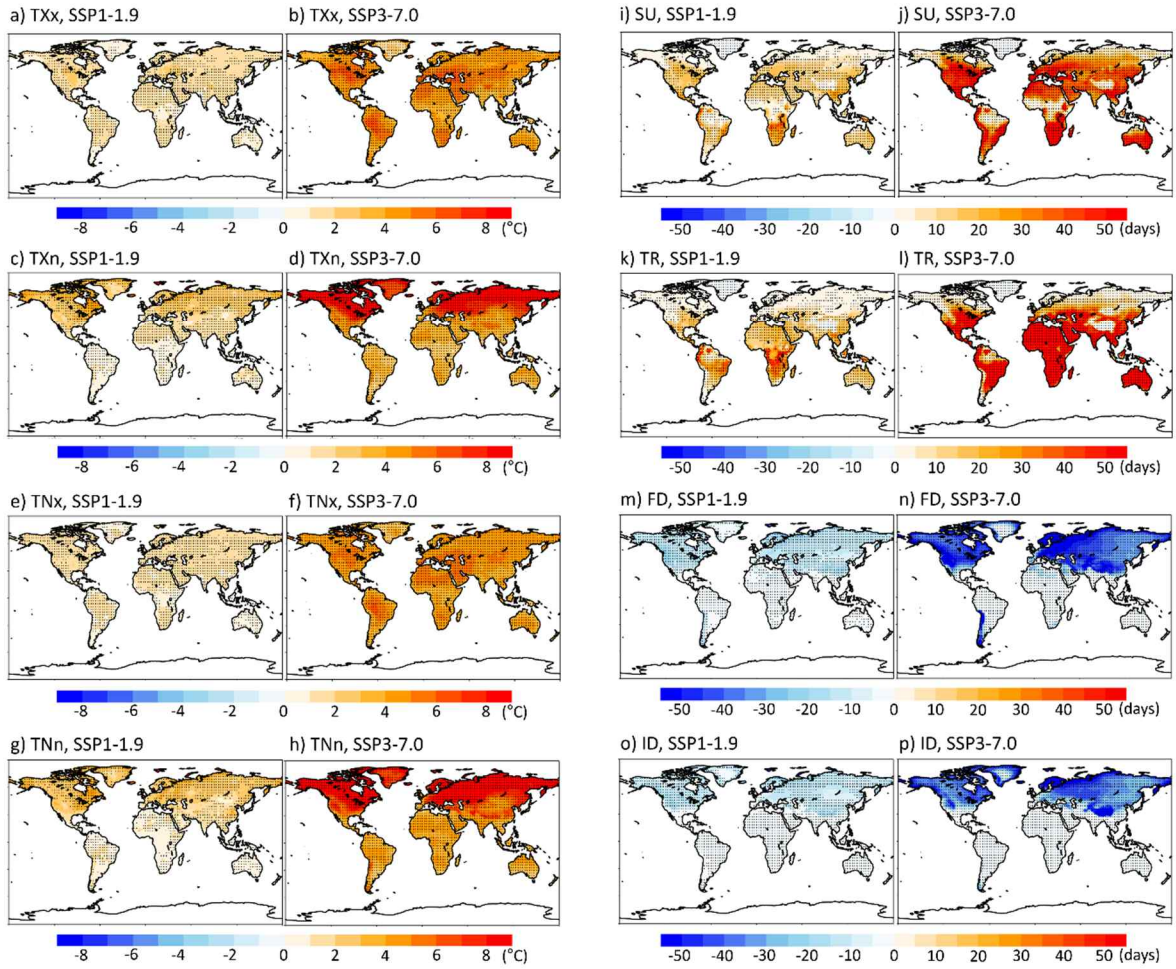

Figure S9. Changes in spatial distribution of temperature-related eight extreme indices in the late 21st century (2071–2100) under the SSP1-1.9 and SSP3-7.0 scenarios compared to the historical period of 1985–2014. The extreme indices are the annual maxima and minima of daily maximum temperature (TXx and TXn, respectively) and minimum temperature (TNx and TNn, respectively), summer days (SU), tropical nights (TR), frost days (FD), and ice days (ID).

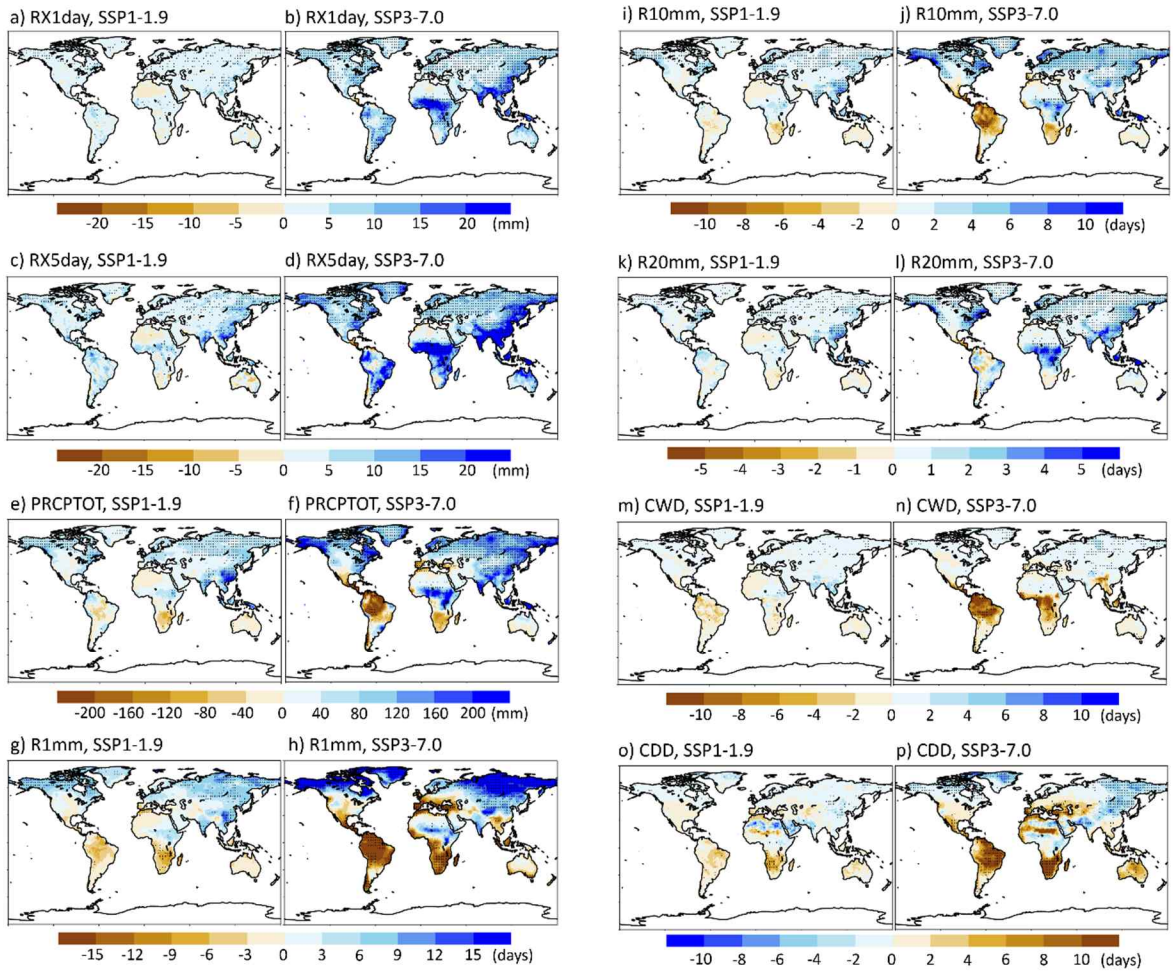

854

855 **Figure S10.** Same as Figure S8 but for precipitation-related eight extreme indices. The extreme
856 indices are the annual maxima of daily precipitation (RX1day) and 5-days-acumulated
857 precipitation (RX5day), total wet-day precipitation (PRCPTOT), number of wet day where the
858 precipitation > 1 mm (R1mm), > 10 mm (R10mm), and > 20 mm (R20mm), consecutive wet
859 days (CWD), and consecutive dry days (CDD).

860

861

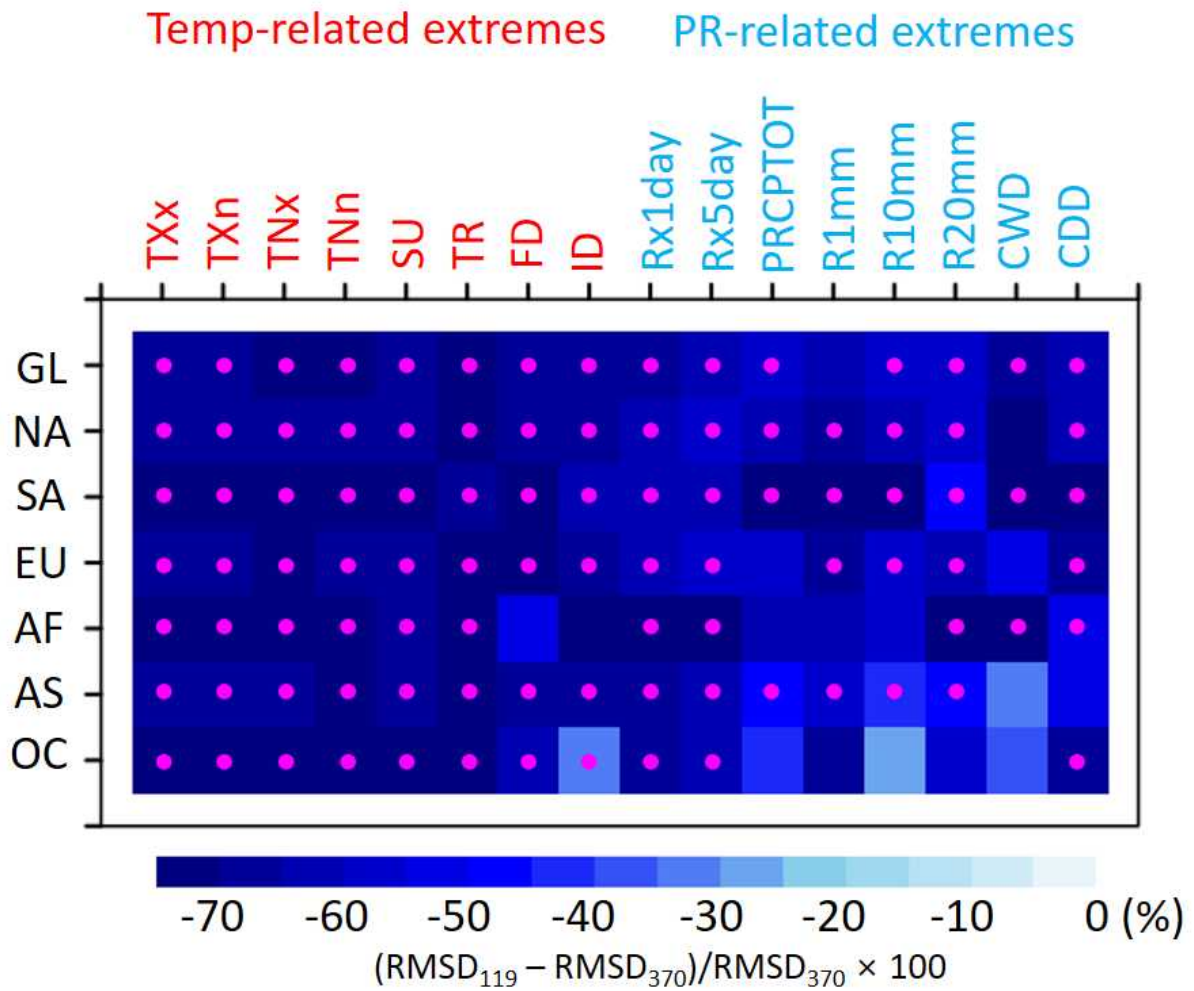

862

863 **Figure S11.** Reduction rate (%) of the root-mean square difference (RMSD) for event
864 frequency in the SSP1-1.9 scenario relative to the SSP3-7.0 scenario in the late 21st century
865 (2071–2100) for 16 extreme indices as shown in Figs. S7 and S8, compared to the historical
866 period of 1985–2014. The CMIP6 multi-model ensemble median is used. A greater negative
867 value implies that the SSP1-1.9 scenario is closer to the current climate state compared to the
868 SSP3-7.0 scenario, highlighting a higher carbon-neutral effect. The pink dot denotes that the
869 difference between the two scenarios is statistically significant at the 95% confidence level.

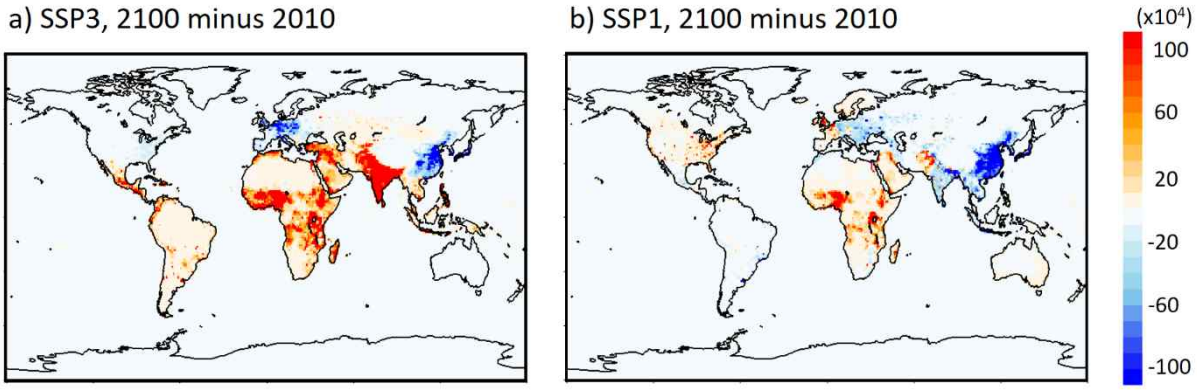

870

871 **Figure S12.** Projected changes of spatial distribution in population counts in year 2010

872 compared to year 2010.

873

874

875

876

877

878

879

880

881

882

883

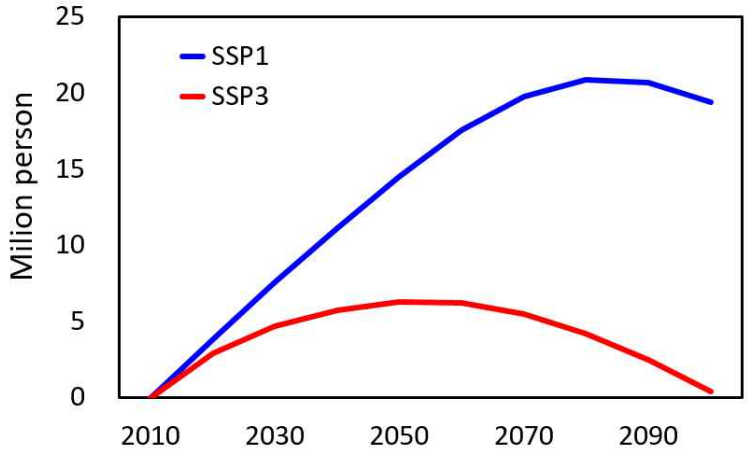

884

885 **Figure S13.** Time series of the population change in Oceania under SSP1 and SSP3 scenarios

886 at ten-year intervals for the period of 2010–2100.

887

888

889

890

891

892

893

894

895

896

897

898

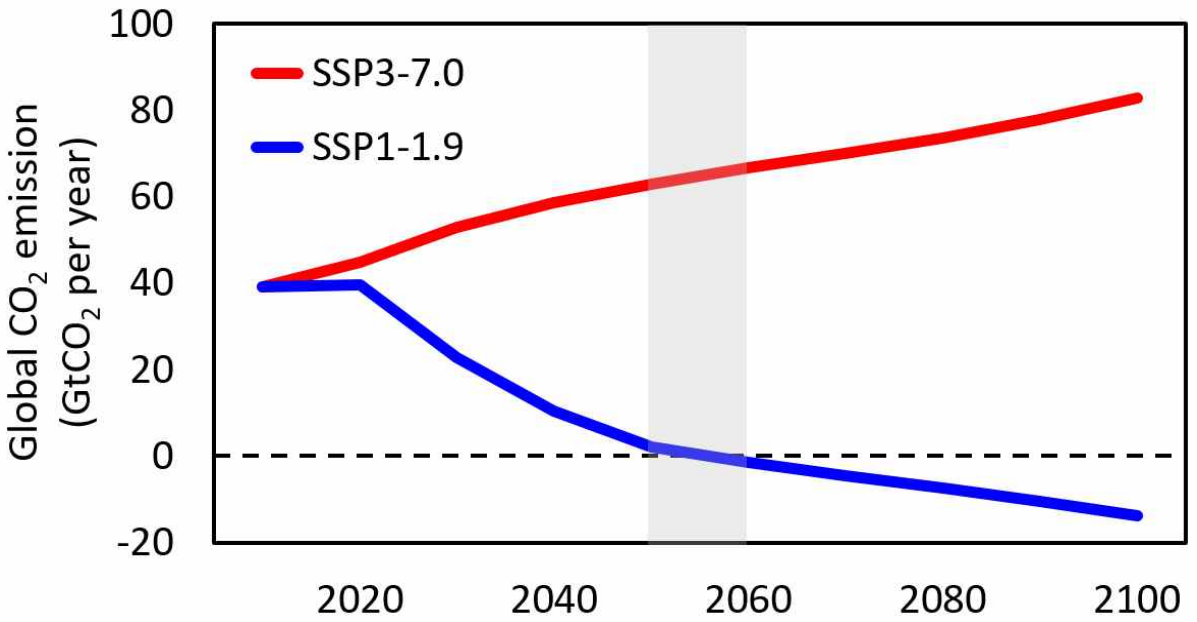
100
80
60
40
20
0
-20
Global CO_2 emission ($GtCO_2$ per year)
SSP3-7.0
SSP1-1.9
2020
2040
2060
2080
2100

899

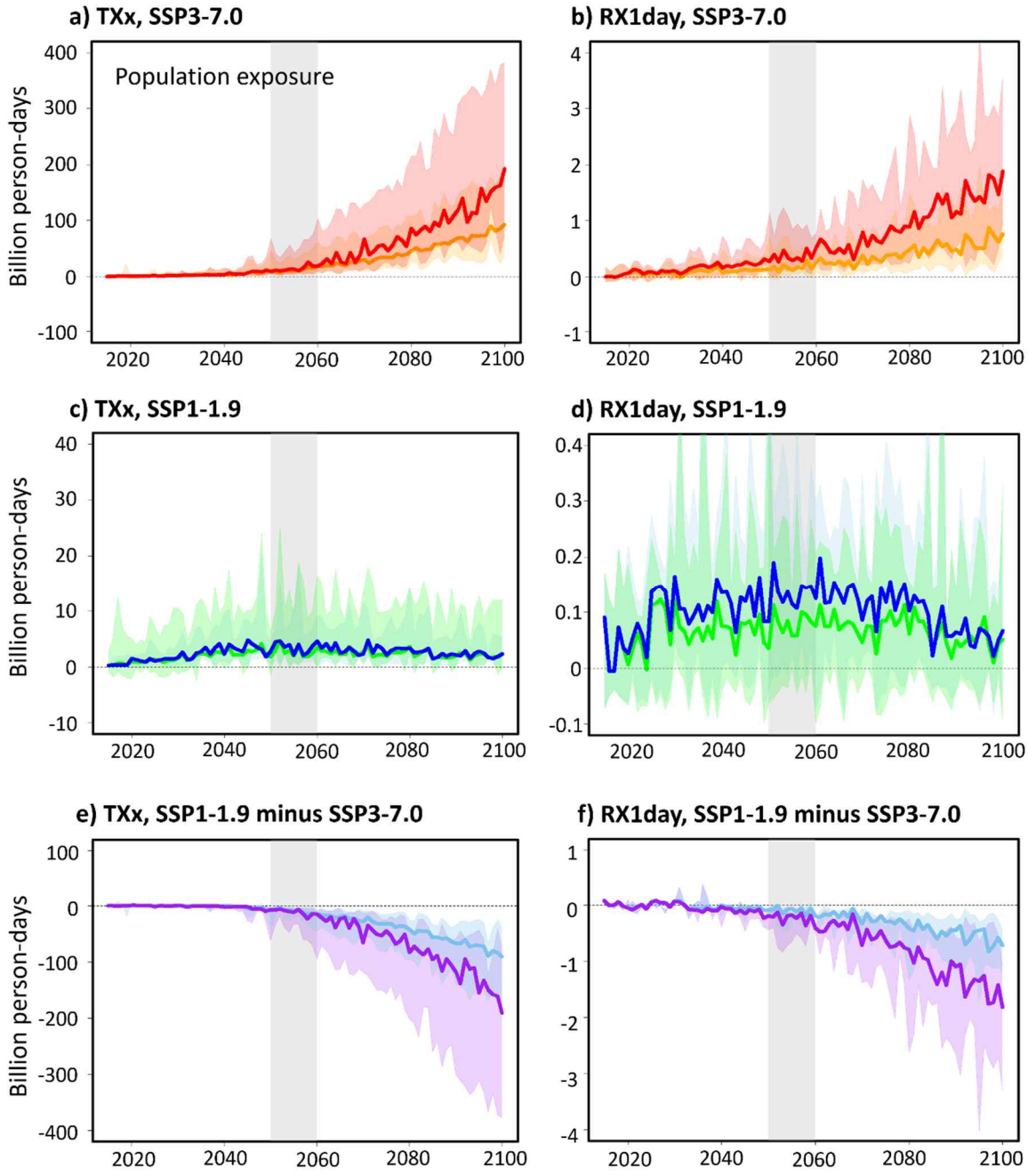
a) TXx, SSP3-7.0
Population exposure
Billion person-days
400
300
200
100
0
-100
2020
2040
2060
2080
2100
b) RX1day, SSP3-7.0
4
3
2
1
0
-1
c) TXx, SSP1-1.9
40
30
20
10
0
-10
d) RX1day, SSP1-1.9
0.4
0.3
0.2
0.1
0
-0.1
e) TXx, SSP1-1.9 minus SSP3-7.0
100
0
-100
-200
-300
-400
f) RX1day, SSP1-1.9 minus SSP3-7.0
1
0
-1
-2
-3
-4

900

901

902

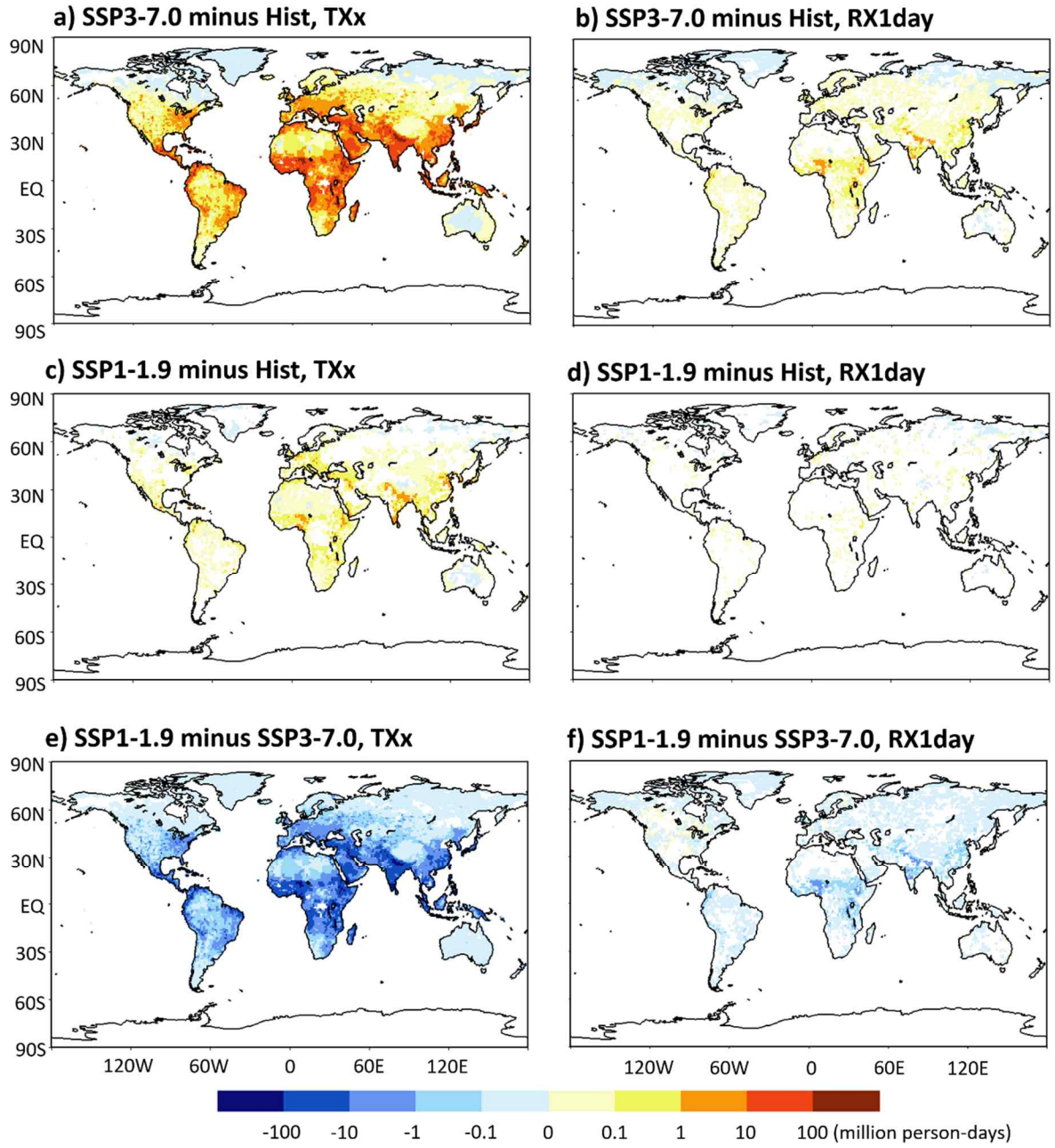
a) SSP3-7.0 minus Hist, TXx
b) SSP3-7.0 minus Hist, RX1day
c) SSP1-1.9 minus Hist, TXx
d) SSP1-1.9 minus Hist, RX1day
e) SSP1-1.9 minus SSP3-7.0, TXx
f) SSP1-1.9 minus SSP3-7.0, RX1day
90N
60N
30N
EQ
30S
60S
90S
120W
60W
0
60E
120E
-100
-10
-1
-0.1
0
0.1
1
10
100 (million person-days)

903

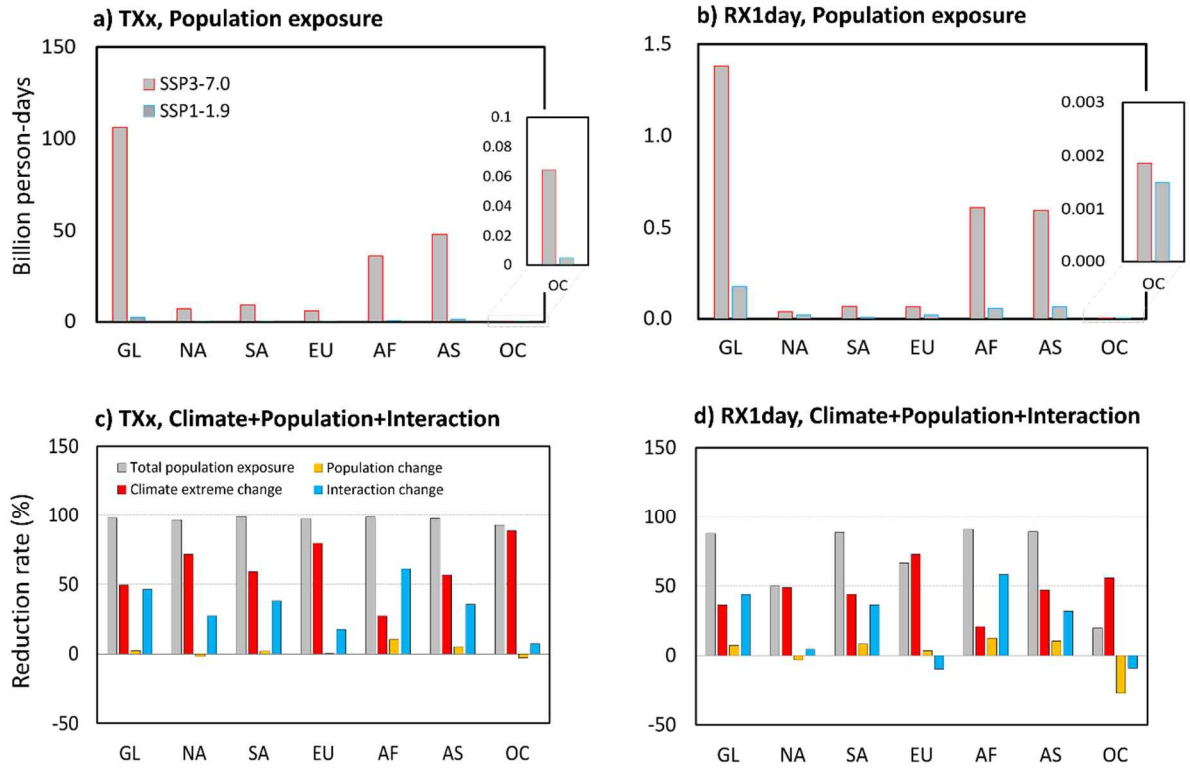

904

905

906

907

908

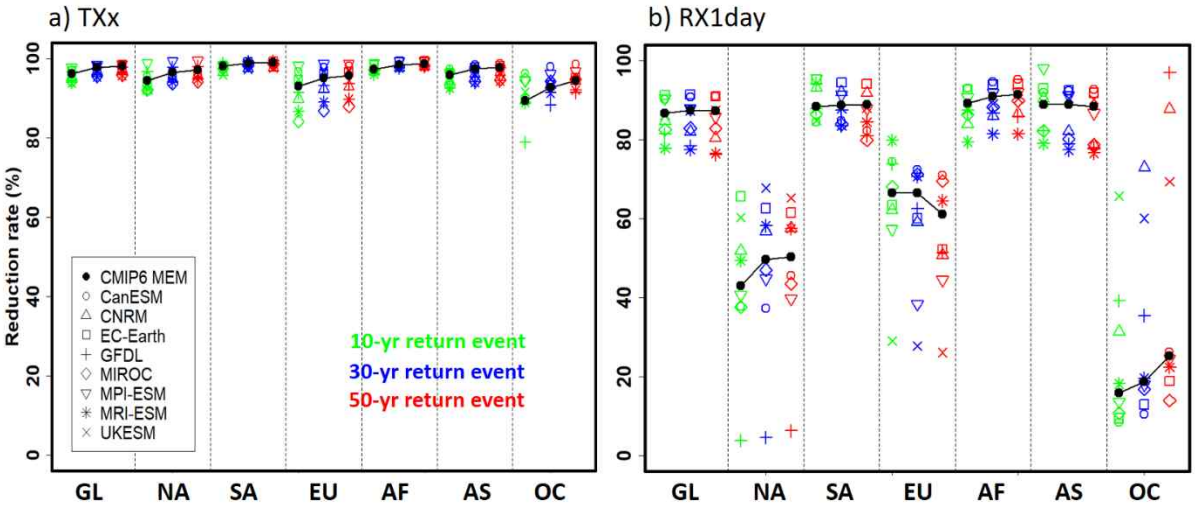
a) TXx
b) RX1day
Reduction rate (%)
0
20
40
60
80
100
CMIP6 MEM
CanESM
CNRM
EC-Earth
GFDL
MIROC
MPI-ESM
MRI-ESM
UKESM
10-yr return event
30-yr return event
50-yr return event
GL
NA
SA
EU
AF
AS
OC

909

910

911

Significant reduction of unequal population exposure to climate extremes by achieving the carbon neutrality

Seok-Geun Oh[1], Jung Choi[1], Min-Jee Kang[1], Sujong Jeong[2,3], Seung-Ki Min[4,5], Sang-Wook Yeh[6], Yeon-Hee Kim[4], and Seok-Woo Son[1,3*]

[1]School of Earth and Environmental Sciences, Seoul National University, Seoul, South Korea

[2]Department of Environmental Planning, Seoul National University, Seoul, South Korea

[3]Climate Technology Center, Seoul National University, Seoul, South Korea

[4]Division of Environmental Science and Engineering, Pohang University of Science and Technology, Pohang, Gyeongbuk, South Korea

[5]Institute for Convergence Research and Education in Advanced Technology, Yonsei University, Incheon, Republic of Korea

[6]Department of Marine Science and Convergence Engineering, Hanyang University, ERICA, Ansan, South Korea

December 2023

***Corresponding author:** Seok-Woo Son (seokwooson@snu.ac.kr)

Key points (Limit 140 character including spaces):

- By the 2050s, carbon neutrality reduces population exposure to climate extremes by 87–98% compared to current global warming rates.
- Africa and Asia are projected to experience the most dramatic reductions in population exposure to climate extremes by achieving the carbon neutrality.
- In North America, Europe, and Oceania, climate extreme change plays a more important role in population exposure to climate extremes.

Abstract

Climate extremes, such as hot temperature and heavy precipitation events, have devastating effects on human societies. As the planet gets warmer, they have become more intense and more frequent. To avoid irreversible damages from climate extremes, many countries have committed to achieving net-zero anthropogenic carbon emissions, or carbon neutrality, by the 2050s. Here, we quantify the impact of carbon neutrality on population exposure to climate extremes using multi-model projections from the Coupled Model Intercomparison Project Phase 6 (CMIP6) Shared Socioeconomic Pathway (SSP)1-1.9 and SSP3-7.0 scenarios. It is found that the increasing population exposure to hot-temperature and heavy-precipitation extremes under SSP3-7.0 scenario can be substantially reduced by 87–98% in the late 21st century by achieving the carbon neutrality based on SSP1-1.9 scenario. The benefits of carbon neutrality are particularly pronounced in Africa and Asia. The potential benefits of carbon neutrality are also significant in North America, Europe, and Oceania, where a reduction in climate extremes is more than twice as important as population decline in reducing population exposure to climate extremes. These results provide important scientific support for ongoing efforts to achieve net-zero carbon emissions by the 2050s to reduce potential climate risk and its inequity across continents.

Plain Language Summary

To avoid irreversible damages from climate extremes in a warming climate, net-zero anthropogenic carbon emissions, or carbon neutrality, has been proposed. However, how much damages from climate extremes can be mitigated by achieving the carbon neutrality has not been quantitatively assessed. Here, we show that achieving carbon neutrality could lead to a significant and widespread reduction in population exposure to hot-temperature and heavy-precipitation extremes by 87–98% in the late 21st century. The benefits of carbon neutrality are particularly large in Africa and Asia. Even in North America, Europe, and Oceania, where the developed countries are concentrated, population exposure to climate extremes is projected to decrease significantly, primarily due to reduced climate extremes with a minor contribution of population decline. This finding underscores the critical importance of ongoing efforts to achieve net-zero carbon emissions by the 2050s to reduce potential climate risk and its inequity across continents.

1. Introduction

As the threat of global warming became a reality, the Paris Agreement was proposed in 2015 to "hold the increase in the global average temperature to well below 2°C against preindustrial levels and pursue efforts to limit the temperature increase to 1.5°C" (UNFCCC, 2015). Its potential benefits have often been highlighted through the analyses of climate model simulations (e.g., Park et al., 2018; King et al., 2021; Nashwan & Shahid, 2022). Such studies have reported that 0.5°C less warming compared to 2°C warming can lead to a significant reduction in the areas damaged by climate change. However, these studies are mainly based on relatively low-emission scenarios compared to high-emission scenarios (e.g., O'Neill et al., 2016; Oin et al., 2021) rather than carbon-neutrality scenarios which take into account socioeconomic and environmental changes, technological development and innovation, and policy coordination to achieve net-zero emissions by the 2050s (Gidden et al., 2018).

While the Paris Agreement focuses on mean surface air temperature (UNFCCC, 2015), more attention should be paid to climate extremes. Climate extremes, such as hot-temperature and heavy-precipitation events, are rapidly increasing with global warming, exerting destructive impacts on human societies (e.g., Kharin et al., 2013; Li et al., 2021; Xie et al., 2022). By reducing CO_2 emissions, the frequency and intensity of climate extremes are projected to decrease significantly (e.g., Jo et al., 2022; Kim et al., 2022; Nashwan & Shahid, 2022). However, it has not yet been quantified how much the population exposure to climate extremes can be reduced by achieving carbon neutrality, although it can provide critical context for establishing effective climate mitigation policies.

Here, we investigate the impact of carbon neutrality on population exposure to hot-temperature and heavy-precipitation events by examining multi-model projections from the Coupled Model Intercomparison Project Phase 6 (CMIP6, Eyring et al., 2016). In particular, we compare the Shared Socioeconomic Pathway (SSP)1-1.9 scenario, which describes a transition to a carbon-neutral society around the 2050s and net carbon absorption thereafter, with the SSP3-7.0 scenario, which is based on regional rivalry over carbon emissions policy (Fig. 1; O'Neill et al., 2016; Oin et al., 2021), and quantitatively assess the projected reduction in global and regional population exposure to hot-temperature and heavy-precipitation extremes. The relative importance of changes in population and extreme events in reducing population exposure to climate extremes is also examined.

2. Data and Methods

2.1. Datasets

To calculate climate extremes, daily maximum temperature and precipitation for historical simulations (1985–2014) and future projections (2015–2100) under two different SSP scenarios from eight CMIP6 models (Eyring et al., 2016) are used (Table 1). Specifically, the SSP3-7.0 and SSP1-1.9 scenarios, which are the high and very low greenhouse gas emission scenarios, respectively (O'Neill et al., 2016; Oin et al. 2021), are compared. The former assumes the current rate of global warming to be maintained until 2100 (i.e., regional rivalry scenario), while the latter assumes net-zero carbon emissions by the 2050s (i.e., carbon neutrality scenario) (Figure 1). All variables of interest are computed at each land grid point

and then intercompared across six continents, i.e., North America, South America, Europe, Africa, Asia, and Oceania (Figure S1; Iturbide et al., 2020).

2.2. Climate extremes based on GEV analysis

This study uses the annual maximum of daily maximum temperature (TXx) and annual maximum daily precipitation (RX1day) as indices of hot temperature and heavy precipitation extremes, respectively, following the Expert Team on Climate Change Detection and Indices (ETCCDI; Zhang et al. 2011). To estimate the rare events occurring once in 10, 30, or 50 years, we first fit TXx and RX1day at every grid point of each model's native resolution to the generalized extreme value (GEV, Kharin et al., 2013) distribution during the historical (1985–2014) and future (2071–2100) periods. The GEV estimation for 30-year time window is based on the assumption that temperature or precipitation extremes remain approximately stationary within 30-year period (Kim et al., 2020; Li et al., 2021).

The cumulative density function (CDF) of the GEV distribution for variable x is defined as follows:

$$F(x;\mu,\sigma,\xi) = \begin{cases} exp\left[-exp\left\{-\frac{x-\mu}{\sigma}\right\}\right] & \text{for } \xi = 0 \\ exp\left[-\left\{1+\xi\frac{x-\mu}{\sigma}\right\}^{-\xi^{-1}}\right] & \text{for } \xi \neq 0 \text{ and } \xi\frac{x-\mu}{\sigma} > -1 \end{cases} \quad (1)$$

where μ, σ, and ξ represent the location, scale, and shape parameters, respectively. The GEV parameters are estimated using the L-moments method (Hosking, 1990), which has been used for the small sample size (Hosking, 1990; Kim et al., 2020). The quantile function of GEV (X)

is derived by inverting a CDF for a given probability p as below.

$$X_p = \begin{cases} \mu - \sigma \ \ln[-\ln(p)] \ \text{ for } \ \ \xi = 0 \\ \mu - \frac{\sigma}{\xi}\ln\left[1 - (-\ln(p))^{-\xi}\right] \ \text{ for } \ \xi \neq 0. \end{cases} \quad (2)$$

The 10-, 30-, and 50-year return values for the historical and future periods are calculated when p=0.90, 0.967, and 0.98 (as the exceedance of the annual extreme with probability = 10%, 3.3%, and 2%), respectively. In this study, we mainly focus on the return values of 30-year, which is the most realistic but large enough period that can be obtained from the current reanalysis dataset (see supporting information). After the GEV estimation, climate extreme indices are interpolated to a common 1°×1° grid using a bilinear remapping, and then multi-model ensemble statistics are computed. This procedure allows to minimize the discrepancy arising from different data resolutions (Kim et al., 2020; Li et al., 2021). Further details on the model evaluation and projection for the historical and future climate extremes can be found in the supporting information.

2.3. Population exposure

Population exposure is one of the key indicators of the impact of climate extremes on human societies (e.g., Jones et al., 2018; Chen & Sun, 2021). It is closely intertwined with climate risk, as the impacts of climate change are felt most acutely by vulnerable populations (e.g., Jones et al., 2018; Chen & Sun, 2021). Population exposure represents the accumulative number of people exposed to climate extremes (unit: person-days), and is computed by multiplying the population count of an area by the number of climate extremes that occur there.

In this study, the 10-, 30-, and 50-year return values of TXx and RX1day, estimated from the historical period of 1985–2014 (Figures S2b and 2e), are used as the threshold values to identify the hot-temperature and heavy-precipitation extremes. The number of climate extreme events at each native model grid is counted as the number of extreme days exceeding the threshold values in each year for the period of 1985–2100. After interpolating the result into a common 1°×1° grid, the historical population exposure is defined as the integrated product of the number of climate extremes from 1985 to 2014 and the historical population count in 2010 (Figure S3a; Jones & O'Neill, 2016). For the future population exposure, the future population counts in 2020, 2030, …, 2090, and 2100 under SSP1 and SSP3 scenarios (Figures S3b–3h; Jones & O'Neill, 2016) are used to match the SSP1-1.9 and SSP3-7.0 scenarios. For example, the population counts in 2020 and 2030 are used to calculate the population exposure for the period of 2020–2029 and 2030–2039, respectively.

2.4. Reduction rate of population exposure and its contributing factor

To quantify the benefit of carbon neutrality, the reduction rate (%, Jones et al., 2018; Zhang et al., 2018; Lei et al., 2022) of population exposure to climate extremes by achieving the carbon neutrality is calculated as follows:

$$\text{Reduction rate (\%)} = \frac{\Delta SSP_{370} - \Delta SSP_{119}}{\Delta SSP_{370}} \times 100 \quad (3)$$

where △ stands for the difference of the aggregated population exposure between the future (2071–2100) and historical (1985–2014) periods. Here, the changes in population exposure can

be attributed to the three factors, i.e., climate extreme, population, and climate extreme-population interaction factors (e.g., Jones et al., 2018; Lei et al., 2022; Zhang et al., 2022) as below:

$$\Delta SSP_{370} = P_{hist} \times \Delta C_{370} + C_{hist} \times \Delta P_{370} + \Delta C_{370} \times \Delta P_{370}$$

$$\Delta SSP_{119} = P_{hist} \times \Delta C_{119} + C_{hist} \times \Delta P_{119} + \Delta C_{119} \times \Delta P_{119} \quad (4)$$

where P and C are the population and the number of extreme days, respectively. The terms ΔP and ΔC are the changes in the population and number of extreme days in the future period with respect to the historical period, respectively. Subscripts of C and P denote the historical climate or SSP scenario. Therefore, the three terms on the right side of Eqn. (4) represent the roles of climate extreme (CLM), population (POP), and their interaction (INT) changes, respectively. By combining Eqns. (3–4), the reduction rate can be decomposed as follows:

$$\text{Reduction rate (\%)} = \frac{CLM_{370} - CLM_{119}}{\Delta SSP_{370}} \times 100 + \frac{POP_{370} - POP_{119}}{\Delta SSP_{370}} \times 100 + \frac{INT_{370} - INT_{119}}{\Delta SSP_{370}} \times 100 \quad (5)$$

The first term represents the contribution of climate extreme changes to the total reduction rate (%) of population exposure to climate extremes. Similarly, the second and third terms represent the contribution of population and climate extreme-population interaction changes, respectively, to the total reduction rate (%).

3. Results

3.1. Global population exposure to climate extremes

Figure 2 presents the time series of global population exposure to hot-temperature and

heavy-precipitation extremes for the period of 2015–2100 under the SSP1-1.9 and SSP3-7.0 scenarios compared to the historical period of 1985–2014. If global warming keeps continuing without a transition to the carbon-neutral society in the 2050s, the population exposures to hot-temperature and heavy-precipitation extremes that exceed the historical 30-year return values (Figures S2b and S2e) are anticipated to increase up to 192 billion and 1.87 billion person-days, respectively, at the end of the century (red lines in Figures 2a and 2b). Given the fact that population exposures in the historical period are 0.21 billion and 0.17 billion person-days, respectively, they are approximately 914 and 11 times larger than the historical values. The increasing trends are particularly noticeable after the 2050s. The inter-model spread does not cross the zero line after the year 2043 for hot-temperature extremes and the year 2067 for heavy-precipitation extremes. This indicates that increasing population exposures to climate extremes under the high-emission scenario are distinct in the late 21st century compared to the historical period. The same trends are also found when population is fixed to the historical level (orange lines in Figures 2a and 2b). However, they are only half of that with time-varying population (compare red and orange lines). This suggests that population changes and climate-population interaction changes are also important in determining population exposure to climate extremes in the high-emission scenario.

The transition to the carbon-neutral society in the 2050s results in a minimal shift in population exposure to climate extremes, accompanied by reduced model spread which indicates the robust multi-model projections (blue lines and shading in Figures 2c and 2d). The population exposure in the carbon neutrality scenario is less than one-tenth of that in the high-

emission scenario (compare Figures 2a,b and 2c,d; note the different scale of the *y*-axis between the two scenarios). The population exposures to hot-temperature and heavy-precipitation extremes slightly increase by approximately 4.65 billion and 0.19 billion person-days (approximately 22 and 1.12 times larger than the historical values), respectively, until the middle of the 21st century, then decrease afterward. However, these changes have a large uncertainty, with a model spread often crossing the zero line, revealing that future population exposures to climate extremes are indistinguishable from historical ones if the carbon neutrality is successfully achieved.

The reduced population exposures to hot-temperature and heavy-precipitation extremes by achieving the carbon neutrality are 187 billion and 1.68 billion person-days in the year 2100, respectively (Figures 2e and 2f). These correspond 90 and 98% reductions for heavy-precipitation and hot-temperature extremes, respectively, from the high-emission scenario (purple lines in Figures 2e and 2f). Inter-model spread does not cross the zero line in the late 21st century for both climate extremes. This result highlights the importance of carbon neutrality in mitigating climate change risks.

3.2. Regional population exposure to climate extremes

The increasing population exposure to climate extremes under the high-emission scenario is more pronounced in densely populated areas. Some land regions, where population is dense (Figure S3a), are expected to have an increasing population exposure to hot-temperature extremes by ten million person-days or more in 2071–2100 (Figure 3a). The people

238 in those regions are anticipated to experience more intense hot-temperature events, over 4 °C
239 hotter than the historical events (upper panel of Figure S4a). In particular, people living in
240 South America, Africa, Arabian Peninsula, and South Asia would be more frequently exposed
241 to heat-related extremes, more than 20 days per year, compared to those living in other regions
242 (bottom row of Figure S4a). For heavy-precipitation extremes, a large population exposure,
243 greater than one million person-days, is projected to occur only in African and Asia monsoon
244 regions (Figure 3b). It is expected that African and Asian people would experience more intense
245 (over 40 mm/day) and frequent (over 0.5–1.0 days per year) heavy-precipitation extremes
246 under the high-emission scenario (Figure S5a).

247 While the global population exposure to climate extremes may increase only
248 marginally under the carbon-neutral scenario, the regional changes remain noteworthy. The
249 large population exposure to hot-temperature extremes, greater than one million person-days,
250 is still found in the late 21st century in African and Asian monsoon regions as well as
251 Mediterranean and western Europe (Figure 3c). It contrasts to the population exposure to
252 heavy-precipitation extremes which is less than one-tenth million person-days in most regions
253 (Figure 3d). This result suggests that even if carbon neutrality is achieved, some regions could
254 be exposed to higher heat-related climate risks than the historical level. However, carbon
255 neutrality can still significantly reduce the number of people, exceeding ten million in each
256 region, who may potentially be exposed to climate extremes under the high-emission scenario
257 (Figures 3e and 3f).

258 To quantify the regional changes in the late 21st century, the area-aggregated total

population exposures to hot-temperature and heavy-precipitation extremes are calculated in Figures 4a and 4b. Globally, an increasing population exposure to hot-temperature extremes is projected to continue under the high-emission scenario, by approximately 106 billion person-days (the first bar in Figure 4a). This value is approximately 461 times higher than the historical value of 0.23 billion person-days. If carbon neutrality is achieved, only 2.50 billion person-days are expected to increase, with the population exposure to hot-temperature extremes being substantially reduced. Although much smaller than hot-temperature extremes, the globally-aggregated population exposure to heavy-precipitation extremes is also expected to increase up to 1.43 billion person-days in the high-emission scenario (approximately 7 times higher than 0.20 billion person-days in the historical period; see the leftmost bar in Figure 4b). If carbon neutrality is achieved, only 0.17 billion person-days are expected to increase, with the population exposure to heavy-precipitation extremes again being substantially reduced.

Such reductions are largest in African and Asian continents (AF and AS in Figures 4a and 4b). If the current "regional rivalry" for the carbon emissions policy is maintained, African and Asian continents would have the highest or second-highest population exposures to both hot-temperature and heavy-precipitation extremes in the late 21st century (Figures 4a and 4b). Their sum accounts for 79% of global population exposure to hot-temperature extremes and 88% of global population exposure to heavy-precipitation extremes. Here, it is important to note that African continent would become the region most suffering from increasing climate extremes despite its relatively low carbon emissions (Mann, 2023). It exemplifies an inequality of climate risk.

3.3. Benefits of carbon neutrality and its contributing factors

The impact of carbon neutrality is further examined by calculating the reduction rate of population exposure to climate extremes (Eq. 3; Figures 4c and 4d). The global reduction rates for hot-temperature and heavy-precipitation extremes in the late 21st century reach up to 98% and 87%, respectively (first gray bars in Figures 4c and 4d). The reduction rate for hot-temperature extremes is similar across all continents, ranging from 93 to 99% (Figure 4c). However, the reduction rate for heavy-precipitation extremes varies considerably from one continent to another, ranging from 20 to 91%, with the largest reduction in Africa, Asia, and South America (Figure 4d; see also Figure S7). This result suggests that the carbon neutrality can reduce the inequality of climate risk across continents.

The relative contributions of climate extreme, population, and their interaction changes on the reduction rate (Eq. 5) are further evaluated in Figures 4c and 4d. The climate extreme change itself explains about half of the global reduction rate (first red bars in Figures 4c and 4d). The contribution of population change is negligible (first yellow bars), while that of interaction change is comparable to climate extreme change (first blue bars). The latter is due to the enormous changes in Africa which is associated with significant future increases in both population and the number of extreme days across all regions of Africa (Figures S3f and S12; see also bottom panel of Figures S4 and S5). It suggests a synergistic effect between climate extreme and population changes in the African continent. Asia is also expected to experience significant increase in population and the number of extreme days (Figure S3g; see also bottom

301 panel of Figures S4 and S5). However, unlike Africa, interaction change contributes less than
302 climate extreme change (AS blue bars in Figures 4c and 4d). Given that climate extreme change
303 is positive across all regions of Asia (bottom panels of Figures S4 and S5), it results from the
304 opposing population trends from one country to another, i.e., an increasing trend in India but a
305 decreasing trend in China (Figure S12). Although South America also shows comparable
306 contributions of climate extreme and interaction changes (SA in Figures 4c and 4d), their
307 absolute values are much smaller than those in Africa and Asia (SA in Figures 4a and 4b).

308 In North America, Europe, and Oceania, the contribution of climate extreme change
309 surpasses that of the interaction change by more than twofold (compare red and blue color bars
310 of NA, EU, and OC in Figures 4c and 4d), because of rather slow and small population growth
311 under the high-emission scenario (Figures S3c, S3e, and S3h; see also Figure S13). In particular,
312 for heavy precipitation extremes, the climate extreme changes dominate the reduction rates in
313 these continents with even negative contributions of the population and interaction changes
314 (Figure 4d). It indicates that climate extreme change plays a predominant role in reducing the
315 population exposure to climate extremes in these continents. This result also suggests that the
316 potential benefits of carbon neutrality can be significant even in developed countries by
317 reducing the occurrence of climate extremes.

318

319 **3.4. Sensitivity to return intervals of climate extremes**

320 More intense climate extremes, that substantially deviate from their climatologies, can
321 result in more significant social damages, particularly when they are beyond the tolerable

ranges of ecological systems and human infrastructures. In this regard, the sensitivity of the reduction rate shown in Figures 4c and 4d to the return intervals of climate extremes is tested. The 10-, 30-, and 50-year return events are particularly considered (Figure 5). Note that all analyses in previous sections are conducted with 30-year return events and repeated here as references. The reduction rate increases for longer return events for hot-temperature extremes (Figure 5a), indicating an increasing benefit of carbon neutrality for more intense hot-temperature extremes. A small inter-model spread for longer return events further indicates that this benefit is robust across all continents (Figure 5a).

In contrast, the reduction rate for heavy-precipitation extremes does not systematically increase for longer return events (black lines in Figure 5b). The inter-model spread is also large, indicating that the risk of heavy-precipitation extremes has a relatively high uncertainty compared to hot-temperature extremes, presumably due to their localized and complex nature. In particular, North America, Europe, and Oceania show a relatively larger inter-model spread because of different climate sensitivity of individual models to the forcing. In these continents, climate extreme change is much more important than the other two factors, with increasing return intervals (Figure S8). Other continents, such as South America, Africa, and Asia, where the population exposure to heavy-precipitation extremes is high, show a relatively small inter-model spread, suggesting a relatively higher model consistency.

4. Discussion and conclusions

The present study evaluates the impact of carbon neutrality on population exposure to

343 climate extremes in the late 21st century. If the current “regional rivalry” over the carbon
344 emissions policy is maintained in this century, population exposures to hot-temperature and
345 heavy-precipitation extremes, exceeding their historical 30-year return values, are projected to
346 increase by 461 and 7 times, respectively, over the historical values. Such drastic increases can
347 be significantly reduced by 87–98% by achieving the carbon neutrality. This result supports
348 the critical importance of ongoing efforts to achieve net-zero carbon emissions by the 2050s to
349 reduce potential climate risks and their inequity across continents.

350 The reduction in population exposure to climate extremes through carbon neutrality is
351 greatest in Africa and Asia. However, as most countries in these continents are currently
352 developing (Figure S6), conflicts between carbon neutrality and economic development may
353 arise. Such conflicts may increase the uncertainty in future projection of population exposure
354 to climate extremes (e.g., Liu et al., 2017; Chen & Suh, 2021; Lei et al., 2022). Another point
355 of note is the contrasting population trends projected for Asian countries, i.e., an increasing
356 trend in India but a decreasing trend in China (Figure S12). This calls for further investigation
357 into the potential benefits of carbon neutrality for individual countries (e.g., Das et al., 2022;
358 Xie et al., 2022). In North America, Europe, and Oceania, reducing climate extremes by
359 achieving carbon neutrality plays a more important role than population decline in reducing
360 population exposure to climate extremes. This indicates that the potential benefits of carbon
361 neutrality can be substantial even in developed countries. It becomes more apparent when
362 considering more intense hot-temperature extremes, for which the reduction rates are much
363 larger with a better agreement between the models (i.e., smaller inter-model spread).

The findings of the present study do not hold only for extremely rare events. Other extreme indices of temperature and precipitation (Zhang et al. 2011) consistently show the net benefits of carbon neutrality (Figures S9–S11). Among others, the number of consecutive dry days, representing drought, in South America and Africa is projected to decrease considerably from the high-emission to carbon-neutrality scenarios (Figures S10o and S10p). This result is consistent with Park et al. (2018), who reported that limiting global warming to 1.5°C constrains the emergence of aridification.

The year of net-zero carbon emissions in the SSP1-1.9 scenario is decades earlier than in other mitigation scenarios (e.g., SSP1-2.6), resulting in weaker warming in the late 21st century (Meinshausen et al., 2020). By conducting the sensitivity experiments for a net-zero carbon emission year by 2050 and 2060, Lei et al. (2022) reported that more active carbon neutrality policy could further reduce the population exposure to heat extremes. The present study supports the need for more active net-zero carbon emissions policy by the 2050s.

It should be recalled that this study is based on concentration-driven simulations from the CMIP6 project (Quilcaille et al., 2023). The concentration-driven simulations often exaggerate future climate changes compared to the emission-driven simulations (Nicholls et al., 2021; Quilcaille et al., 2023). In this regard, the emissions-driven simulations may be more useful for investigating the merits of the Paris Agreement's goals (Terhaar et al., 2022).

While this study has addressed the impact of carbon neutrality on climate extremes and population exposure, it is still important to explore the importance of vulnerability which serves as a critical determinant in assessing the extent to which communities and ecosystems

fare in a warming climate (Cardona et al., 2012; Jones et al., 2018). Because vulnerability depends on regional location, social and economic development, and the nature of climate extremes (e.g., Cardona et al., 2012; Jones et al., 2018), assessing the impact of carbon neutrality on vulnerability may be useful in developing and implementing equitable and sustainable climate risk mitigation strategies.

Acknowledgements

This research was supported by Basic Science Research Program through the National Research Foundation of Korea (NRF) funded by the Ministry of Education (RS-2023-00238065). This research was also supported by the Research Program for the carbon cycle between oceans, land, and atmosphere of the NRF funded by the Ministry of Science and ICT (2021M3I6A1086807), and Korea Environment Industry & Technology Institute (KEITI) through Project for developing an observation-based GHG emissions geospatial information map, funded by Korea Ministry of Environment (MOE) (RS-2023-00232066). All authors thank every group involved in Coupled Model Intercomparison Project Phase 6 (CMIP6) model output data provided by World Climate Research Programme (WCRP) CMIP6 Community. We also thank Jones & O'Neill and Iturbide & co-authors for sharing their dataset and providing guidance. Special thanks for two anonymous reviewers for their relevant contribution in the different processes of the revisions of this work.

Conflict of Interest

The authors declare no conflicts of interest relevant to this study.

Open Research

The data of eight global climate models from the Coupled Model Intercomparison Project Phase 6 (CMIP6) can be accessed at https://esgf-node.llnl.gov/search/cmip6/, and can also be accessed in Eyring et al. (2016). The projected gridded population dataset under Shared Socioeconomic Pathway 1 (SSP1) and SSP3 scenarios can be obtained in Jones and O'Neill (2016) or via http://sedac.ciesin.columbia.edu/data/set/popdynamics-1-8th-pop-base-year-projection-ssp-2000-2100-rev01/data-download. The mask dataset for the six continents in this study is available in Iturbide et al. (2020). The above raw data were post-processed using Fortran90 (https://www.intel.com/content/www/us/en/developer/articles/tool/oneapi-standalone-components.html#fortran), R version 4.0.3 (https://cran.r-project.org/bin/windows/base/old/4.0.3/), Grads version 2.2.1 (http://cola.gmu.edu/grads/downloads.php). The relevant post-processed dataset and analysis codes for Figures 1 to 5 in the main text are available at https://zenodo.org/records/10408749

Author contributions

All authors contributed to the study conception and design. Material preparation, data collection and analysis were performed by S.-G. Oh under supervision of S.-W. Son. The first draft of the manuscript was written by S.-G. Oh, J. Choi, M.-J. Kang, S. Jeong, S.-K. Min, S.-W. Yeh, Y.-H. Kim, and S.-W. Son and all authors commented on previous versions of the

manuscript. All authors read and approved the final manuscript.

Additional information

The methods and results of the model evaluation for the historical period of 1985–2014 are presented in the Supporting Information. The future changes in intensity and frequency of climate extremes under the SSP1-1.9 and SSP3-7.0 scenarios are also discussed in the Supporting Information.

References

Cardona, O. D., van Aalst, M. K., Birkmann, J., Fordham, M., McGregor, G., & Perez, R., et al. (2012). in Determinants of risk: exposure and vulnerability (eds Field, C. B. et al.) *Managing the Risks of Extreme Events and Disasters to Advance Climate Change Adaptation*. pp. 65–108 (Cambridge University Press, Cambridge, UK, and New York, NY, USA, 2012). A Special Report of Working Groups I and II of the Intergovernmental Panel on Climate Change (IPCC).

Chen, H., & Sun, J. (2021). Significant increase of the global population exposure to increased precipitation extremes in the future. *Earth's Future*, *9(9)*, e2020EF001941.

Das, J., Manikanta, V., & Umamahesh, N. V. (2022). Population exposure to compound extreme events in India under different emission and population scenarios. *Science of The Total Environment*, *806*, 150424.

Eyring, V., Bony, S., Meehl, G. A., Senior C. A., Stevens, B., Stouffer, R. J., & Taylor K. E.

448 (2016). Overview of the coupled model intercomparison project phase 6 (CMIP6)
449 experimental design and organization [Dataset]. *Geoscientific Model Development*, *9*,
450 1937–1958.

451 Gidden, M. J., Riahi, K., Smith, S. J., Fujimori, S., Luderer, G., & Kriegler, E. et al. (2018).
452 Global emissions pathways under different socioeconomic scenarios for use in CMIP6:
453 a dataset of harmonized emissions trajectories through the end of the century. *Geosci.*
454 *Model Dev. Discuss.*, https://doi.org/10.5194/gmd-2018-266

455 Hosking, J. R. M. (1990). L-moments: analysis and estimation of distributions using linear
456 combinations of order statistics. *Journal of the Royal Statistical Society*, *522*, 105–124.

457 Iturbide, M., Gutierrez, J. M., Alves, L. M., Bedia, J., Cerezo-Mota, R., & Cimadevilla E., et
458 al. (2020). An update of IPCC climate reference regions for subcontinental analysis of
459 climate model data: definition and aggregated datasets [Dataset]. *Earth System Science*
460 *Data*, *12*, 2959–2970.

461 Jo, S. Y., Seong, M. G., Min, S. K., Kug, J. S., Yeh, S. W., & An, S. I., et al. (2022). Hysteresis
462 behaviors in East Asian extreme precipitation frequency to CO2 pathway. *Geophysical*
463 *Research Letters*, *49*, e2022GL099814.

464 Jones, B., & O'Neill B. C. (2016). Spatially explicit global population scenarios consistent with
465 the shared socioeconomic pathways [Dataset]. *Environmental Research Letters*, *11*,
466 084003.

467 Jones, B., Tebaldi, C., O'Neill B. C., Oleson, K., & Gao J. (2018). Avoiding population

468 exposure to heat-related extremes: demographic change vs climate change. *Climatic*
469 *Change*, *146*, 423–472.

470 Kharin, V. V., Zwiers, F. W., Zhang, X., & Wehner, M. (2013). Changes in temperature and
471 precipitation extremes in the CMIP5 ensemble. *Climatic Change*, *119*, 345–357.

472 Kim, S. K., Shin, J., An, S. I., Kim, H. J., Im, N., & Xie, S. P., et al. (2022). Widespread
473 irreversible changes in surface temperature and precipitation in response to CO2 forcing.
474 *Nature Climate Change*, *12*, 834–840.

475 Kim, Y. H., Min, S. K., Zhang, X., Sillmann, J., & Sandstad, M. (2020). Evaluation of the
476 CMIP6 multi-model ensemble for climate extreme indices. *Weather and Climate*
477 *Extremes*, *29*, 100269.

478 King, A. D., Borowiak, A., Brown, J. R., Frame, D. J., Harrington, L. J., & Min, S. K., et al.
479 (2021). Transient and quasi-equilibrium climate states at 1.5°C and 2°C global warming.
480 *Earth's Future*, *9*, https://doi.org/10.1029/2021EF002274

481 Lei, Y., Wang, Z., Zhang, X., Che, H., Yue, X., & Tian, C., et al. (2022). Avoided population
482 exposure to extreme heat under two scenarios of global carbon neutrality by 2050 and
483 2060. *Environmental Research Letters*, *17*, 094041.

484 Li, C., Zwiers, F., Zhang, X., Li, G., Sun, Y., & Wehner, M. (2021). Changes in annual extremes
485 of daily temperature and precipitation in CMIP6 model. *Journal of Climate*, *34*, 3441–
486 3460.

487 Liu, Z., Anderson, B., Yan, K., Dong, W., Liao, H., & Shi, P. (2017). Global and regional

changes in exposure to extreme heat and the relative contributions of climate and population change. *Scientific Reports*, *7*(1), 43909.

Mann, M. E. (2023, October 24). G*reenhouse gas*. *Encyclopedia Britannica*. https://www.britannica.com/science/greenhouse-gas

Meinshausen, M., Nicholls, Z. R., Lewis, J., Gidden, M. J., Vogel, E., Freund, M., ... & Wang, R. H. (2020). The shared socio-economic pathway (SSP) greenhouse gas concentrations and their extensions to 2500. *Geoscientific Model Development*, *13*(8), 3571-3605.

Nashwan, M. S., & Shahid, S. (2022). Future precipitation changes in Egypt under the 1.5 and 2.0°C global warming goals using CMIP6 multimodel ensemble. *Atmospheric Research*, *265*, 105908.

Nicholls, Z., Meinshausen, M., Lewis, J., Corradi, M. R., Dorheim, K., Gasser, T., ... & Woodard, D. L. (2021). Reduced complexity Model Intercomparison Project Phase 2: Synthesizing Earth system knowledge for probabilistic climate projections. *Earth's Future*, *9*(6), e2020EF001900.

Oin, J., Su, B., Tao, H., Wang, Y., Huang, J., & Jiang T. (2021). Projection of temperature and precipitation under SSPs-RCPs scenarios over northwest China. *Frontiers of Earth Science*, *15(1)*, 23–37.

O'Neill, B. C., Tebaldi, C., van Vuuren, D. P., Eyring, V., Friedlingstein, P., & Hurtt, G., et al. (2016). The scenario model intercomparison project (ScenarioMIP) for CMIP6. *Geoscientific Model Development*, *9*, 3461–3482.

508 Park, C. E., Jeong, S. J., Joshi, M., Osborn, T. J., Ho, C. H., & Piao, S., et al. (2018). Keeping
509 global warming within 1.5°C constrains emergence of aridification. *Nature Climate*
510 *Change*, *8*, 70–74.

511 Quilcaille, Y., Gasser, T., Ciais, P., & Boucher, O. (2023). CMIP6 simulations with the compact
512 Earth system model OSCAR v3. 1. *Geoscientific Model Development*, *16*(3), 1129–
513 1161.

514 Terhaar, J., Frölicher, T. L., Aschwanden, M. T., Friedlingstein, P., & Joos, F. (2022). Adaptive
515 emission reduction approach to reach any global warming target. *Nature climate*
516 *change*, *12*(12), 1136–1142.

517 UNFCCC (2015). Conference of the Parties. Adoption of the Paris Agreement.
518 FCCC/CP/2015/10/Add.1, pp. 1–32, Paris.

519 Xie, W., Zhou, B., Han, Z., & Xu Y. (2022). Substantial increase in daytime-nighttime
520 compound heat waves and associated population exposure in China projected by the
521 CMIP6 multimodel ensemble. *Environmental Research Letters*, *17*, 045007.

522 Zhang, G., Wang, H., Gan, Y. Y., Zhang, S., Shi, L., & Zhao, J., et al. (2022). Climate change
523 determines future population exposure to summertime compound dry and hot events.
524 *Earth's Future*, *10(11)*, e2022EF003015.

525 Zhang, W., Zhou, T., Zou, L., Zhang, L., & Chen, X. (2018). Reduced exposure to extreme
526 precipitation from 0.5°C less warming in global land monsoon regions. *Nature*
527 *Communications*, *9*, 3153.

528 Zhang, X., Alexander, L., Hegerl, G. C., Jones, P., Tank, A. K., & Peterson, T. C. (2011) Indices
529 for monitoring changes in extremes based on daily temperature and precipitation data.
530 *WIREs Climate Chang*, *2*, 851–870.

531

532

533

534

535

536

537

538

539

540

541

542

543

544

545

546

547

548

549 **Table 1.** CMIP6 models used in this study.

No.	Model	Ensemble information	Institution	Horizontal Resolution (Lon x Lat)
1	CanESM5	r1i1p1f1	Canadian Earth System Model version 5, Canadian Centre for Climate Modelling and Analysis (Canada)	128 x 64
2	CNRM-ESM2-1	r1i1p1f2	National Center for Meteorological Research (France)	256 x 128
3	EC-Earth3	r4i1p1f1	ICHEC, The Irish Centre for High-End Computing, National University of Ireland (Ireland)	512 x 256
4	GFDL-ESM4	r1i1p1f1	NOAA/Geophysical Fluid Dynamics Laboratory, Earth System Model version 4 (USA)	288 x 180
5	MIROC-ES2L	r1i1p1f2	Atmosphere and Ocean Research Institute (The University of Tokyo), National Institute for Environmental Studies, and Japan Agency for Marine-Earth Science and Technology (Japan)	128 x 64
6	MPI-ESM-LR	r1i1p1f1	Max Planck Institute for Meteorology (Germany)	192 x 96
7	MRI-ESM2-0	r1i1p1f1	Meteorological Research Institute (Japan)	320 x 160
8	UKESM1-0-LL	r1i1p1f2	Met Office Hadley Centre (UK)	192 x 144

550

551

552

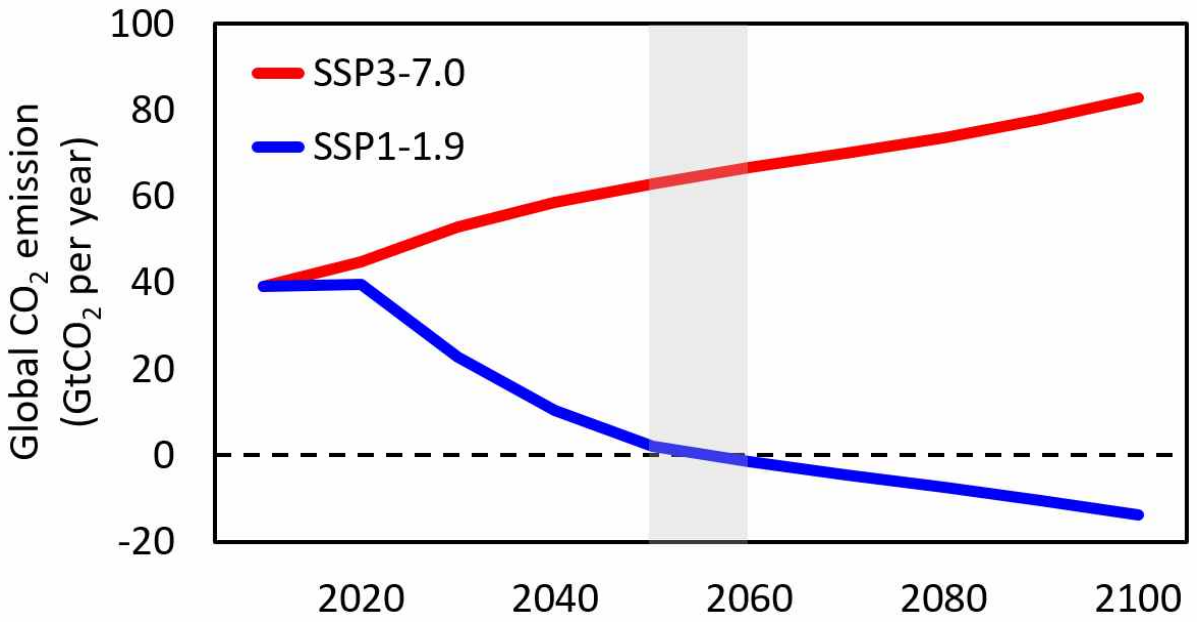

Figure 1. Time series of global CO_2 emissions in SSP1-1.9 and SSP3-7.0 scenarios. The vertical gray shading indicates the 2050s when net-zero emissions are achieved in the SSP1-1.9 scenario.

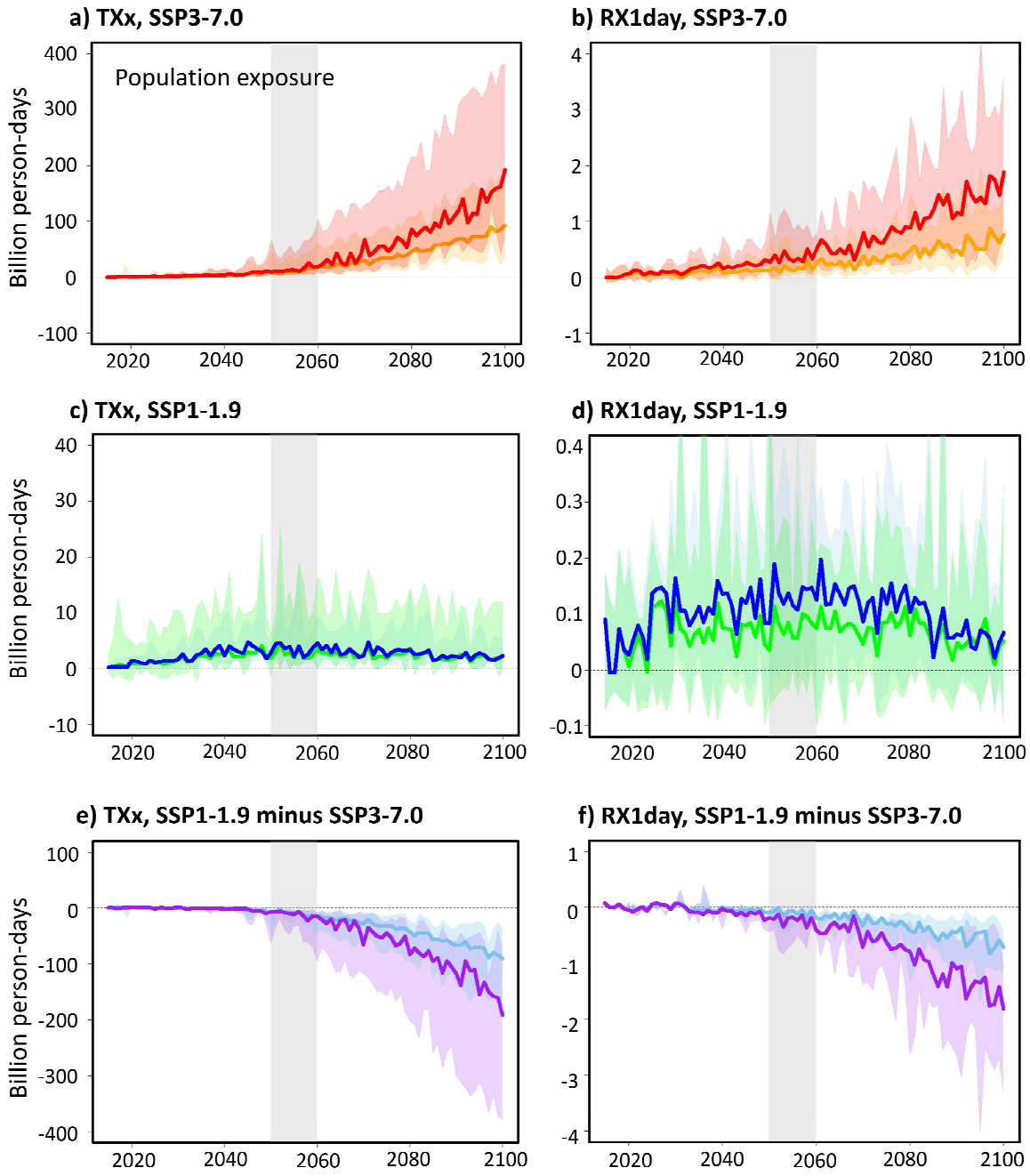

557

558 **Figure 2.** Temporal evolution of global population exposure to climate extremes. Time series
559 of global population exposure (unit: person-days) to 30-year return events of (a) hot-
560 temperature (TXx) and (b) heavy-precipitation (RX1day) for the period of 2015–2100. Blue

and red lines indicate the CMIP6 multi-model ensemble median with population change under SSP1-1.9 and SSP3-7.0 scenarios against the historical period of 1985–2014. Green and orange lines are the same as blue and red ones but with a fixed population to the historical period. Purple and sky-blue lines in the bottom row are the differences between SSP1-1.9 and SSP3-7.0 scenarios with time-varying and time-fixed populations, respectively. Shadings indicates the inter-model spread defined by the full range (min-max) for each scenario. The vertical gray shading denotes the 2050s when net-zero CO2 emissions occur in Fig. 1. Note that the range of the y-axis in SSP1-1.9 scenario is only one-tenth of that in SSP3-7.0 scenario.

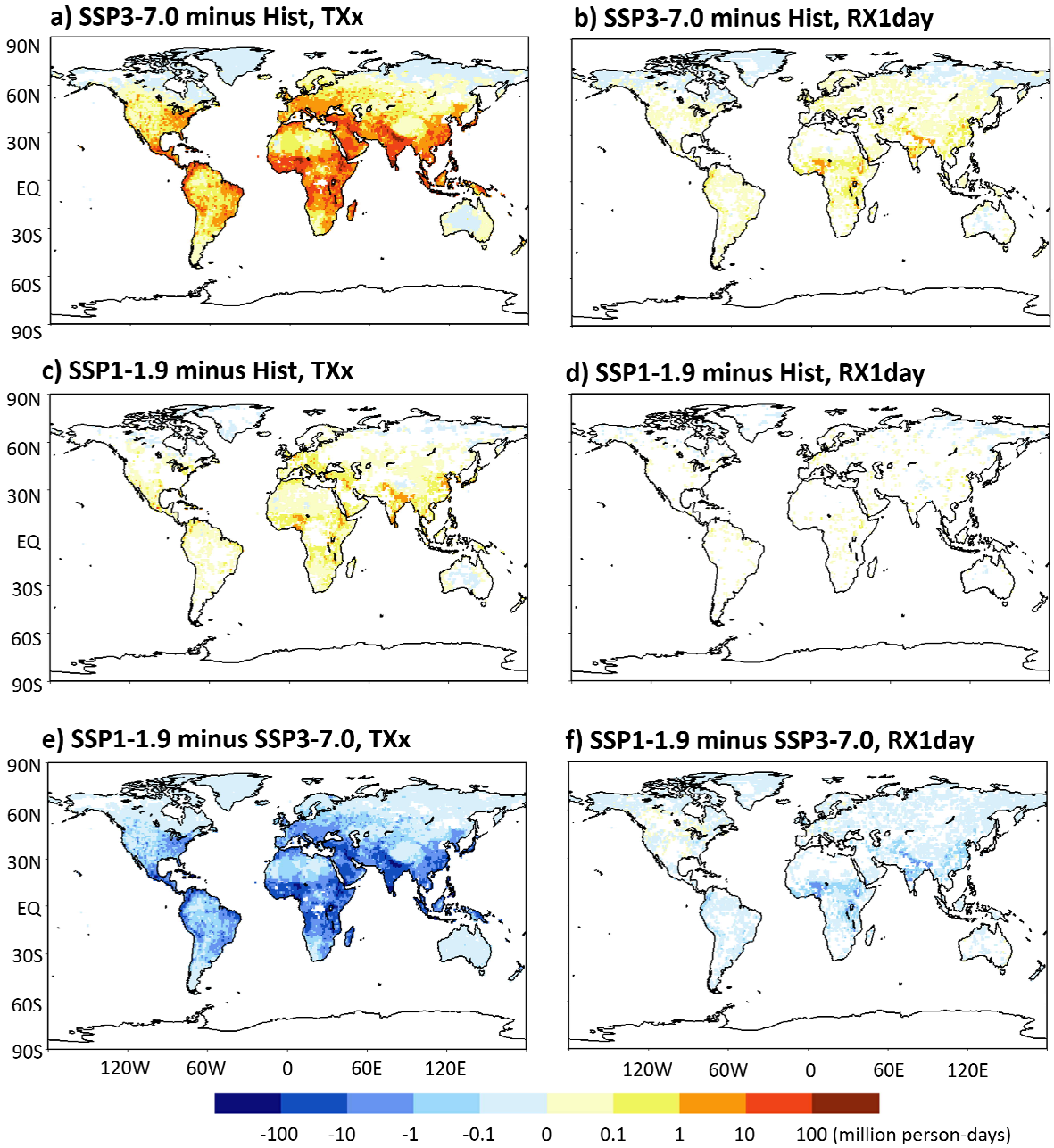

573

574 **Figure 3.** Projected changes of 30-year mean population exposure to climate extremes in the
575 late 21st century (2071–2100) compared to the historical period of 1985–2014. Changes of the
576 population exposure (unit: person-days) to 30-year return events of hot-temperature extreme

(TXx) under (a) SSP3-7.0 and (c) SSP1-1.9 scenarios and (e) their differences. Only grids where more than three-quarters of the models show the same sign to the multi-model ensemble median are presented. (b, d, f) Same as (a, c, e), but for heavy-precipitation extreme (RX1day).

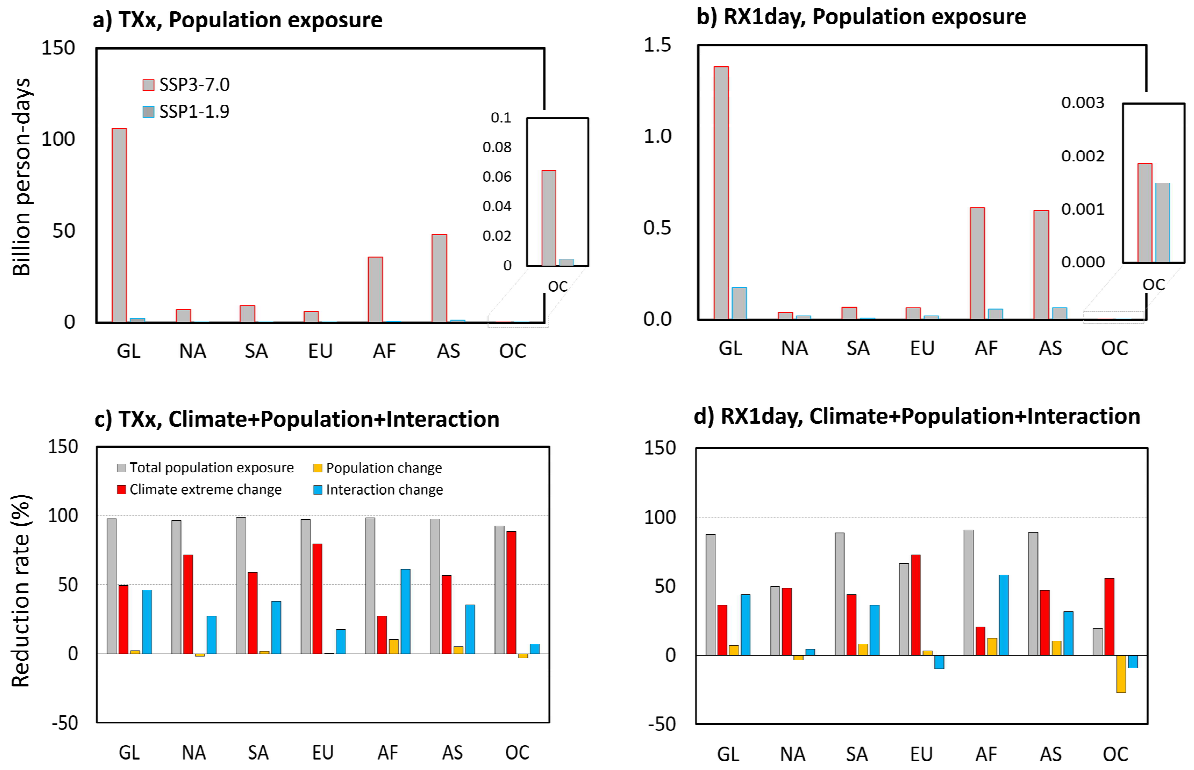

594

595 **Figure 4.** Changes of 30-year mean regionally-aggregated population exposures to climate
596 extremes in the late 21st century (2071–2100) compared to the historical (1985–2014) values,
597 and their reduction rate from SSP3-7.0 to SSP1-1.9 scenarios. (a) Area-aggregated population
598 exposure to 30-year return events of TXx over the globe (GL), North America (NA), South
599 America (SA), Europe (EU), Africa (AF), Asia (AS), and Oceania (OC). Red and blue outlined
600 bars indicate the SSP3-7.0 and SSP1-1.9 scenarios, respectively. (c) The reduction rate (%) of
601 population exposure to TXx from SSP3-7.0 scenario to SSP1-1.9 scenarios (gray), and the
602 relative contributions of climate (red), population (yellow), and climate-population interaction
603 (blue) changes. (b, d) Same as (a, c) but for RX1day. Note that the range of the y-axis is
604 different in (a) and (b).

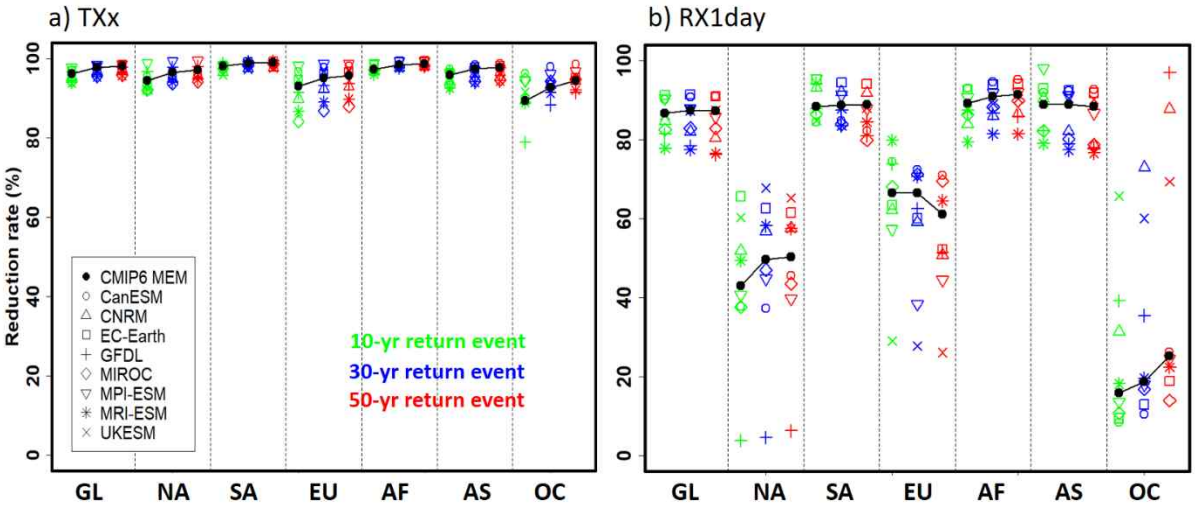

Figure 5. Regionally-aggregated reduction rate of population exposures to climate extremes for varying return periods. Area-averaged reduction rate (%) of population exposure to (a) TXx and (b) RX1day is shown for 10-year (green), 30-year (blue), and 50-year (red) return events. The periods of 1985–2014 and 2071–2100 are used as in Figs. 3c and d. Closed circles denote the CMIP6 multi-model ensemble median results, whereas other marks indicate individual models.

[Earth's Future]

Supporting Information for

Significant reduction of unequal population exposure to climate extremes by achieving the carbon neutrality

Seok-Geun Oh[1], Jung Choi[1], Min-Jee Kang[1], Sujong Jeong[2,3], Seung-Ki Min[4,5], Sang-Wook Yeh[6], Yeon-Hee Kim[4], and Seok-Woo Son[1,3*]

[1]School of Earth and Environmental Sciences, Seoul National University, Seoul, South Korea

[2]Department of Environmental Planning, Seoul National University, Seoul, South Korea

[3]Climate Technology Center, Seoul National University, Seoul, South Korea

[4]Division of Environmental Science and Engineering, Pohang University of Science and Technology, Pohang, Gyeongbuk, South Korea

[5]Institute for Convergence Research and Education in Advanced Technology, Yonsei University, Incheon, Republic of Korea

[6]Department of Marine Science and Convergence Engineering, Hanyang University, ERICA, Ansan, South Korea

December 2023

***Corresponding author:** Seok-Woo Son (seokwooson@snu.ac.kr)

Contents of this file

- **Text S1 to S3**
- **Figures S1 to S13**

Text S1. Model evaluation.

The fifth generation of the European Centre for Medium-Range Weather Forecast global reanalysis (ERA5, Hersbach et al. 2020) for the historical period of 1985–2014 is used as reference to evaluate the Coupled Model Intercomparison Phase 6 (CMIP6) models. The ERA5 data has higher spatial (30 km) and time resolution (hourly) than the other reanalysis data (i.e., ERA40, Uppala et al. 2005; ERA-Interim, Dee et al., 2011; NCEP/NCAR Reanalysis 1, Kalnay et al., 1996; NCEP-DOE Reanalysis 2, Kanamitsu et al., 2002), potentially making it more suitable to estimate and evaluate the climate extremes. Therefore, this dataset has been widely utilized as a reference data for temperature and precipitation extremes (e.g., Kim et al., 2020; Li et al., 2021; Oh & Sushama, 2021). The daily temperature and precipitation data at approximately 30 km resolution into common into 1°×1° grid and then calculated climate extreme indices, TXx and RX1day (Zhang et al. 2011), and Generalized Extreme Value (GEV) estimation to reduce the difference in spatial scales from CMIP6 models (1–2°).

This study uses the multi-model ensemble median (MEM), which is a more valid representative measure than the multi-model mean, because extremely large or small values can distort the mean. The model performance is basically evaluated based on the bias, root-mean-square error (RMSE), and correlation for spatial patterns of the estimated extreme values for the historical period of 1985–2014. The equations of the bias, RMSE and correlation are as

follow:

$$bias = \frac{1}{n}\sum_{i=1}^{n}(M_i - R_i)$$

$$RMSE = \sqrt{\frac{1}{n}\sum_{i=1}^{n}(M_i - R_i)^2}$$

$$correlation = \frac{\sum_{i=1}^{n}(M_i - \bar{M})(R_i - \bar{R})}{\sqrt{\sum_{i=1}^{n}(M_i - \bar{M})}\sqrt{\sum_{i=1}^{n}(R_i - \bar{R})}}$$

where n is the number of the total grids at land areas. The M_i and R_i denote the model and reanalysis at i th grid, respectively. The $\bar{M}$ nd $\bar{R}$ present the mean values over the land areas in the model and reanalysis, respectively. To compare the performance of MEM with that of each model, the combined metric of the RMSE and Taylor skill score (TSS, Taylor, 2001) is also used. The equation of TSS is like below:

$$TSS = \frac{(1 + correlation)^4}{4(SDR + \frac{1}{SDR})^2}$$

where SDR is the ratio of the spatial standard deviations of the model against to that of the reanalysis data. This score quantifies the similarity in the distribution and amplitude of the spatial pattern between the model and the reanalysis. The relative RMSE and TSS for each model and MEM are calculated by using their median values.

Text S2. Performance of CMIP6 MEM for historical period.

Compared with the ERA5 data, the CMIP6 MEM reproduces the spatial distribution

of the 30-year return value of TXx and RX1day reasonably well for the historical period of 1985–2014, with the spatial correlations of 0.95 and 0.84, respectively (Figures S2a–S2f). The 30-year return value of TXx is slightly overestimated by 0.1 to 3.0 °C in most land areas except for the high-latitude regions of the Northern Hemisphere, resulting in the global land average bias of 0.28 °C (Figure S2c). For the 30-year return value of RX1day, the CMIP6 MEM well captures typical large-scale features such as the intense precipitation extreme in the intertropical convergence zone (ITCZ) and African and Asian monsoon regions. However, the models underestimate the extreme precipitation by 20 to 100 mm/day depending precipitation zone, resulting in a global land average bias of -11.41 mm/day (Figure S2f).

Compared to a single model, the MEM shows a better performance in both the 30-year return values of TXx and RX1day (Figure S2g and S2h). This result is consistent with previous studies showing that the multi-model ensemble shows superior performance in reproducing mean and extreme climates than a single model (e.g., Oh & Suh, 2017; Kim et al., 2020; Li et al., 2021). Similar results are found for other return events, i.e., 10- and 50-year return value (not shown). It provides justification for the use of the CMIP6 MEM for future projection of the rare extreme events with varying return years.

Text S3. Response of climate extremes in the late 21st century to carbon neutrality.

If the current global warming is continued (i.e., SSP3-7.0 scenario), hot-temperature and heavy-precipitation extremes are expected to be strengthened in the late 21st century. The hot-temperature extreme is projected to experience a more intense warming event of above

4 °C over all land regions except Greenland (the first row of Figure S4a). Such extreme is expected to occur more than total 1000 days in South America, Africa, Arabia peninsula, and South Asia regions during the future period of 2071–2100 (the second row of Figure S4a). The heavy-precipitation extreme also reveals more intense and frequent events (Figure S5a) particularly in the African and Asian monsoon region where a dense population exists (Figure S3a).

Even if the transition to a carbon-neutral society is successful (i.e., SSP1-1.9 scenario), the intensity in both hot-temperature and heavy-precipitation extremes are still expected to increase with a range of 0.5–2°C and 0–20 mm/day, respectively. On a global average, the number of days in hot-temperature (heavy-precipitation) extreme increases up to total 100 days (5 days) compared to the historical period (Figures S4b and S5b). Although more intense and frequent climate extremes are also evident in the carbon neutrality scenario, the reduction rates, which estimate the benefit of carbon neutrality compared to the high emission scenario, are substantially large (Figures S4c and S5c; see Methods in main paper). Globally, a 71% decrease is found in the intensity of hot-temperature extreme (the first row of Figure S4c), while a more significant decrease (97%) is found in its frequency (the second row of Figure S4c). Similar reduction rates are revealed in the heavy-precipitation extreme, i.e., 75 and 76% decreases in its intensity and frequency, respectively (Figure S5c).

The difference between the scenarios with and without the net-zero carbon emission shows a large regional dependency, especially for the frequency (Figures S4c and S5c). For example, the frequency of the hot-temperature extreme exhibits large differences in the South

America, African, and Asian continents, while that of heavy-precipitation extreme shows a large difference in the African, North America, and Asian continents. Interestingly, the reduction rates of the intensity and frequency of the hot-temperature extremes are 68–81% and 94–98%, respectively, which implies a higher benefit of carbon neutrality in the frequency than in the intensity for all the continents (Figures S4c). On the other hand, the intensity and frequency of the heavy-precipitation extremes are reduced by 66–85% and 69–87% in net-zero carbon emission scenario, respectively. This result suggests that there are larger differences in reduction rate across continents, but smaller differences between frequency and intensity compared to hot-temperature extreme (Figure S5c). In summary, a transition to a carbon-neutral society around 2050 can lead to a more than twofold of reduction in both the intensity and frequency of hot-temperature and heavy-precipitation extremes for all the continents.

Acknowledgements

This research was supported by Basic Science Research Program through the National Research Foundation of Korea (NRF) funded by the Ministry of Education (RS-2023-00238065). This research was also supported by the Research Program for the carbon cycle between oceans, land, and atmosphere of the NRF funded by the Ministry of Science and ICT (2021M3I6A1086807), and Korea Environment Industry & Technology Institute (KEITI) through Project for developing an observation-based GHG emissions geospatial information map, funded by Korea Ministry of Environment (MOE) (RS-2023-00232066).

Reference

Dee, D. P., Uppala, S. M., Simmons, A. J., Berrisford, P., Poli, P., & Kobayashi, S., et al. (2011). The ERA-Interim reanalysis: configuration and performance of the data assimilation system. *Quarterly Journal of the Royal Meteorological Society*, *137*, 553–597.

Hersbach, H., Bell, B., Berrisford, P., Hirahara, S., Horanyi, A., & Munoz-Sabater, J., et al. (2020). The ERA5 global reanalysis. *Quarterly Journal of the Royal Meteorological Society*, *146*, https://doi.org/10.1002/qj.3803.

Kalnay, E., Kanamitsu, M., Kistler, R., Collins, W., Deaven, D., & Gandin, L., et al. (1996). The NCEP/NCAR 40-year reanalysis project. *Bulletin of the American Meteorological Society*, *77*, 437–472.

Kanamitsu, M., Ebisuzaki, W., Woollen, J., Yang, S.-K., Hnilo, J. J., & Fiorino, M., et al. (2002). NCEP-DOE AMIP-II reanalysis (R-2). *Bulletin of the American Meteorological Society*, *83*, 1631–1643.

Kim, Y. H., Min, S. K., Zhang, X., Sillmann, J., & Sandstad, M. (2020). Evaluation of the CMIP6 multi-model ensemble for climate extreme indices. *Weather and Climate Extremes*, *29*, 100269.

Kummu, M., Taka, M., & Guillaume, J. H. A. (2018). Gridded global datasets for gross domestic product and human development index over 1990 2015. *Scientific data*, *5*, 180004.

Li, C., Zwiers, F., Zhang, X., Li, G., Sun, Y., & Wehner, M. (2021). Changes in annual extremes of daily temperature and precipitation in CMIP6 model. *Journal of Climate*, *34*, 3441–3460.

761 Oh, S. G. & Sushama, L. (2021). Urban-climate interactions during summer over eastern North
762 America. *Climate Dynamics*, *57*, 3015–3028.

763 Oh, S. G., & Suh, M. S. (2017). Comparison of projection skills of deterministic ensemble
764 methods using pseudo-simulation data generated from multivariate Gaussian
765 distribution. *Theoretical and Applied Climatology*, 129, 243–262 .

766 Taylor K. E. (2001) Summarizing multiple aspects of model performance in a single diagram.
767 *Journal of Geophysical Research*, *106*, 7183–7192.

768 Uppala, S. M., KÅllberg, P. W., Simmons, A. J., Andrae, U., Bechtold, V. D. C., & Fiorino, M.,
769 et al. (2005). The ERA-40 Reanalysis. *Quarterly Journal of the Royal*
770 *Meteorological Society*, *131*, 2961–3012.

771 Zhang, W., Zhou, T., Zou, L., Zhang, L., & Chen, X. (2018). Reduced exposure to extreme
772 precipitation from 0.5°C less warming in global land monsoon regions. *Nature*
773 *Communications*, *9*, 3153.

774

775

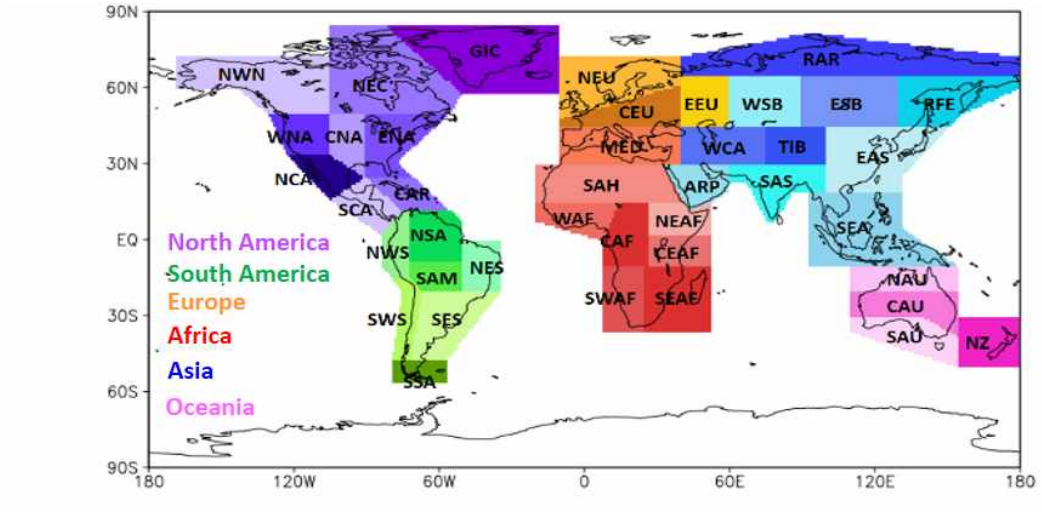

776

777 **Figure S1.** Sub-regional domain in the global land adopted from Iturbide et al. (2020). The
778 shaded colors indicate different continents: North America (purple series), South America
779 (green), Europe (orange), Africa (red), Asia (blue), and Oceania (pink).

780

781

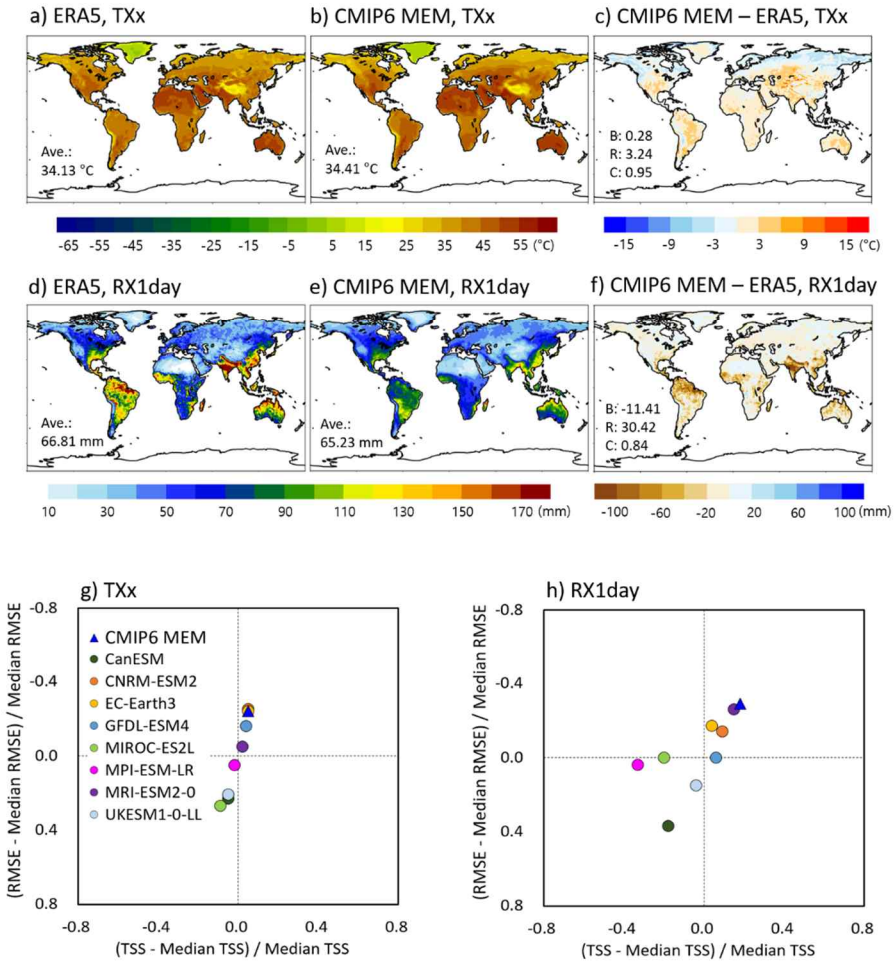

782

783 **Figure S2.** Estimates of 30-year return values of hot-temperature (TXx) and heavy-
784 precipitation (RX1day) extremes of (a, d) ERA5 reference data and (b, e) CMIP6 multi-model
785 ensemble median for the present period of 1985–2014, and (c, f) their differences. The area-
786 averaged value (Ave.), bias (B), root-mean-square error (R), and correlation (C) between the
787 CMIP6 multi-model ensemble median and ERA5 are indicated in sub-plot. Only land areas are
788 considered. (g, h) The relative performance of the CMIP6 models for 30-year return values of
789 TXx and RX1day, based on the root-mean-square error (RMSE) and Taylor skill score (TSS).
790 The symbol closer to the upper right corner indicates better performance.

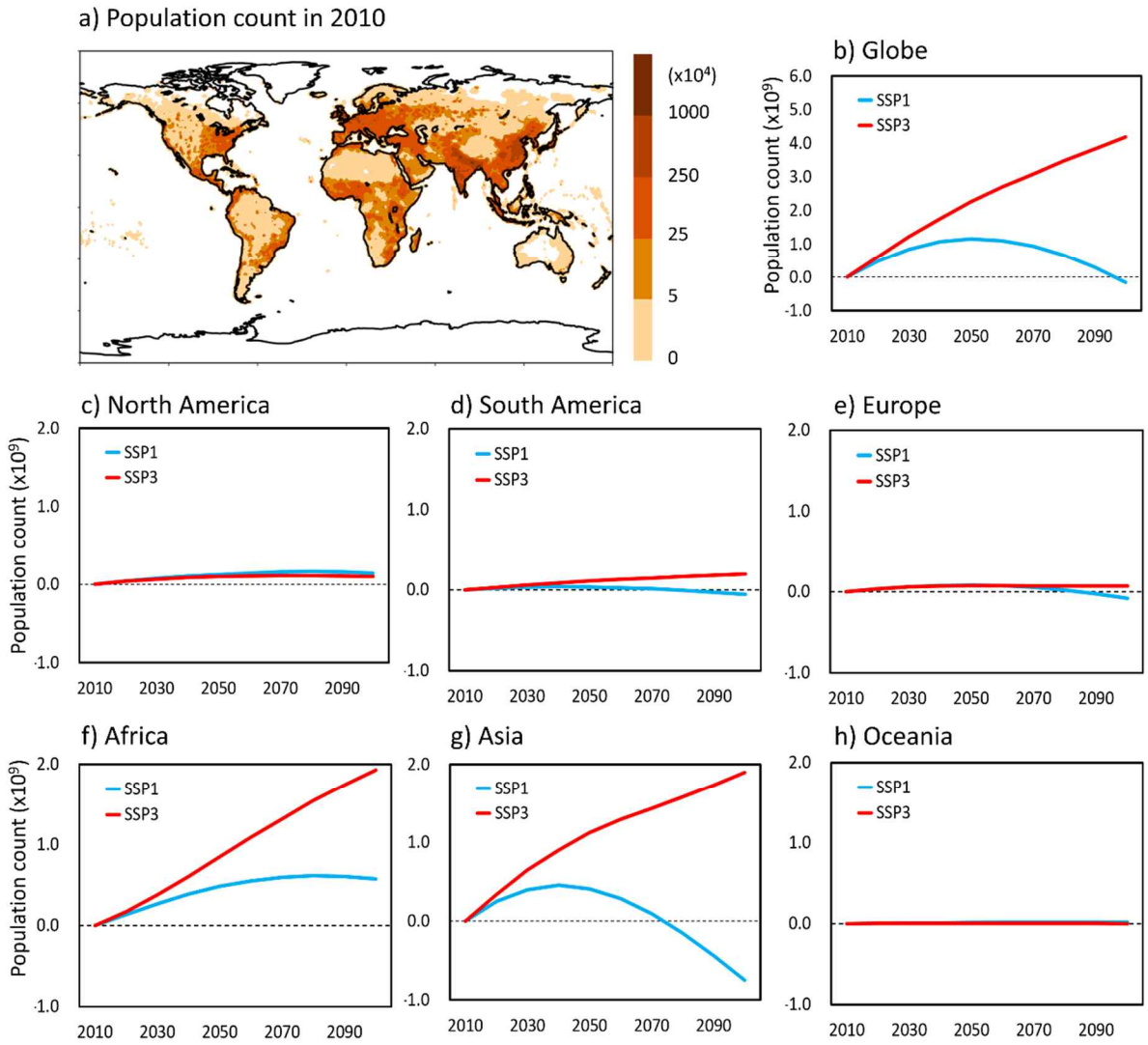

791

792 **Figure S3.** Spatial distribution of (a) population count (unit: number of persons) in 2010
793 estimated by NASA Socioeconomic Data and Application Center, and (b–h) time series of the
794 population change in the globe (GL), North America (NA), South America (SA), Europe (EU),
795 Africa (AF), Asia (AS), and Oceania (OC) under SSP1 and SSP3 scenarios at ten-year intervals
796 for the period of 2010–2100. Note that the y-axis range for GL is different from that of each
797 continent.

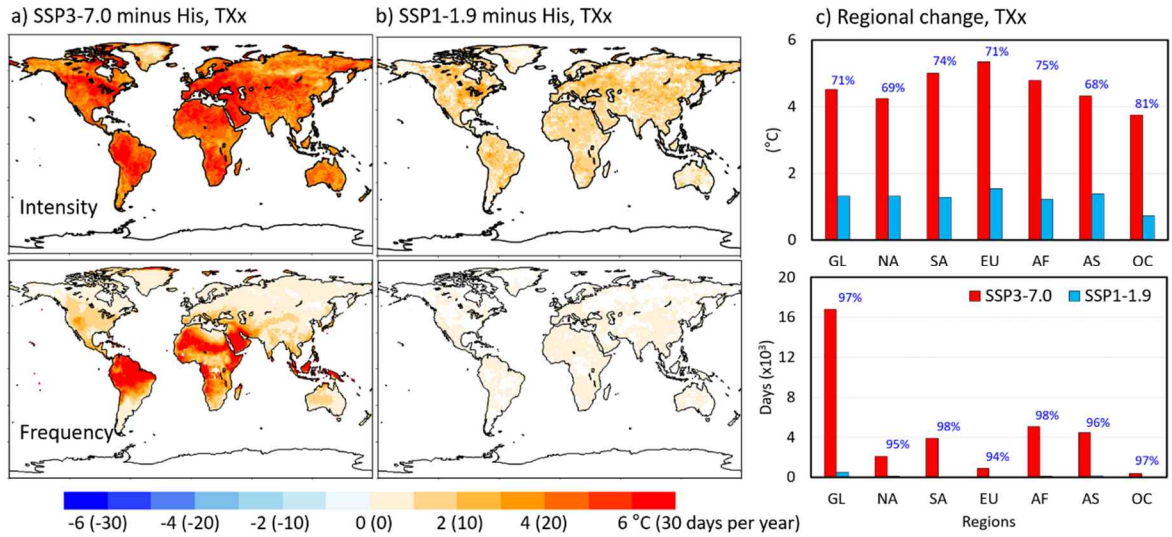

Figure S4. Projected changes of (a, b) spatial distribution in 30-year return value of TXx in the late 21st century (2071–2100) compared to the historical period of 1985–2014. (c) Changes in regionally-averaged or aggregated 30-year return value and its exceeding occurrence days for the North America (NA), South America (SA), Europe (EU), Africa (AF), Asia (AS), and Oceania (OC) are also presented. The CMIP6 multi-model ensemble median under the SSP1-1.9 and SSP3-7.0 scenarios are used. Only grids where more than three-quarters of the models used show the same sign are presented. Note that the relative reduction rate (%) in the SSP1-1.9 scenario compared to the SSP3-7.0 scenario is shown in blue above each bar.

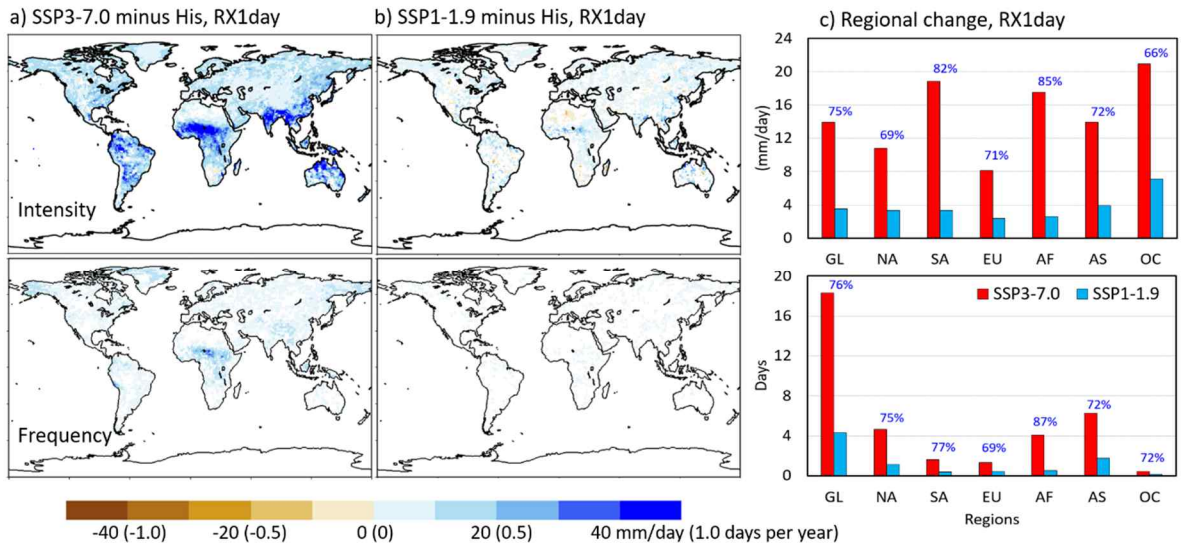

Figure S5. Same as Figure S4 but for 30-year return value of RX1day.

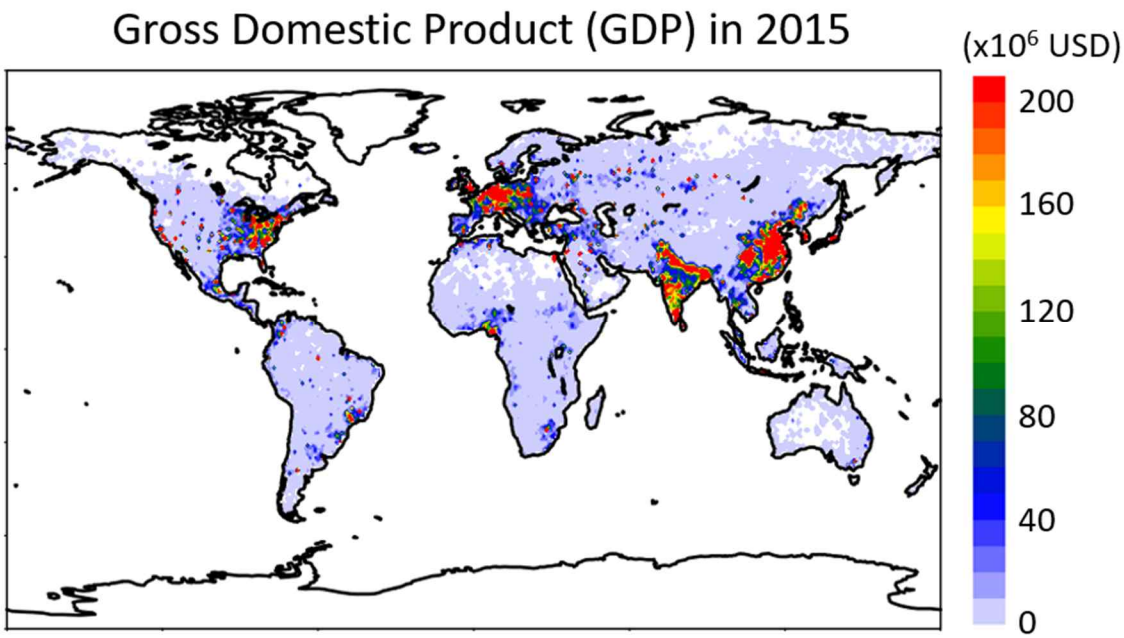

822

823 **Figure S6.** Gross Domestic Product (GDP, unit: US dollar) in 2015 estimated by Kummu et al.

824 (2020).

825

826

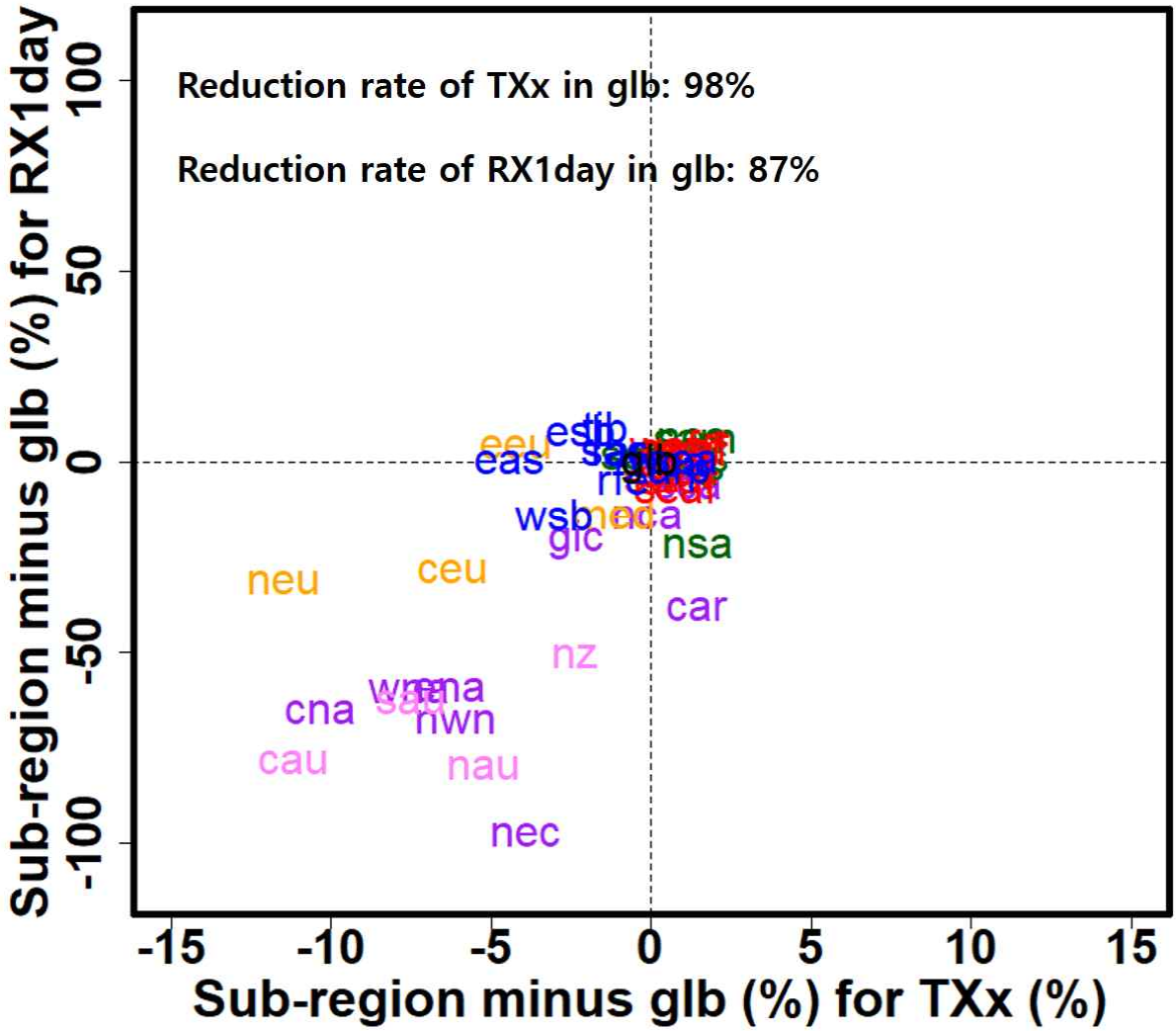

827

828 **Figure S7.** Comparison of relative reduction rate (%) of population exposure to extremely
829 high-temperature and heavy-precipitation events, that exceed the historical 30-year return
830 value of TXx and RX1day, in 41 sub-regions against that of the global region (glb). The
831 reduction rate (%) is calculated by comparing the population exposure changes under the SSP1-
832 1.9 scenario against the SSP3-7.0 scenario. Shaded colors indicate different continents: North
833 America (purple series), South America (green), Europe (orange), Africa (red), Asia (blue), and
834 Oceania (pink).

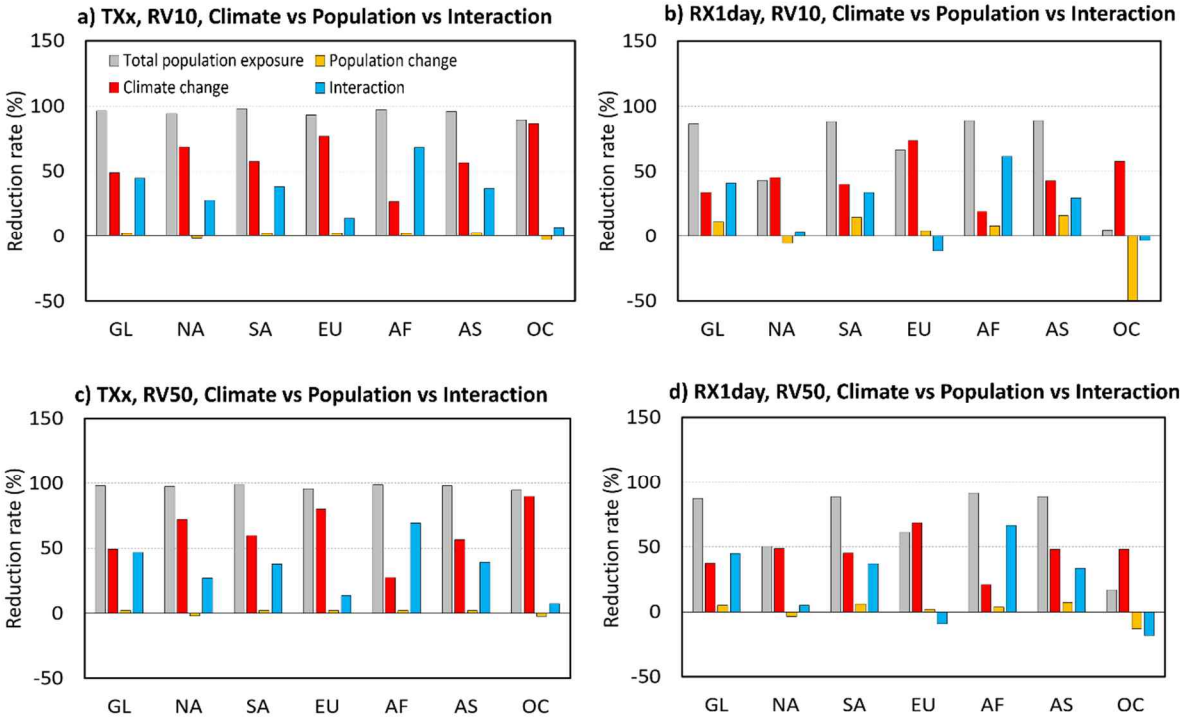

Figure S8. Reduction rate (%) of regionally aggregated population exposure for the 10- and 50-year return events (RV10 and RV50) of hot-temperature and heavy-precipitation in SSP1-1.9 relative to SSP3-7.0 scenarios and the relative contribution of climate, population, and climate-population interaction in the reduction rate.

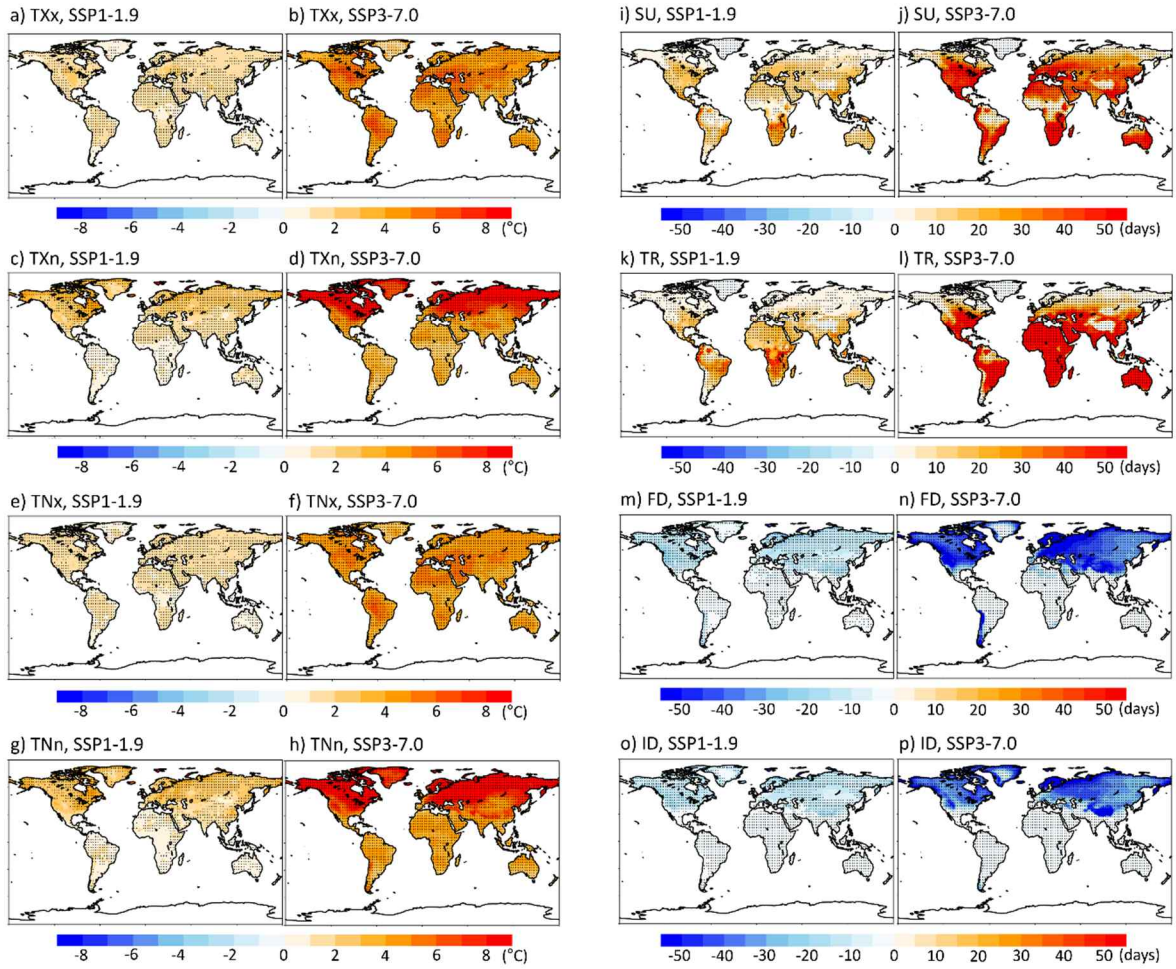

Figure S9. Changes in spatial distribution of temperature-related eight extreme indices in the late 21st century (2071–2100) under the SSP1-1.9 and SSP3-7.0 scenarios compared to the historical period of 1985–2014. The extreme indices are the annual maxima and minima of daily maximum temperature (TXx and TXn, respectively) and minimum temperature (TNx and TNn, respectively), summer days (SU), tropical nights (TR), frost days (FD), and ice days (ID).

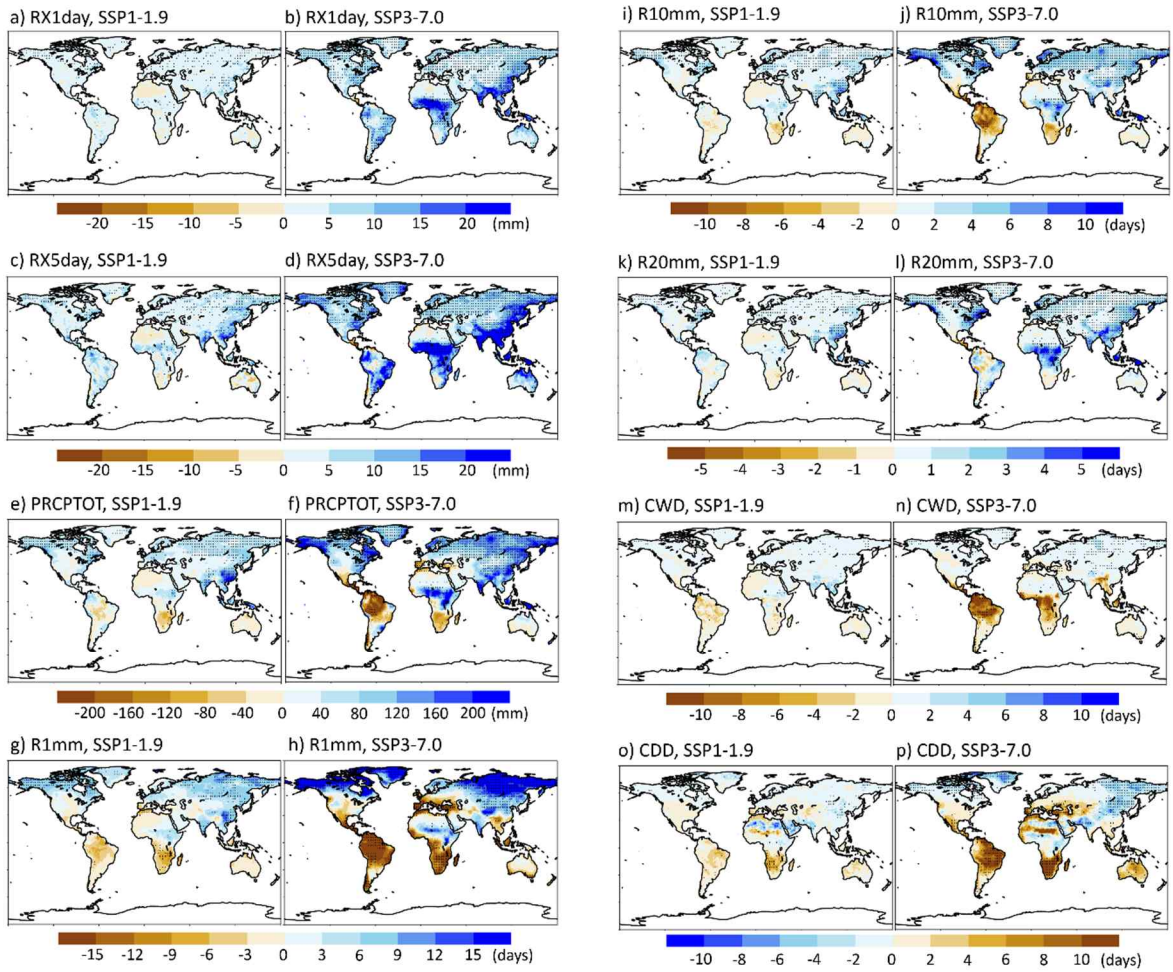

854

855 **Figure S10.** Same as Figure S8 but for precipitation-related eight extreme indices. The extreme
856 indices are the annual maxima of daily precipitation (RX1day) and 5-days-acumulated
857 precipitation (RX5day), total wet-day precipitation (PRCPTOT), number of wet day where the
858 precipitation > 1 mm (R1mm), > 10 mm (R10mm), and > 20 mm (R20mm), consecutive wet
859 days (CWD), and consecutive dry days (CDD).

860

861

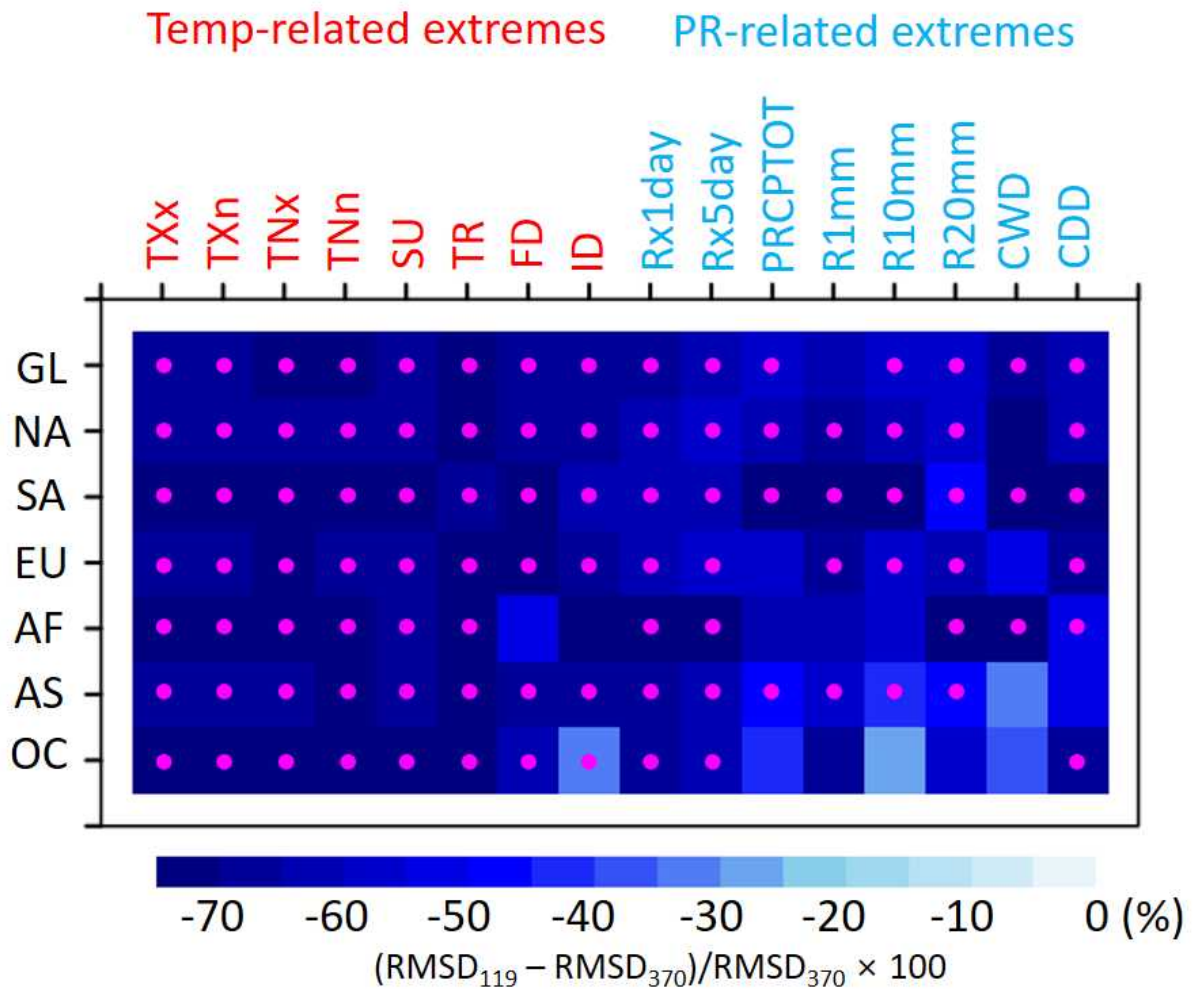

862

863 **Figure S11.** Reduction rate (%) of the root-mean square difference (RMSD) for event
864 frequency in the SSP1-1.9 scenario relative to the SSP3-7.0 scenario in the late 21st century
865 (2071–2100) for 16 extreme indices as shown in Figs. S7 and S8, compared to the historical
866 period of 1985–2014. The CMIP6 multi-model ensemble median is used. A greater negative
867 value implies that the SSP1-1.9 scenario is closer to the current climate state compared to the
868 SSP3-7.0 scenario, highlighting a higher carbon-neutral effect. The pink dot denotes that the
869 difference between the two scenarios is statistically significant at the 95% confidence level.

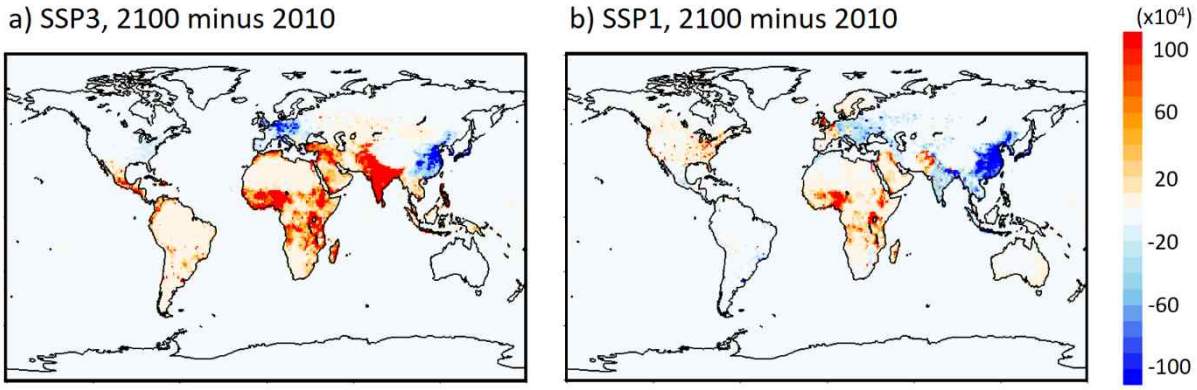

870

871 **Figure S12.** Projected changes of spatial distribution in population counts in year 2010

872 compared to year 2010.

873

874

875

876

877

878

879

880

881

882

883

884

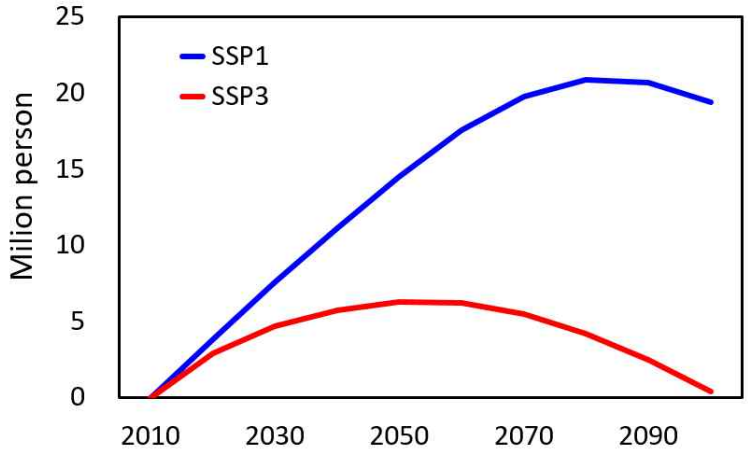

885 **Figure S13.** Time series of the population change in Oceania under SSP1 and SSP3 scenarios
886 at ten-year intervals for the period of 2010–2100.

887

888

889

[Earth's Future]

Supporting Information for

Significant reduction of unequal population exposure to climate extremes by achieving the carbon neutrality

Seok-Geun Oh[1], Jung Choi[1], Min-Jee Kang[1], Sujong Jeong[2,3], Seung-Ki Min[4,5], Sang-Wook Yeh[6], Yeon-Hee Kim[4], and Seok-Woo Son[1,3*]

[1]School of Earth and Environmental Sciences, Seoul National University, Seoul, South Korea

[2]Department of Environmental Planning, Seoul National University, Seoul, South Korea

[3]Climate Technology Center, Seoul National University, Seoul, South Korea

[4]Division of Environmental Science and Engineering, Pohang University of Science and Technology, Pohang, Gyeongbuk, South Korea

[5]Institute for Convergence Research and Education in Advanced Technology, Yonsei University, Incheon, Republic of Korea

[6]Department of Marine Science and Convergence Engineering, Hanyang University, ERICA, Ansan, South Korea

December 2023

***Corresponding author:** Seok-Woo Son (seokwooson@snu.ac.kr)

Contents of this file

- **Text S1 to S3**
- **Figures S1 to S13**

Text S1. Model evaluation.

The fifth generation of the European Centre for Medium-Range Weather Forecast global reanalysis (ERA5, Hersbach et al. 2020) for the historical period of 1985–2014 is used as reference to evaluate the Coupled Model Intercomparison Phase 6 (CMIP6) models. The ERA5 data has higher spatial (30 km) and time resolution (hourly) than the other reanalysis data (i.e., ERA40, Uppala et al. 2005; ERA-Interim, Dee et al., 2011; NCEP/NCAR Reanalysis 1, Kalnay et al., 1996; NCEP-DOE Reanalysis 2, Kanamitsu et al., 2002), potentially making it more suitable to estimate and evaluate the climate extremes. Therefore, this dataset has been widely utilized as a reference data for temperature and precipitation extremes (e.g., Kim et al., 2020; Li et al., 2021; Oh & Sushama, 2021). The daily temperature and precipitation data at approximately 30 km resolution into common into 1°×1° grid and then calculated climate extreme indices, TXx and RX1day (Zhang et al. 2011), and Generalized Extreme Value (GEV) estimation to reduce the difference in spatial scales from CMIP6 models (1–2°).

This study uses the multi-model ensemble median (MEM), which is a more valid representative measure than the multi-model mean, because extremely large or small values can distort the mean. The model performance is basically evaluated based on the bias, root-mean-square error (RMSE), and correlation for spatial patterns of the estimated extreme values for the historical period of 1985–2014. The equations of the bias, RMSE and correlation are as follow:

$$bias = \frac{1}{n}\sum_{i=1}^{n}(M_i - R_i)$$

$$RMSE = \sqrt{\frac{1}{n}\sum_{i=1}^{n}(M_i - R_i)^2}$$

$$correlation = \frac{\sum_{i=1}^{n}(M_i - \bar{M})(R_i - \bar{R})}{\sqrt{\sum_{i=1}^{n}(M_i - \bar{M})}\sqrt{\sum_{i=1}^{n}(R_i - \bar{R})}}$$

where n is the number of the total grids at land areas. The M_i and R_i denote the model and reanalysis at i th grid, respectively. The $\bar{M}$ nd $\bar{R}$ present the mean values over the land areas in the model and reanalysis, respectively. To compare the performance of MEM with that of each model, the combined metric of the RMSE and Taylor skill score (TSS, Taylor, 2001) is also used. The equation of TSS is like below:

$$TSS = \frac{(1 + correlation)^4}{4(SDR + \frac{1}{SDR})^2}$$

where *SDR* is the ratio of the spatial standard deviations of the model against to that of the reanalysis data. This score quantifies the similarity in the distribution and amplitude of the spatial pattern between the model and the reanalysis. The relative RMSE and TSS for each model and MEM are calculated by using their median values.

Text S2. Performance of CMIP6 MEM for historical period.

Compared with the ERA5 data, the CMIP6 MEM reproduces the spatial distribution of the 30-year return value of TXx and RX1day reasonably well for the historical period of 1985–2014, with the spatial correlations of 0.95 and 0.84, respectively (Figures S2a–S2f). The 30-year return value of TXx is slightly overestimated by 0.1 to 3.0 °C in most land areas except

for the high-latitude regions of the Northern Hemisphere, resulting in the global land average bias of 0.28 °C (Figure S2c). For the 30-year return value of RX1day, the CMIP6 MEM well captures typical large-scale features such as the intense precipitation extreme in the intertropical convergence zone (ITCZ) and African and Asian monsoon regions. However, the models underestimate the extreme precipitation by 20 to 100 mm/day depending precipitation zone, resulting in a global land average bias of -11.41 mm/day (Figure S2f).

Compared to a single model, the MEM shows a better performance in both the 30-year return values of TXx and RX1day (Figure S2g and S2h). This result is consistent with previous studies showing that the multi-model ensemble shows superior performance in reproducing mean and extreme climates than a single model (e.g., Oh & Suh, 2017; Kim et al., 2020; Li et al., 2021). Similar results are found for other return events, i.e., 10- and 50-year return value (not shown). It provides justification for the use of the CMIP6 MEM for future projection of the rare extreme events with varying return years.

Text S3. Response of climate extremes in the late 21st century to carbon neutrality.

If the current global warming is continued (i.e., SSP3-7.0 scenario), hot-temperature and heavy-precipitation extremes are expected to be strengthened in the late 21st century. The hot-temperature extreme is projected to experience a more intense warming event of above 4 °C over all land regions except Greenland (the first row of Figure S4a). Such extreme is expected to occur more than total 1000 days in South America, Africa, Arabia peninsula, and South Asia regions during the future period of 2071–2100 (the second row of Figure S4a). The heavy-precipitation extreme also reveals more intense and frequent events (Figure S5a) particularly in the African and Asian monsoon region where a dense population exists (Figure

S3a).

Even if the transition to a carbon-neutral society is successful (i.e., SSP1-1.9 scenario), the intensity in both hot-temperature and heavy-precipitation extremes are still expected to increase with a range of 0.5–2°C and 0–20 mm/day, respectively. On a global average, the number of days in hot-temperature (heavy-precipitation) extreme increases up to total 100 days (5 days) compared to the historical period (Figures S4b and S5b). Although more intense and frequent climate extremes are also evident in the carbon neutrality scenario, the reduction rates, which estimate the benefit of carbon neutrality compared to the high emission scenario, are substantially large (Figures S4c and S5c; see Methods in main paper). Globally, a 71% decrease is found in the intensity of hot-temperature extreme (the first row of Figure S4c), while a more significant decrease (97%) is found in its frequency (the second row of Figure S4c). Similar reduction rates are revealed in the heavy-precipitation extreme, i.e., 75 and 76% decreases in its intensity and frequency, respectively (Figure S5c).

The difference between the scenarios with and without the net-zero carbon emission shows a large regional dependency, especially for the frequency (Figures S4c and S5c). For example, the frequency of the hot-temperature extreme exhibits large differences in the South America, African, and Asian continents, while that of heavy-precipitation extreme shows a large difference in the African, North America, and Asian continents. Interestingly, the reduction rates of the intensity and frequency of the hot-temperature extremes are 68–81% and 94–98%, respectively, which implies a higher benefit of carbon neutrality in the frequency than in the intensity for all the continents (Figures S4c). On the other hand, the intensity and frequency of the heavy-precipitation extremes are reduced by 66–85% and 69–87% in net-zero carbon emission scenario, respectively. This result suggests that there are larger differences in

reduction rate across continents, but smaller differences between frequency and intensity compared to hot-temperature extreme (Figure S5c). In summary, a transition to a carbon-neutral society around 2050 can lead to a more than twofold of reduction in both the intensity and frequency of hot-temperature and heavy-precipitation extremes for all the continents.

Acknowledgements

This research was supported by Basic Science Research Program through the National Research Foundation of Korea (NRF) funded by the Ministry of Education (RS-2023-00238065). This research was also supported by the Research Program for the carbon cycle between oceans, land, and atmosphere of the NRF funded by the Ministry of Science and ICT (2021M3I6A1086807), and Korea Environment Industry & Technology Institute (KEITI) through Project for developing an observation-based GHG emissions geospatial information map, funded by Korea Ministry of Environment (MOE) (RS-2023-00232066).

Reference

Dee, D. P., Uppala, S. M., Simmons, A. J., Berrisford, P., Poli, P., & Kobayashi, S., et al. (2011). The ERA-Interim reanalysis: configuration and performance of the data assimilation system. *Quarterly Journal of the Royal Meteorological Society*, *137*, 553–597.

Hersbach, H., Bell, B., Berrisford, P., Hirahara, S., Horanyi, A., & Munoz-Sabater, J., et al. (2020). The ERA5 global reanalysis. *Quarterly Journal of the Royal Meteorological Society*, *146*, https://doi.org/10.1002/qj.3803.

Kalnay, E., Kanamitsu, M., Kistler, R., Collins, W., Deaven, D., & Gandin, L., et al. (1996). The NCEP/NCAR 40-year reanalysis project. *Bulletin of the American Meteorological Society*, *77*, 437–472.

Kanamitsu, M., Ebisuzaki, W., Woollen, J., Yang, S.-K., Hnilo, J. J., & Fiorino, M., et al. (2002). NCEP-DOE AMIP-II reanalysis (R-2). *Bulletin of the American Meteorological Society*, *83*, 1631–1643.

Kim, Y. H., Min, S. K., Zhang, X., Sillmann, J., & Sandstad, M. (2020). Evaluation of the CMIP6 multi-model ensemble for climate extreme indices. *Weather and Climate Extremes*, *29*, 100269.

Kummu, M., Taka, M., & Guillaume, J. H. A. (2018). Gridded global datasets for gross domestic product and human development index over 1990 2015. *Scientific data*, *5*, 180004.

Li, C., Zwiers, F., Zhang, X., Li, G., Sun, Y., & Wehner, M. (2021). Changes in annual extremes of daily temperature and precipitation in CMIP6 model. *Journal of Climate*, *34*, 3441–3460.

Oh, S. G. & Sushama, L. (2021). Urban-climate interactions during summer over eastern North America. *Climate Dynamics*, *57*, 3015–3028.

Oh, S. G., & Suh, M. S. (2017). Comparison of projection skills of deterministic ensemble methods using pseudo-simulation data generated from multivariate Gaussian distribution. *Theoretical and Applied Climatology*, 129, 243–262 .

Taylor K. E. (2001) Summarizing multiple aspects of model performance in a single diagram. *Journal of Geophysical Research*, *106*, 7183–7192.

Uppala, S. M., KÅllberg, P. W., Simmons, A. J., Andrae, U., Bechtold, V. D. C., & Fiorino, M., et al. (2005). The ERA-40 Reanalysis. *Quarterly Journal of the Royal Meteorological Society*, *131*, 2961–3012.

Zhang, W., Zhou, T., Zou, L., Zhang, L., & Chen, X. (2018). Reduced exposure to extreme precipitation from 0.5°C less warming in global land monsoon regions. *Nature*

157 *Communications*, *9*, 3153.

158

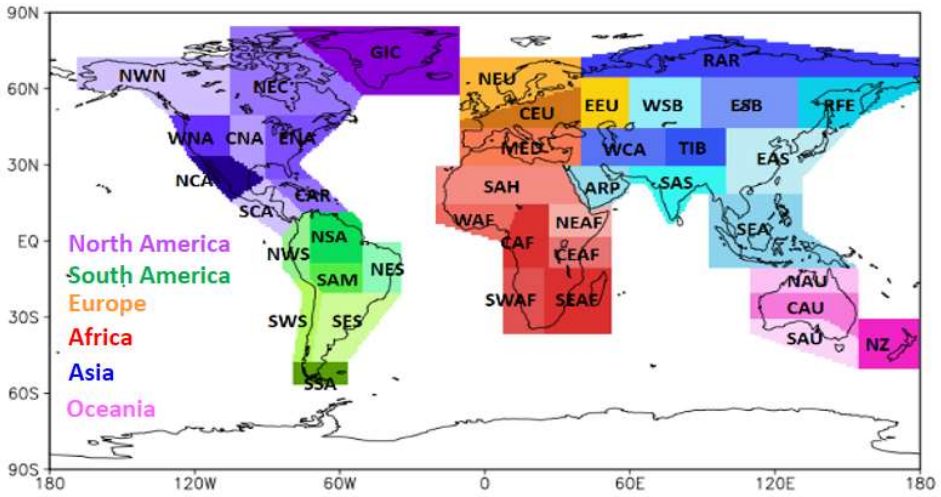

159

160 **Figure S1.** Sub-regional domain in the global land adopted from Iturbide et al. (2020). The
161 shaded colors indicate different continents: North America (purple series), South America
162 (green), Europe (orange), Africa (red), Asia (blue), and Oceania (pink).

163

164

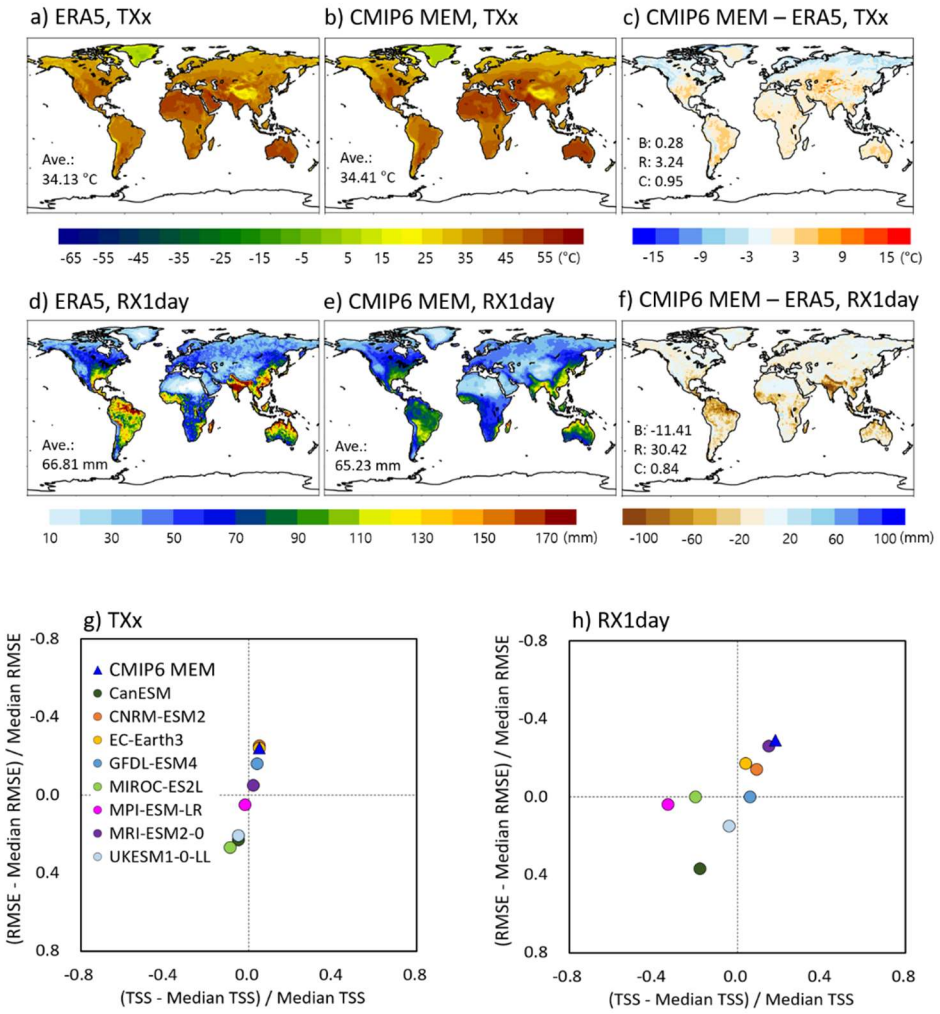

165

166 **Figure S2.** Estimates of 30-year return values of hot-temperature (TXx) and heavy-
167 precipitation (RX1day) extremes of (a, d) ERA5 reference data and (b, e) CMIP6 multi-model
168 ensemble median for the present period of 1985–2014, and (c, f) their differences. The area-
169 averaged value (Ave.), bias (B), root-mean-square error (R), and correlation (C) between the
170 CMIP6 multi-model ensemble median and ERA5 are indicated in sub-plot. Only land areas are
171 considered. (g, h) The relative performance of the CMIP6 models for 30-year return values of
172 TXx and RX1day, based on the root-mean-square error (RMSE) and Taylor skill score (TSS).
173 The symbol closer to the upper right corner indicates better performance.

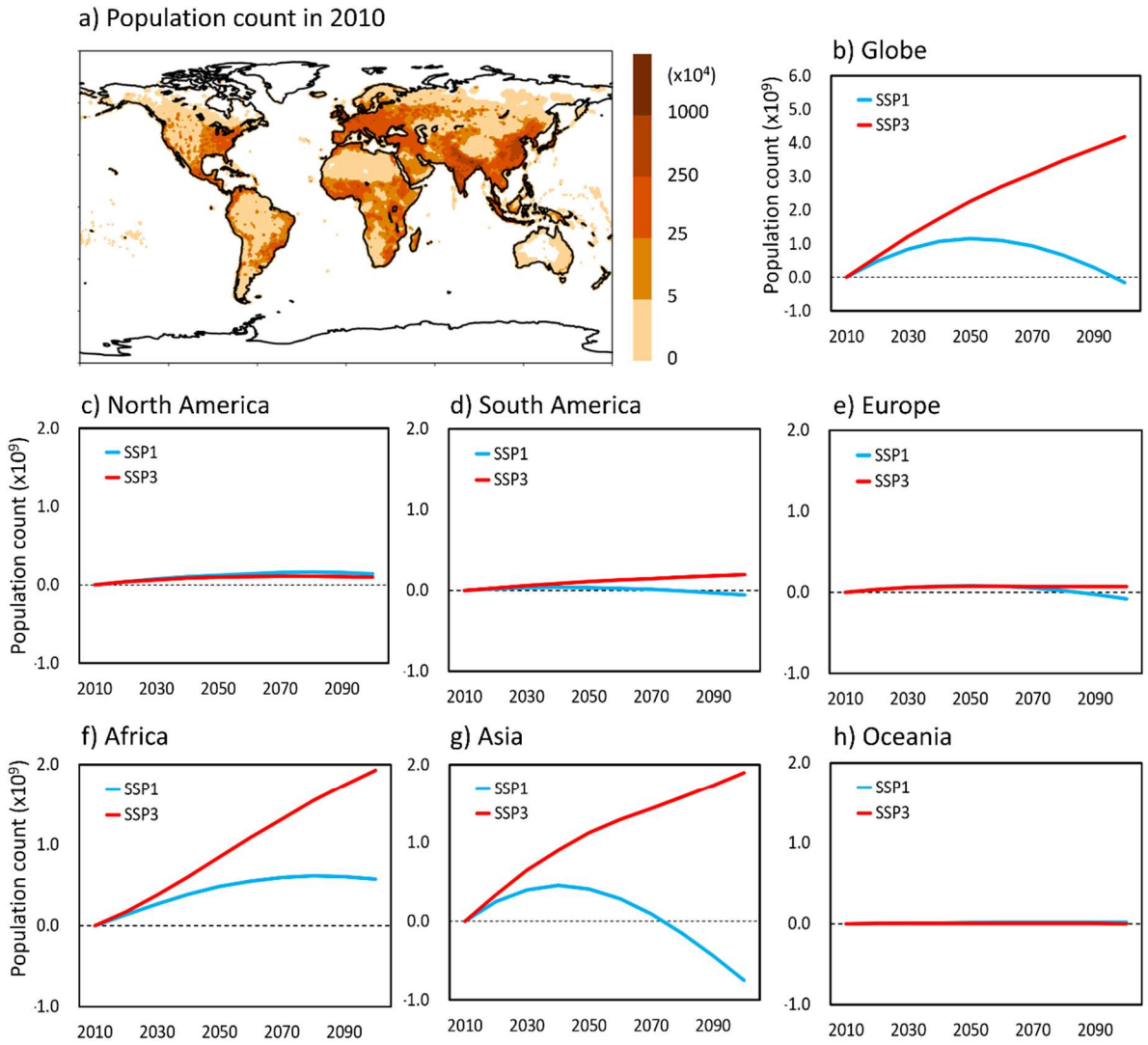

174

175 **Figure S3.** Spatial distribution of (a) population count (unit: number of persons) in 2010
176 estimated by NASA Socioeconomic Data and Application Center, and (b–h) time series of the
177 population change in the globe (GL), North America (NA), South America (SA), Europe (EU),
178 Africa (AF), Asia (AS), and Oceania (OC) under SSP1 and SSP3 scenarios at ten-year intervals
179 for the period of 2010–2100. Note that the y-axis range for GL is different from that of each
180 continent.

181

182

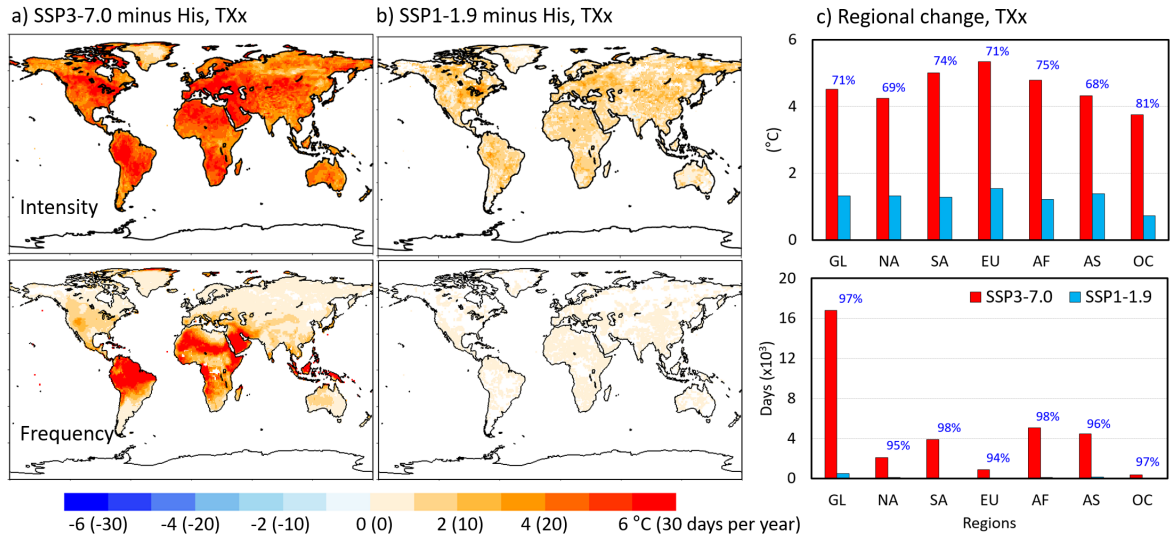

Figure S4. Projected changes of (a, b) spatial distribution in 30-year return value of TXx in the late 21st century (2071–2100) compared to the historical period of 1985–2014. (c) Changes in regionally-averaged or aggregated 30-year return value and its exceeding occurrence days for the North America (NA), South America (SA), Europe (EU), Africa (AF), Asia (AS), and Oceania (OC) are also presented. The CMIP6 multi-model ensemble median under the SSP1-1.9 and SSP3-7.0 scenarios are used. Only grids where more than three-quarters of the models used show the same sign are presented. Note that the relative reduction rate (%) in the SSP1-1.9 scenario compared to the SSP3-7.0 scenario is shown in blue above each bar.

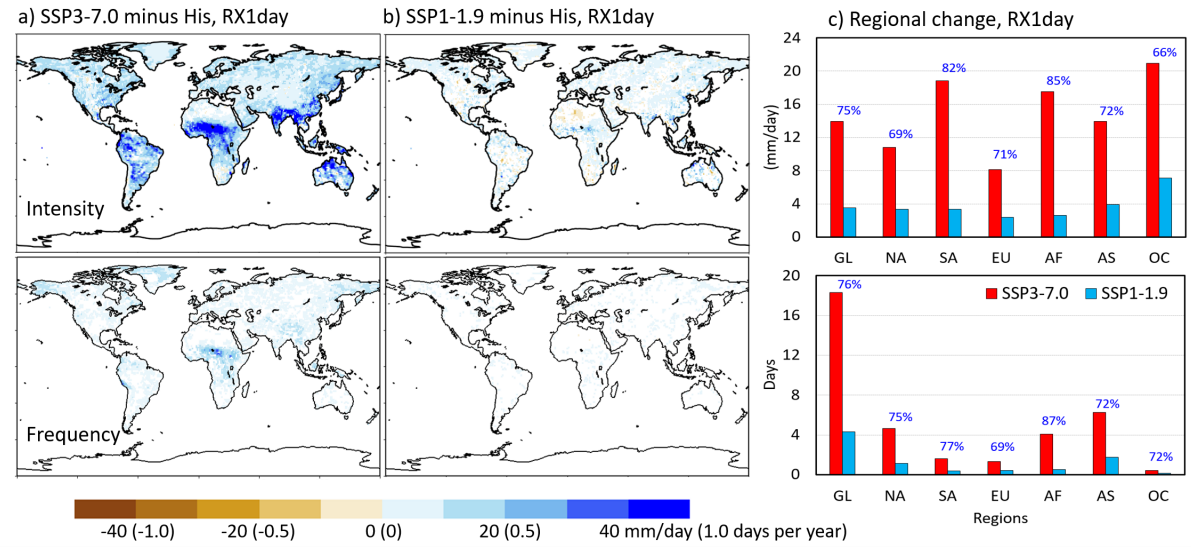

Figure S5. Same as Figure S4 but for 30-year return value of RX1day.

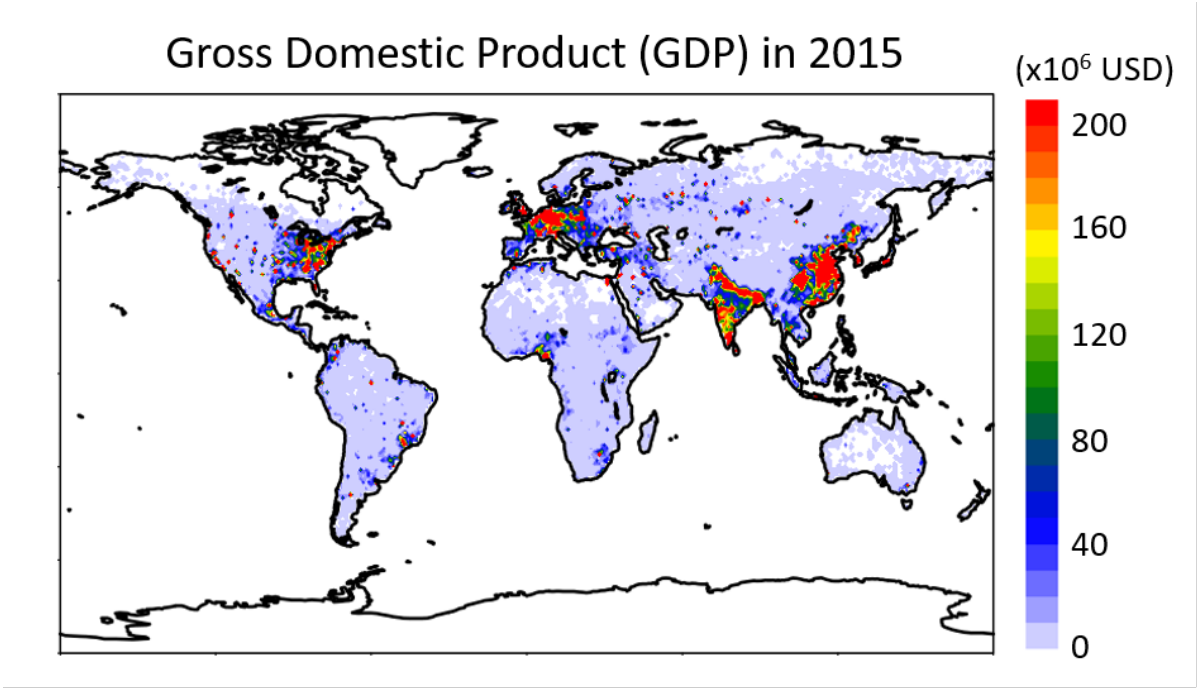

Figure S6. Gross Domestic Product (GDP, unit: US dollar) in 2015 estimated by Kummu et al. (2020).

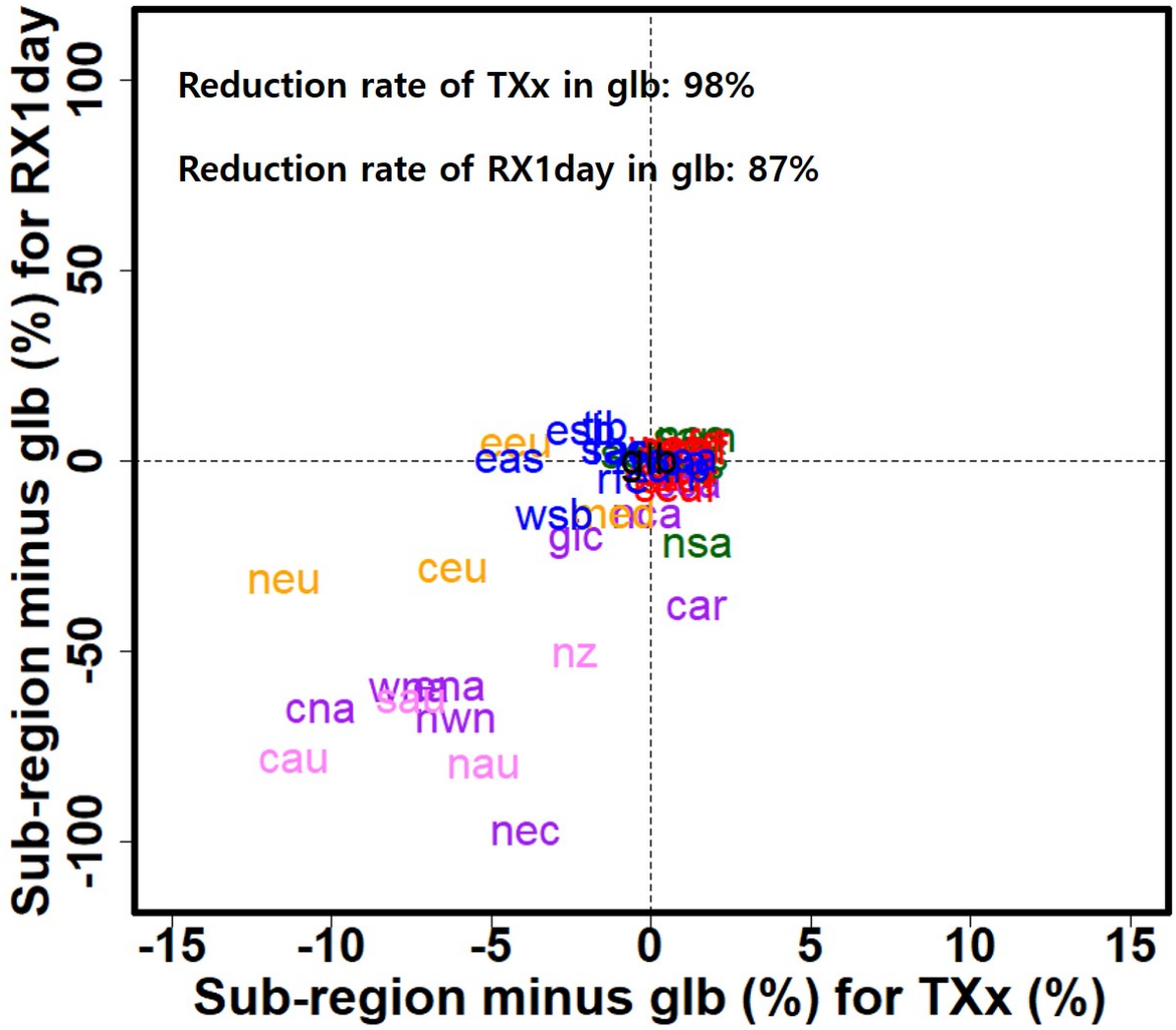

Figure S7. Comparison of relative reduction rate (%) of population exposure to extremely high-temperature and heavy-precipitation events, that exceed the historical 30-year return value of TXx and RX1day, in 41 sub-regions against that of the global region (glb). The reduction rate (%) is calculated by comparing the population exposure changes under the SSP1-1.9 scenario against the SSP3-7.0 scenario. Shaded colors indicate different continents: North America (purple series), South America (green), Europe (orange), Africa (red), Asia (blue), and Oceania (pink).

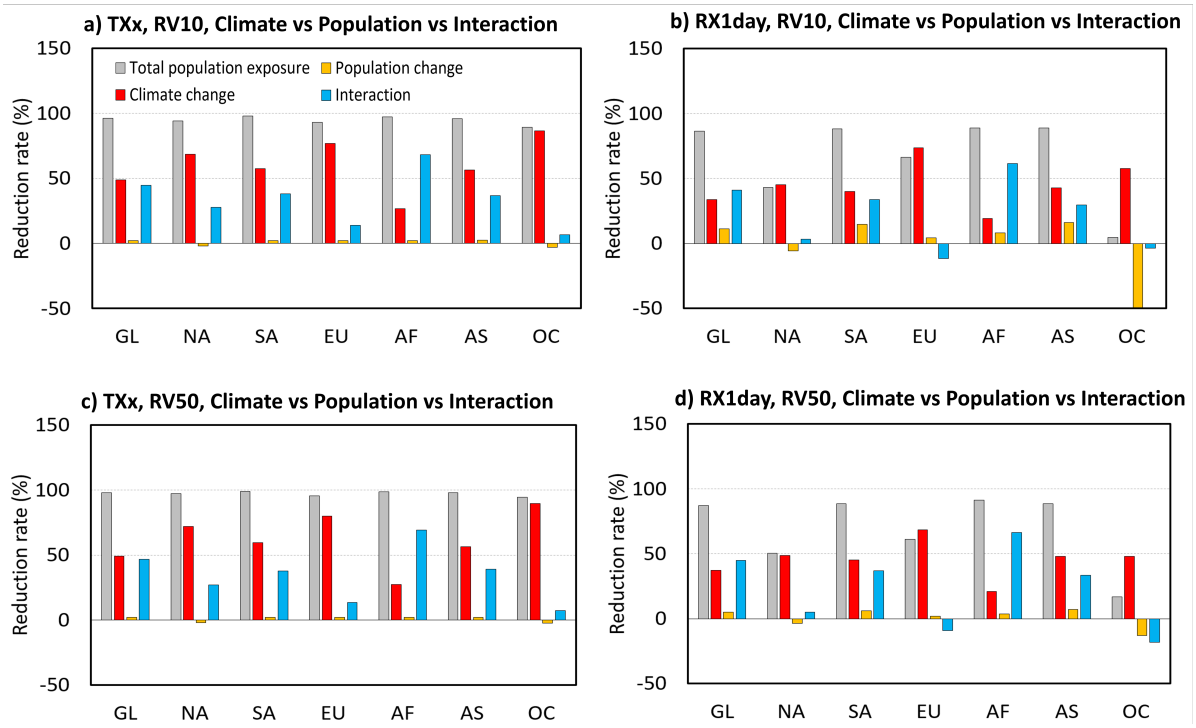

Figure S8. Reduction rate (%) of regionally aggregated population exposure for the 10- and 50-year return events (RV10 and RV50) of hot-temperature and heavy-precipitation in SSP1-1.9 relative to SSP3-7.0 scenarios and the relative contribution of climate, population, and climate-population interaction in the reduction rate.

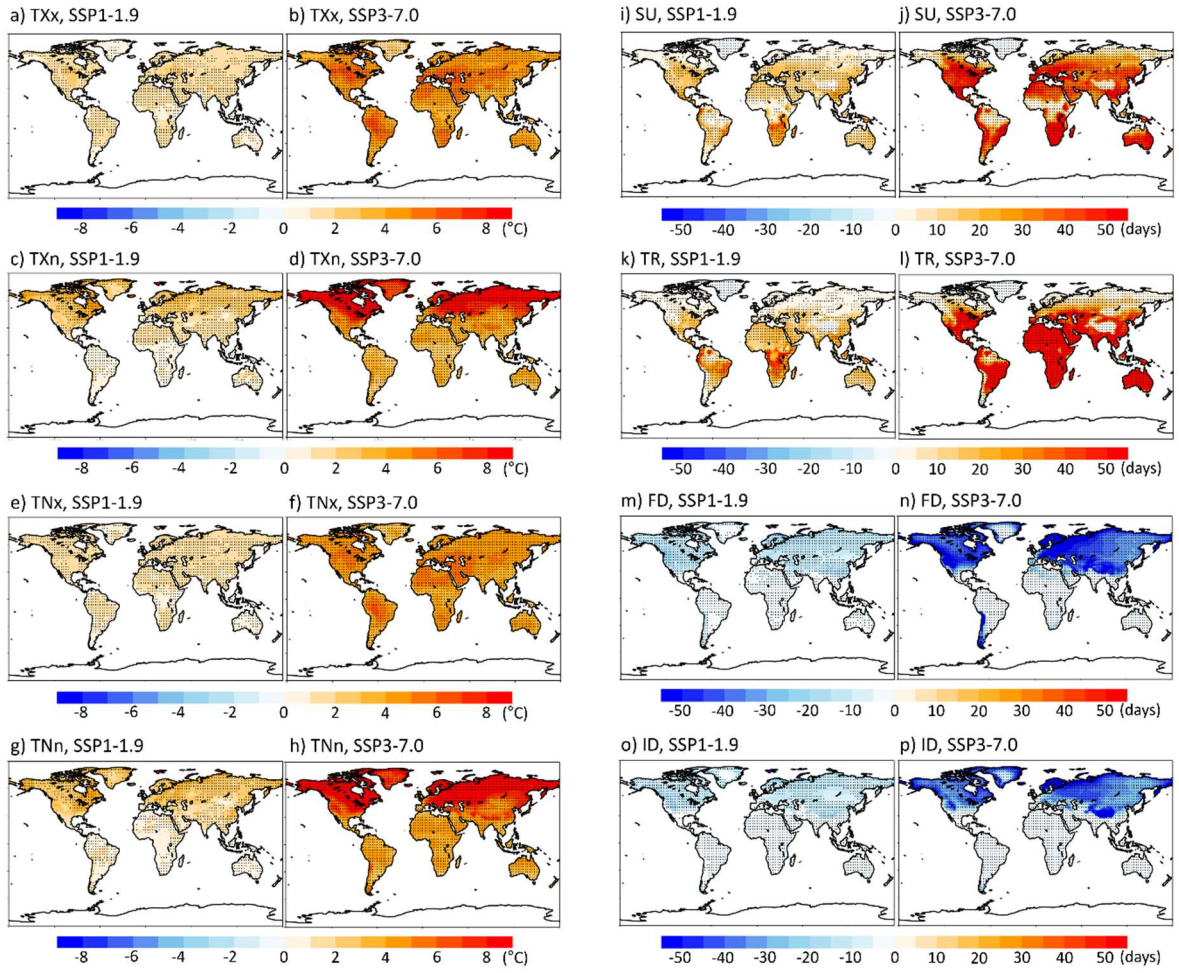

235

236 **Figure S9.** Changes in spatial distribution of temperature-related eight extreme indices in the
237 late 21st century (2071–2100) under the SSP1-1.9 and SSP3-7.0 scenarios compared to the
238 historical period of 1985–2014. The extreme indices are the annual maxima and minima of
239 daily maximum temperature (TXx and TXn, respectively) and minimum temperature (TNx and
240 TNn, respectively), summer days (SU), tropical nights (TR), frost days (FD), and ice days (ID).

241

242

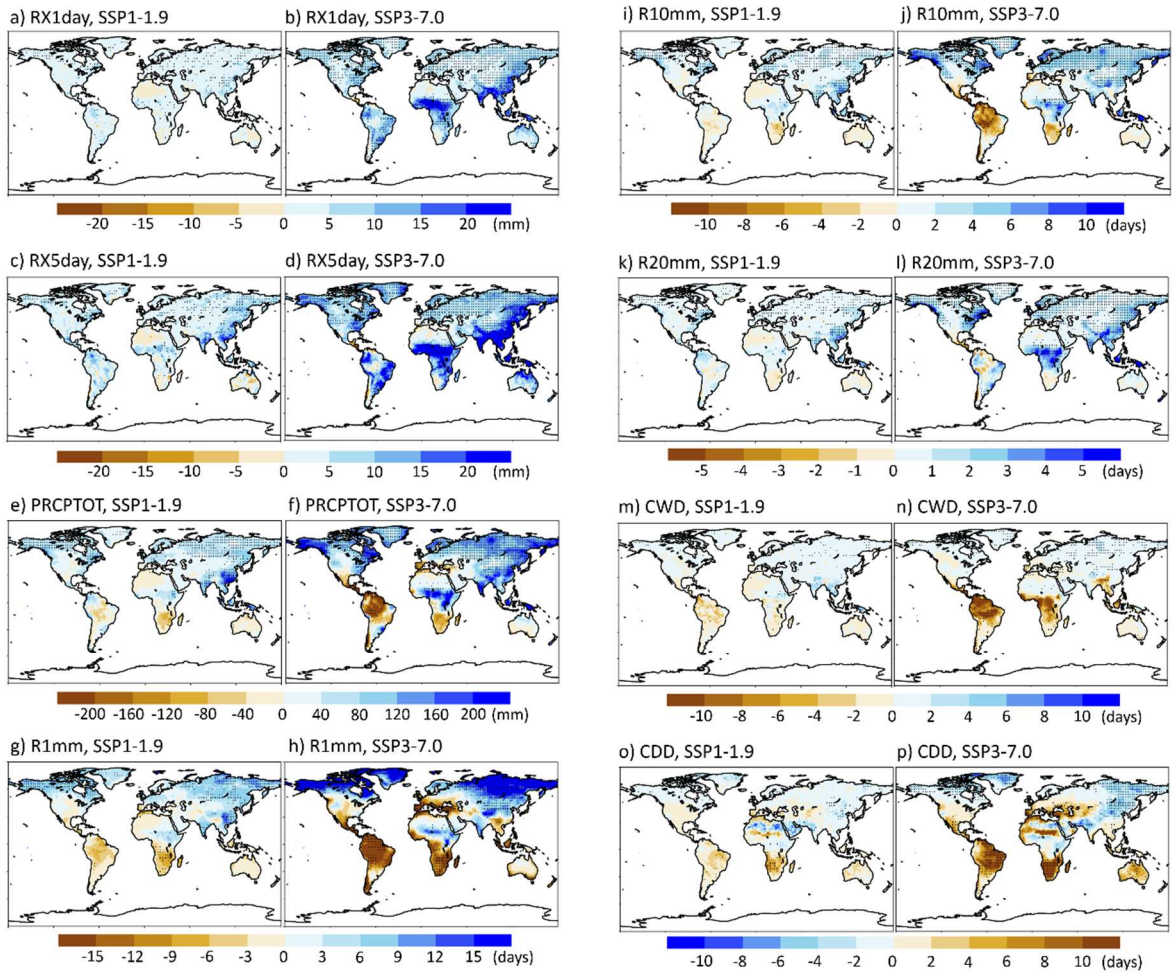

Figure S10. Same as Figure S8 but for precipitation-related eight extreme indices. The extreme indices are the annual maxima of daily precipitation (RX1day) and 5-days-acumulated precipitation (RX5day), total wet-day precipitation (PRCPTOT), number of wet day where the precipitation > 1 mm (R1mm), > 10 mm (R10mm), and > 20 mm (R20mm), consecutive wet days (CWD), and consecutive dry days (CDD).

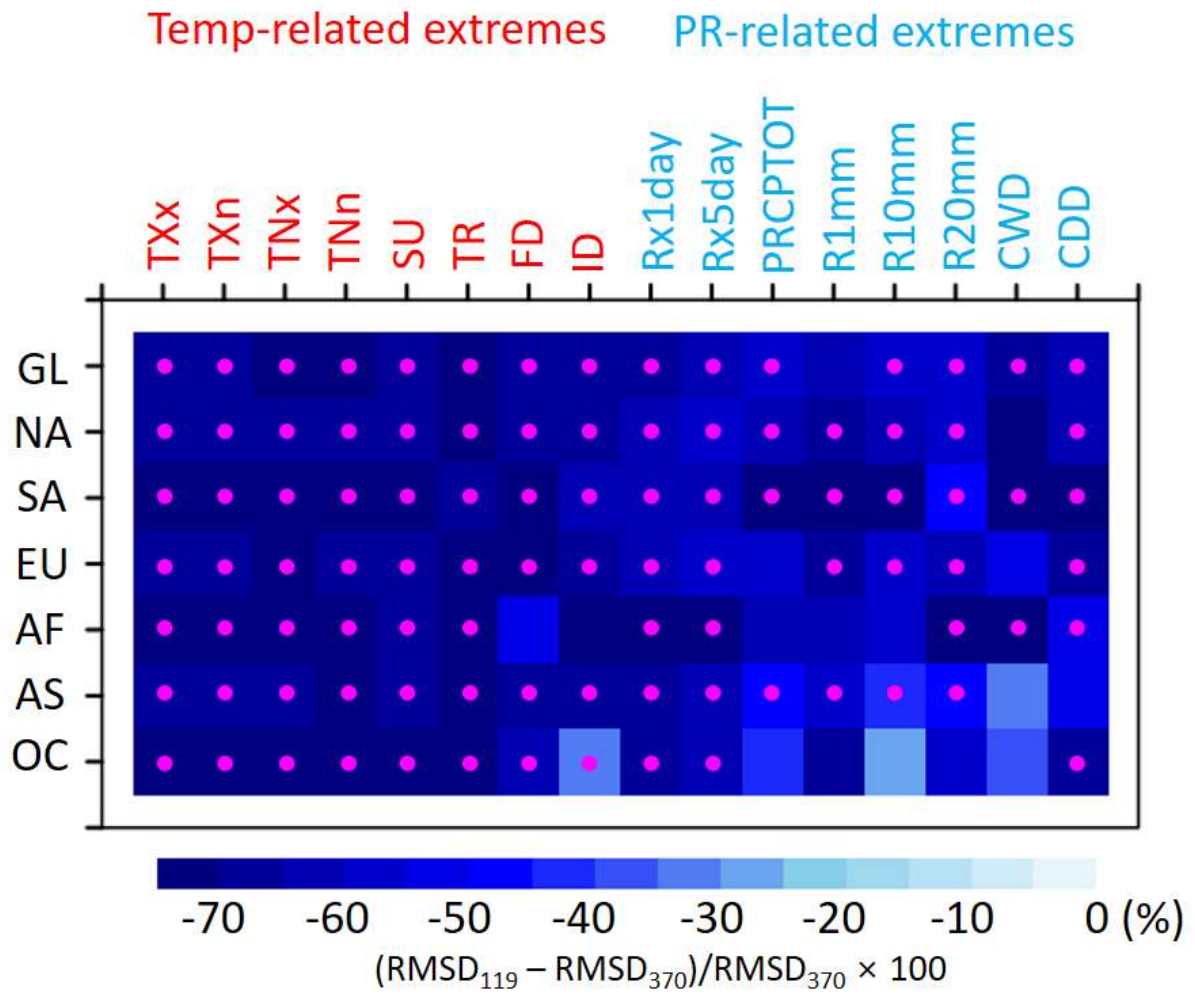

Figure S11. Reduction rate (%) of the root-mean square difference (RMSD) for event frequency in the SSP1-1.9 scenario relative to the SSP3-7.0 scenario in the late 21st century (2071–2100) for 16 extreme indices as shown in Figs. S7 and S8, compared to the historical period of 1985–2014. The CMIP6 multi-model ensemble median is used. A greater negative value implies that the SSP1-1.9 scenario is closer to the current climate state compared to the SSP3-7.0 scenario, highlighting a higher carbon-neutral effect. The pink dot denotes that the difference between the two scenarios is statistically significant at the 95% confidence level.

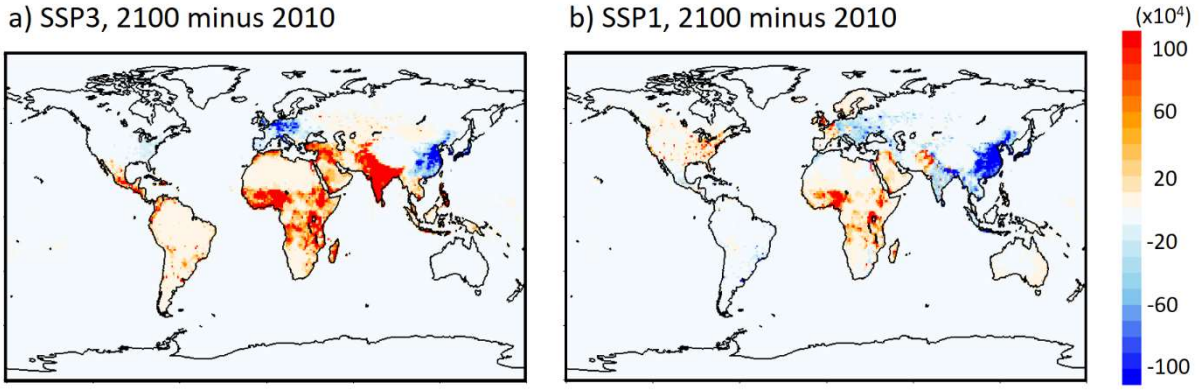

Figure S12. Projected changes of spatial distribution in population counts in year 2010 compared to year 2010.

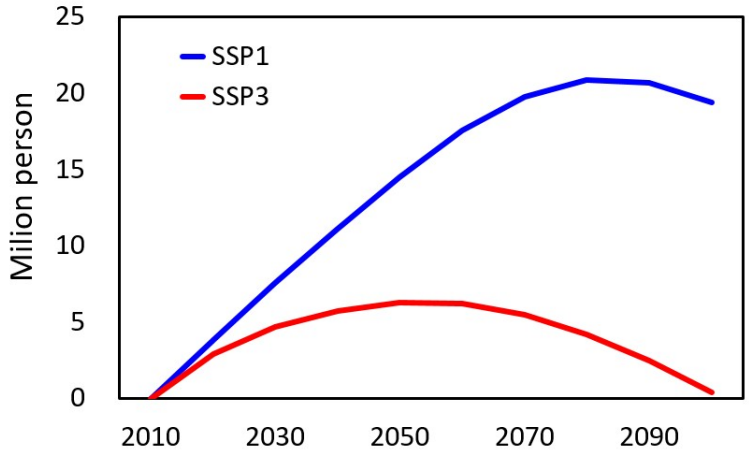

278

279 **Figure S13.** Time series of the population change in Oceania under SSP1 and SSP3 scenarios

280 at ten-year intervals for the period of 2010–2100.

281